MOLECULAR CHARACTERIZATION OF GLUCOCORTICOID-INDUCED AUTOPHAGY AND EXOSOME RELEASE IN MLO-Y4 OSTEOCYTE-LIKE CELLS

REINALDO BORGES GONÇALVES

This thesis is submitted to the University of Western Australia

in fulfilment of the requirements for the degree of

Bachelor of Medical Science (Honours)

2014

The work presented in this thesis was performed at the University of Western Australia, School of Surgery and Pathology, Centre for Orthopaedic Research, Queen Elizabeth II Medical Centre, Nedlands, Perth, Western Australia

STATEMENT

This is to certify that all the work contained herein was performed by myself, except where indicated otherwise

Reinaldo Borges Gonçalves

Asst/Prof. Tak Cheng
Supervisor

W/Prof. Ming-Hao Zheng
Supervisor/Director

TABLE OF CONTENTS

Table of Contents i

Acknowledgements v

Abbreviations vi

List of Figures viii

CHAPTER ONE – LITERATURE REVIEW

1.1 Introduction 1

1.2 The Osteocyte 2

1.3 Osteocyte Morphology 3

1.4 Osteocyte Function 5

1.4.1 Osteocyte: A Mechanosensory Cell 5

1.4.2 Osteocyte: Orchestrator of Osteoclastic and Osteoblastic Functions and Phosphate Metabolism 6

1.4.2.1 Receptor Activator of Nuclear Factor-kappa B Ligand (RANKL) 6

1.4.2.2 Sclerostin (SOST) 6

1.4.2.3 Fibroblast Growth Factor 23 (FGF23) 7

1.5 Autophagy: A crucial mechanism for bone maintenance 7

1.5.1 Autophagy Machinery 8

1.5.2 Autophagy Signaling Cascade 9

1.5.2.1 mTORC1 10

1.5.2.2 mTORC2 11

1.6 Intercellular Communication – The Role of Exosomes 13

1.7 Autophagy and Exosome Biogenesis and Secretion – The Convergence Point 16

1.8 Summary 18

CHAPTER TWO – RESEARCH PROPOSAL

2.1 Research Proposal 20

2.2 Hypothesis 21

2.3 Aims 21

CHAPTER THREE - MATERIALS AND METHODS

3.1 Materials **22**

3.1.1 Chemical Reagents 22

3.1.2 Molecular Products 23

3.1.3 Commercially Purchased Kits 24

3.1.4 Oligonucleotide Primers 24

3.1.5 Western Blot/Immunoblot Antibodies 25

3.1.6 Secondary Antibodies 27

3.1.7 Antibodies, Markers and Dyes Immunofluorescence Microscopy 27

3.1.7.1 Primary Antibodies 27

3.1.7.2 Secondary Antibodies 28

3.1.8 Other Materials and Equipments 28

3.1.9 Softwares 30

3.1.10 Solutions and Buffers 30

3.1.11 Cells 34

3.1.12 Cell Culture Medium and Reagents 34

3.2 Cell Culture **35**

3.2.1 Culturing of MLO-Y4 Cells 35

3.2.2 Culturing of Primary Calvarial Osteoblasts 36

3.2.3 Culturing of Primary Bone Marrow Monocytes and Osteoclasts 36

3.3 Protein Analysis **36**

3.3.1 Total Cellular Protein (TCP) Extraction 36

3.3.2 Protein Concentration Quantitation 36

3.3.3 SDS Polyacrylamide Gel (SDS-PAGE) Analysis of Protein Profile 37

3.3.4 Protein Transfer to Nitrocellulose Membrane for Western Blotting 38

3.3.5 Ponceau S Red Staining 40

3.3.6 Western Blot/Immunoblot Analysis 40

3.3.7 Stripping and and Reprobing of Membranes 41

3.4 Isolation and Purification of MLO-Y4-derived Exosomes **41**

3.5 RNA Extraction and Quantitation **43**

3.5.1 General Handling Procedures 43

3.5.2 Extraction of Total RNA 43

3.5.3 Quantification of RNA Concentration 44
3.6 Reverse Transcription – Generation of cDNAs 44
3.7 DNA Amplification of Target Genes by Semi-Quantitative PCR 45
3.8 DNA Agarose Gel Electrophoresis 46
3.9 Quantitative Real Time PCR (qPCR) 47
3.10 Transient Transfection of MLO-Y4 cells 48
3.10.1 Transformation of pCMV6-AC-Redd1-GFP plasmid 48
3.10.2 Overexpression of pCMV6-AC-Redd1-GFP in MLO-Y4 cells 51
3.10.3 REDD1 Silencing in MLO-Y4 Cells 51
3.11 Immunofluorescence Staining 52
3.11.1 Confocal Microscopy 53

CHAPTER FOUR - MOLECULAR MECHANISMS OF GC-INDUCED AUTOPHAGY IN MLO-Y4 OSTEOCYTE-LIKE CELLS
4.1 Introduction 54
4.2 Results 55
4.2.1 Effect of GC (Dex) on Autophagy in MLO-Y4 Osteocyte-like Cells 55
4.2.2 Effect of GC (Dex) on *redd1* and *mkp1* Gene Expression 57
4.2.3 Effect of GC (Dex) on MKP1 and REDD1 Protein Expression 64
4.2.4 Effect of REDD1 Overexpression on mTORC1 Signaling Pathway 64
4.2.5 Effect of REDD1 Silencing on GC (Dex)-induced Autophagy 73
4.3 Discussion and Conclusion 73

CHAPTER FIVE - CHARACTERIZATION AND PROFILING OF MLO-Y4 CELLS-DERIVED EXOSOMES
5.1 Introduction 80
5.2 Results 81
5.2.1 Effect of GC (Dex) on MLO-Y4 Morphology 81
5.2.2 Optimization of Exosomes Isolation Protocol 81
5.2.3 Characterization of MLO-Y4-derived Exosomes 86
5.2.4 Effects of MLO-Y4 cells-derived Exosomes on Bone Marrow Monocytes 91
5.3 Discussion and Conclusion 93

CHAPTER SIX - OVERVIEW OF THESIS

6.1 General Discussion 99

6.2 Future Directions 104

CHAPTER SEVEN – REFERENCES

7.1 References 107

ABBREVIATIONS

A	Ampere
bp	Base pairs
BSA	Bovine Serum Albumin
cDNA	Complementary deoxyribonucleic acid
CO_2	Carbon dioxide
ddH_2O	Double distilled Water
Dex	Dexamethasone
DMEM	Dulbecco's Modification of Eagle Medium
DMSO	Dimethyl sulphoxide
DNA	Deoxyribonucleic acid
dNTP	Deoxyribonucleotide triphosphate
EDTA	Ethylenediaminetetracetic acid
ECM	Exosomes conditioned media
Exo	Exosomes
FBS	Fetal bovine serum
FCS	Fetal calf serum
GC	Glucocorticoid
kDa	Kilodaltons
L	Litre
LCS	Lacunar-canalicular system
mL	Millilitre
MQ ddH_2O	MilliQue double distilled water
MKP1	Mitogen-activated protein kinase phosphatase-1
PBS	Phosphate Buffered Saline

PCR	Polymerase Chain Reaction
PMSF	Phenylmethylsulfonyl fluoride
RANK	Receptor Activator of NF-Kb
RANKL	Receptor Activator of NF-Kb Ligand
Redd1	Regulated in development and DNA damage responses 1
rpm	Revolutions per minute
RT	Reverse Transcriptase
RT-PCR	Reverse transcriptase polymerase chain reaction
S	Conditioned media supplemented with serum
SDS	Sodium dodecyl sulphate
SDS-PAGE	SDS-Polyacrylamide Gel
SF	Serum-free
TAE	Tris-acetate EDTA
TBS	Tris buffered saline
TCP	Total cellular protein
TEMED	N, N, N', N'-tetra-methyl-ethylenediamine
V	Volts
µg	Microgram
µL	Microlitre

LIST OF FIGURES

		Page
Chapter 1		
Figure 1.1	**Osteocyte image by scanning electron microscopy**	4
Figure 1.2	**Upstream regulators of mTORC1**	12
Figure 1.3	**Proposed model of the signaling cascade for GC-induced autophagy**	14
Figure 1.4	**Simplified model of exosome biogenesis and release**	15
Figure 1.5	**Mechanisms of action of released exosomes**	17
Chapter 3		
Figure 3.1	**Assembly of the Mini-PROTEAN 3 Cell Electrophoresis System**	39
Figure 3.2	**Flow chart for the exosome purification procedure based on differential ultracentrifugation**	42
Figure 3.3	**Quantitative real-time qPCR plate layout**	49
Figure 3.4	**pCMV6-AC-GFP vector map and multiple cloning sites**	50
Chapter 4		
Figure 4.1	**Dexamethasone-induced autophagy in MLO-Y4 osteocyte-like cells**	56
Figure 4.2	**Nuclear localization of glucocorticoid receptor (GR) in MLO-Y4 cells following Dex treatment**	58
Figure 4.3	**Semi-quantitative RT-PCR analysis of *mkp1* and *redd1* gene expression**	60
Figure 4.4	**Quantitative real-time qPCR analysis of *mkp1* gene expression (dose-dependent Effect)**	61
Figure 4.5	**Quantitative real-time qPCR analysis of *mkp1* gene expression (dose- and time-dependent effect)**	62
Figure 4.6	**Quantitative real-time qPCR analysis of *redd1* gene**	63
Figure 4.7	**Immunoblot analysis of REDD1 protein expression following Dex treatment**	65
Figure 4.8	**Immunoblot analysis of MKP1 protein expression**	66

	following Dex treatment	
Figure 4.9	**Confirmation of Redd1-GFP transfection into MLO-Y4**	68
Figure 4.10	**Immunoblot analysis of the effect of REDD1-GFP overexpression on mTORC1 signaling cascade**	69
Figure 4.11	**Raw densitometric quantitation of protein expression following REDD1 overexpression**	70
Figure 4.12	**Normalized densitometric quantitation of protein expression following REDD1 overexpression**	71
Figure 4.13	**REDD1 silencing attenuates GC (Dex)-induced autophagy**	74
Chapter 5		
Figure 5.1	**Dex-induced retraction of MLO-Y4 cell dendritic processes**	82
Figure 5.2	**Immunoblot analysis of isolated MLO-Y4 exosomes in the presence and absence of serum**	84
Figure 5.3	**Immunoblot analysis of 2nd and 3rd batches of isolated exosomes from MLO-Y4 cells cultured under serum-free conditions**	85
Figure 5.4	**Exosome secretion by MLO-Y4 cells is markedly reduced following Dex treatment**	**87**
Figure 5.5	**MLO-Y4 cells-derived exosomes expresses sclerostin, cathepsin K and V-ATPases**	90
Figure 5.6	**Effect of MLO-Y4 cells-derived exosomes on osteoclast precursors, bone marrow monocytes**	92

CHAPTER ONE

LITERATURE REVIEW

1.1 Introduction

Bone the basic element of the skeletal system, is a porous mineralized structure made up of cells, blood vessels, extracellular matrix (largely mineralized) and collagen (Hadjidakis and Androulakis 2006). Bone plays an essential role in the human body, providing support, bearing body weight, protecting vital organs, supporting mechanical movement, serves as reservoir for the formation of hematopoietic cells, and importantly maintains calcium, phosphate and iron homeostasis (Hadjidakis and Androulakis 2006). Moreover, bone is a highly dynamic tissue undergoing constant remodeling. Bone remodeling is a complex process that results from the action of bone forming osteoblasts and bone resorbing osteoclasts. The activity of the osteoblasts and osteoclasts are co-ordinately orchestrated by the bone-embedded osteocyte. During normal homeostasis, a balance between osteoblastic bone formation and osteoclastic bone resorption is precisely maintained (Heino *et al*. 2002; Hadjudakis and Androulakis 2006). Perturbations of this balance leading to excessive osteoclastic bone resorption results in debilitating osteolytic bone diseases such as osteoporosis. Osteoporosis is characterised by a systemic impairment of bone mass and microarchitecture resulting in fragility fractures (Rachner, Khosla and Hofbauer 2011).

Glucocorticoids (GCs) are extensively used for the treatment of chronic inflammatory and autoimmune diseases. However, prolonged use of GC results in reduction of bone mineral density (BMD) and increased risk of bone fragility (Weinstein 2012). GC-induced osteoporosis is the third leading form of osteoporosis and the most common cause of drug-related osteoporosis in the last decade (Weinstein 2001). Histomorphometric analyses of patients with GC-induced osteoporosis consistently showed fewer osteoblasts and increased prevalence of osteocyte apoptosis, as compared with normal controls (Canalis *et al.* 2007; Weinstein *et al*. 1998; O`Brien *et al*. 2004). Furthermore, GCs have been shown to directly reduce new osteoclast formation, prolong the lifespan of already formed osteoclasts, and decrease osteoblast survival. Therefore, with long-term GC therapy, the number of osteoclasts is maintained in the normal range, whereas the number of osteoblasts is dramatically reduced with concomitant decrease in bone formation (Weinstein *et al.* 1998).

Interestingly, more recent studies have demonstrated that low dose GC treatment (1.4 mg/kg/d for 28 days) results in the induction of autophagy (self catabolism) in osteocytes both *in vitro* and *in vivo* (Jia *et al.* 2011). Similarly, Xia and colleagues

(2010) have also reported that GC treatment induced the development of autophagy in a murine osteocyte-like cell line, MLO-Y4 (Xia *et al.* 2010). Similar induction of autophagy was also observed in primary osteocytes from mice that received prednisolone (synthetic GC) treatment (Xia *et al.* 2010). Inhibition of autophagy reversed the protective effects of GC (Xia *et al.* 2010). These observations offer novel insights into the possibility that osteocytic autophagy may serve as an initial major self-protective mechanism to guard against metabolic stress conditions induced by GC treatment. However, higher and persistent stress as observed in long-term or high dose GC treatment may overwhelm the self-protective autophagic mechanism leading to cell death and consequently, a reduction in bone strength and elevated bone loss. Thus, autophagy may provide a promising new target in the prevention of GC-induced bone fragility however, further investigation into the detailed molecular mechanism that regulates the development and progression of autophagy in osteocytes in response to GC treatment is required.

1.2 The Osteocyte

The osteocyte is the most abundant cell in the bone tissue, ranging from 20,000 to 80,000 osteocytes/mm^2 of bone, a number twenty times higher than osteoblasts (Rochefort *et al*. 2010). Osteocytes are terminally-differentiated cells descended from osteoblasts (Bonewald 2011). During the differentiation process, osteoblasts undergo structural and ultra-structural modifications leading to loss of some organelles and gain of long cell projections, which are responsible for keeping osteocytes in contact with other cells on the bone surface and with other osteocytes (Aarden *et al*. 1994).

Osteocyte differentiation was first thought to be a passive process, in which 10 to 20% of active osteoblasts were buried within the bone matrix, by a neighbouring osteoblast. However, the dramatic cellular changes that happen during entombment suggests that osteocyte differentiation is actually an active process (Bonewald 2011; Rochefort *et al*. 2010). Newly formed osteocytes keep several ultra-structural features of osteoblasts. They retain characteristics of a highly protein-synthesizing cell, with abundant Golgi complex and rich and well-structured granular endoplasmic reticulum. Furthermore, these osteocytes continue to produce osteoblastic factors, such as osteocalcin, which are typically produced by late osteoblasts (Bonewald 2011). On the other hand, osteocytes located far from the active bone-forming zone, have sparse

granular endoplasmic reticulum and a smaller Golgi region. However, despite their "inactive" appearance, mature osteocytes are involved in several biological processes, including signal transdution, mechanosensoring and mineral homeostasis (Zhao *et al*. 2000).

As soon as the osteoblast is "buried" within the bone matrix, it is called an osteoid osteocyte. One of the first morphologic changes that occurs during osteocyte differentiation is the formation of dendritic processes. These cellular projections allow the osteocyte to communicate with the vascular space, bone surface and other bone cells (Bonewald 2011). During osteocyte differentiation, expression of some osteoblast protein markers, such as alkaline phosphatase (ALP), type I collagen (Col1), bone morphogenetic protein 2 (BMP-2), osteoblast specific factor 2 (OSF-2, also known as periostin), Cbfa1, Osterix, casein kinase II, bone sialoprotein and Runx2 are downregulated, representing the transition towards an osteocytic phenotype (Bonewald 2011; Mullen *et al*. 2013; Rochefort *et al*. 2010). On the other hand, the expression of E11/gp38, the first osteocyte-selective protein to be expressed when osteoblast initiates differentiation, is upregulated and localized along the dendritic processes and on the cell surface and, together with MT1-MMP, plays an important role in controlling osteocyte morphology (Zhang *et al*. 2006; Zhao *et al*. 2000). As the differentiating osteocyte begins to extend its dendritic processes and mineralize its surrounding matrix (mineralizing osteocyte), additional marker are expressed, such as dentin matrix protein-1 (DMP-1), and CapG. At the latest stage, the mature osteocyte expresses Sclerostin, FGF23 and ORP150. (Bonewald 2011, Mullen *et al*. 2013).

1.3 Osteocyte Morphology

The final differentiated osteocyte is a spindle-shaped, flattened cell, with about 50 cytoplasmic processes radiating from the cell body (Fig. 1) (Sugawara *et al*. 2005). The cellular morphology is variable depending on the bone type in which it is embedded. Osteocytes found into trabecular bone are more rounded, while those ones found into cortical bone adopt a more elongated shape. The percentage of the total cell surface occupied by the dendritic processes ranges up to 52%. In addition, the total length of all cytoplasmic processes together (1 mm) is 100 times bigger than the average osteocyte length (10 to 15 μm) (Sugawara *et al*. 2005).

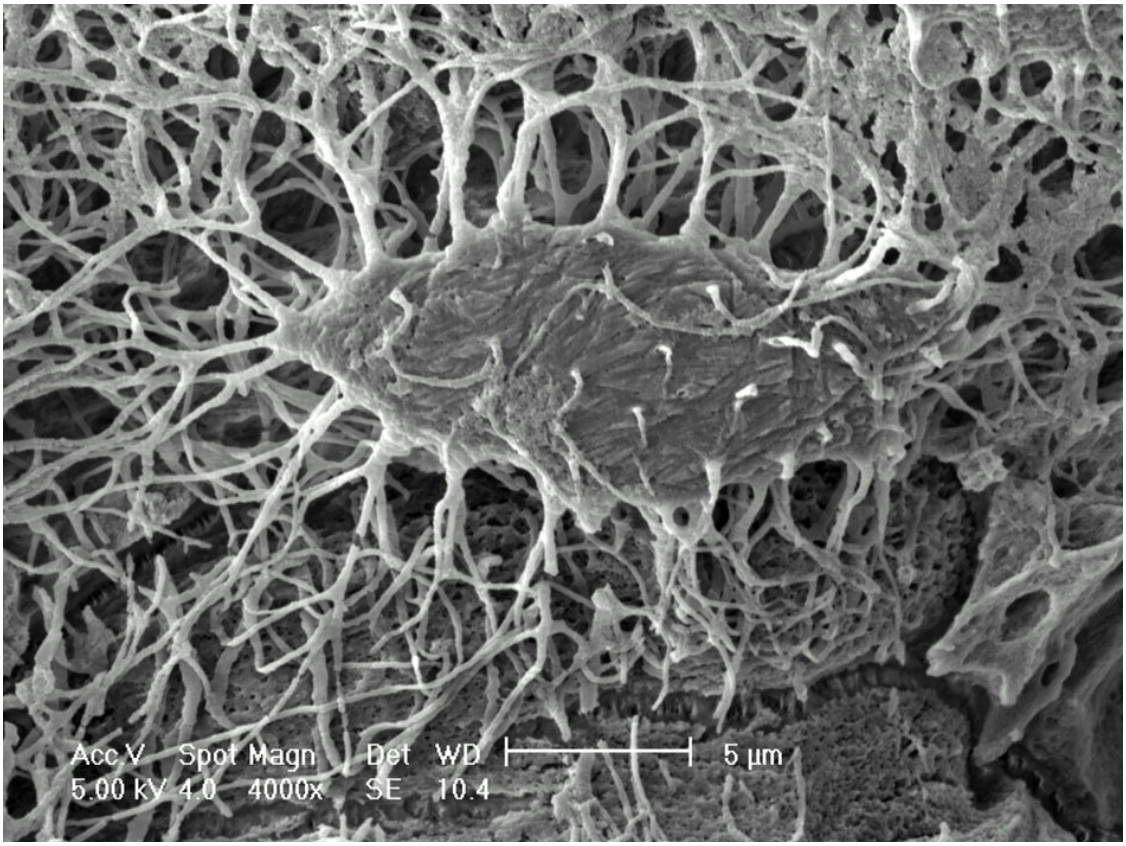

Figure 1.1. Osteocyte Image by Scanning Electron Microscopy (Image taken from Pajevic, 2009). The bone-embedded osteocyte is a spindle-shaped cell with multiple cytoplasmic projections/dendrites radiating from the cell body. On average, the surface area occupied by the dendritic processes is higher than the cell body. These dendritic processes significantly increase the cell surface area in contact with bone matrix and plays essential role in osteocytic mechanosensory function as well as a means of intercellular communication with neighbouring osteocytes and cells on the bone surface.

Osteocyte dendritic processes, which are rich in actin filaments, occupy the large and complex intercellular network of canaliculi in the bone matrix. They are essential for maintaining osteocytic function and bone homeostasis. In this complex canalicular network, each osteocyte occupies a lacunae within the bone matrix from which radiates dendritic process which connects the osteocyte with neighbouring osteocytes, periosteal and endosteal lining cells, bone marrow cells and osteoclasts (Sheng *et al*. 2014). This interconnected network provides the osteocytes with fluids and nutrients essential for maintaining metabolic exchange and nutrition. Furthermore, these canaliculi allows soluble signalling molecules, released by osteocytes, to diffuse to blood vessels and other bone cells fostering intercellular communications (Sheng *et al*. 2014). Thus, osteocyte occupies a privileged place in bone, as it is in contact with a huge bone surface area and is highly interconnected to several cells.

1.4 Osteocyte Function

Osteocytes function in several important biological processes, including phosphate regulation, vitamin D metabolism, response to mechanical strain, and regulation of bone turnover and bone fracture repair (Zhao *et al*. 2002; Heino *et al*. 2002; Bouillon and Suda 2014; Jing *et al*. 2014). Moreover, osteocytes can act as an endocrine organ, secreting soluble factors, such as fibroblast growth factors (FGF) and insulin-like growth factors (IGF), which can modulate other organs functions (e.g. kidney) and even determine internal organs size during development (Sheng et al. 2014).

1.4.1 Osteocyte: A Mechanosensory Cell

One of the most well established osteocytic functions is that of mechanoreception/transduction. It has been shown that the osteocytic dendritic processes acquired during differentiation, are more mechanosensitive than the cell body, and thus serve as the major site of signal transduction, from mechanical to biochemical signals (Adachi *et al*. 2009). How the osteocytes sense the mechanical load on bone and coordinate adaptive alterations in bone mass and architecture is not yet completely understood. However, it is widely accepted that mechanical load placed on bones drive the flow of interstitial fluid through the lacunar-canalicular system (LCS) to the pericellular matrix surrounding osteocytes (Weinbaum *et al.* 1994; Piekarski and Munro 1997). Apparently, several events, acting simultaneously, can trigger mechanosensation

and transduction, including cell deformations in response to strain and shear stress along the cell body, ciliar structures or dendritic processes (Bonewald 2006). This flow or sheer force activate the osteocytes via as yet unknown mechanism, producing signaling molecules that orchestrate the activities of effector cells (Nakashima *et al.* 2011, Xiong *et al.* 2011), namely the osteoclasts and the osteoblasts, to maintain healthy bone structure and homeostasis (Huiskes et al. 2000).

1.4.2 Osteocyte: Orchestrator of Osteoclastic and Osteoblastic Functions and Phosphate Metabolism

The osteocyte plays a crucial role in maintaining healthy bone turnover through the release of several soluble molecules, signaling factors and cytokines that regulate osteoclastic and osteoblastic differentiation and function. Recent data have demonstrated that osteocyte-produced endocrine factors that play a vital role in the regulation of phosphate homeostasis.

1.4.2.1 Receptor Activator of Nuclear Factor-kappa B Ligand (RANKL)

RANKL is a membrane-bound factor expressed by several cell types (osteocytes, osteoblasts, T-cells and bone marrow cells). Osteocytes produce almost all RANKL secreted in bone matrix (Nakashima *et al*. 2011; Xiong *et al.*, 2011) and this cytokine is widely known as the most important regulator of osteoclast differentiation and, consequently, bone resorption. The crucial role of this cytokine in osteoclastogenesis was demonstrated by Sobacci and colleagues (2007) who showed that mutation in the gene encoding RANKL leads to autosomal recessive osteopetrosis, due to the lack of osteoclasts. Being an important activator of osteoclast formation and bone resorption, a specific antibody against RANKL (Denosumab) has been developed for the treatment of osteolytic diseases characterized by excessive osteoclast activity.

1.4.2.2 Sclerostin (SOST)

Sclerostin is a glycoprotein, encoded by the gene SOST, secreted exclusively by osteocytes. It plays crucial role in reducing bone formation by inhibiting the differentiation of osteoblastic precursor cells (Winkler *et al*. 2003; Li *et al*. 2008). The importance of sclerostin on bone homeostasis is evidenced by a rare genetic disease, Scleroteosis, caused by an inactivating mutation in gene SOST. This disorder is characterized by a highly increased bone mass, progressive bone overgrowth and

gigantism (Winkler et al. 2003). Similarly loss of function or gain of function of sclerostin in mouse models results in increased and decreased bone mass respectively (Babij *et al.* 2003). Because of its profound role in regulating bone mass, monoclonal antibodies directed against sclerostin have been developed as potential anabolic therapeutics for osteoporosis.

1.4.2.3 Fibroblast Growth Factor 23 (FGF23)

Fibroblast Growth Factor 23 is an important regulator of phosphorus homeostasis expressed in several tissues, such as kidney medulla, liver, thyroid, kidney cortex and in bone (Mirams *et al.* 2004). In bone, this 32kDa peptide is predominantly expressed by osteocytes and secreted in response to blood phosphate availability (Riminucci et al. 2003). Since its discovery, FGF23 remains one of the most important endocrine factors secreted by osteocytes. Elevations in phosphate serum concentrations, increase FGF23 levels and the opposite effect occurs when phosphate availability is low. One of the most important targets of FGF23 is the kidney, with signalling between the bone and kidney being vital for the maintenance of serum phosphate levels. FGF23 downregulates the expression of the NaPi-IIa and NaPi-IIc sodium phosphate cotransporters in the kidney both of which are required for renal phosphate reabsorption (Gattineni et al. 2009, Larsson et al. 2004). This leads to increased urinary excretion of phosphate. The crucial role of FGF23 in phosphate homeostasis is evidenced by the occurrence of high levels of FGF23 in individuals with tumor-induced rickets/osteomalacia, a disease characterized by increased urinary phosphate excretion, low serum phosphate and, consequently, imbalance in bone metabolism. In these patients, FGF23 level in the plasma can be 24 times higher than in healthy individuals (Yamazaki et al. 2002). Similarly, transgenic mice overexpressing FGF23 demonstrate growth retardation, osteomalacia, and impaired phosphate homeostasis (Larsson et al. 2004)

1.5 Autophagy: A crucial mechanism for bone maintenance

Autophagy is a term derived from greek roots "auto" (self) and "phage" (eating). It is a catabolic cellular process characterized by degradation of cellular components and organelles via the lysosome degradation system. It is a fundamental process for recycling of cellular products and is a major cell adaptive mechanism for self-preservation, against intrinsic cellular damage during unfavourable and stressful

conditions. However, this process is a 'double-edged sword' that can also lead to self-destruction, destroying cellular components leading to autophagy-induced cell death (ACD). Thus, eukaryotic cells have developed a regulatory mechanism through which autophagy induction is tightly coupled to the regulation of cell growth. Osteocytes, being extremely long-lived cells (up to decades) as well as being isolated and entombed in bone, are highly susceptible to changes in chemical and mechanical signals within the bone microenvironment and thus autophagy serves as an important process for cellular maintenance (Rubinsztein *et al.* 2011).

Osteocyte autophagy has been demonstrated to be crucial for skeletal maintenance. Suppression of autophagy by deletion of autophagy gene Atg7, in osteocytes, results in bone mass loss, increase in cortical porosity and decrease in spongy bone volume and cortical thickness. These changes are typically observed in skeletal aging (Onal *et al*. 2013). Similarly, recent *in vitro* and *in vivo* studies have also shown that GC upregulates autophagy in osteocytes (Jia *et al.* 2011, Xia et al. 2010). The induction of osteocyte autophagy by GC can be considered an adaptive response to chemical stress. While these studies were among the first to directly implicate osteocyte autophagy in skeletal maintenance, the precise molecular mechanism(s) regulating osteocyte autophagy remains unclear.

1.5.1 Autophagy Machinery

Autophagy is characterized by several ultra-structural phenomena and a complex signalling cascade that can be divided into four key stages: initiation, elongation, maturation and fusion with the lysosome (Ravikumar *et al*. 2010). The whole process of formation of autophagosomes requires a group of proteins called autophagy proteins (ATG). In its simplest form, upon autophagy induction, an early autophagic structure called the isolation membrane (IM) is formed around the material that is to be recycled/degraded. This membrane structure is the precursor of autophagosome. After formation, the IM grows and curves around engulfing a portion of cytoplasmic contents, eventually each membrane edges are sealed together, forming a double membrane vesicle, called an autophagosome (Juhasz and Neufeld 2006). The membrane source of IM and autophagosome is a long-standing question that remains elusive and a topic of debate (Axe *et al.* 2008).

After initiation and elongation, the fully formed autophagosome starts moving along microtubules, preferentially towards the microtubule organization centre (MTOC), where it finally fuses to a lysosome. After autophagosome and lysosome fusion, this newly formed membrane structure is called autophagolysosome or autolysosome (Ravikumar *et al*. 2010). As autophagy depends on the microtubule network, depolymerization of microtubules or inhibition of polymerization results in defective autophagy (Kochl *et al.* 2006). In addition to an intact microtubule network, normal lysosomal function is indispensable for autophagosome and lysosome fusion. Inhibition of the lysosomal V-ATPases, proton pumps that are responsible for acidifying the lysosomal vesicles, significantly decreases autophagosome fusion with lysosome (Yamamoto *et al*. 1998).

1.5.2 Autophagy Signaling Cascade

In the past decade, many second messengers and signalling cascades have been shown to regulate autophagy in mammalian cells (Esclatine *et al*. 2009). Among these, TOR (target of rapamycin) complexes are considered the master regulators and key components that coordinately regulate the balance between growth and autophagy in response to physiological conditions and environmental stress (Ravikumar *et al*. 2010). Despite the significant progress in the field of autophagy, the mechanism by which TOR regulates autophagy remains to be fully understood (Jung *et al.* 2010). The activity of TOR is inhibited under nutrient starvation, a crucial step for the induction of autophagy in eukaryotic cells (Noda and Oshumi 1998; Scott, Schuldiner and Neufeld 2004). TOR was first described in the early 90s as a target for the anti-fungal and immunosuppressant agent, rapamycin (Heitman. Movva and Hall 1991). In yeast, TOR activity is regulated by the availability of nutrients such as nitrogen and carbon (Wullschleger, Loewith and Hall 2006). Similarly, mammalian TOR (mTOR) activity is regulated by amino acid and glucose levels (Inoki, Zhu and Guan 2003). Inhibition of mTOR by rapamycin results in the induction of autophagy to reduce protein synthesis and enhance the clearance of accumulated intracellular proteins aggregates (King *et al.* 2008, Wyttenbach *et al*. 2008). In mammalian cells, mTOR is the catalytic subunit of two molecular complexes, mTORC1 (mTOR complex1) and mTORC2 (mTOR complex 2) (Hara *et al.* 2002; Kim et al. 2002; Sarbassov et al. 2004). Although these complexes share some components, the downstream substrates phosphorylated by these

complexes are different and consequently, play different roles in autophagy (Loewith *et al*. 2002).

1.5.2.1 mTORC1

Rapamycin sensitive mTORC1 consists of 5 distinct proteins: mTOR the serine/threonine protein, that belongs to the phosphatidylinositol kinase-related kinase (PIKK) family, GβL/mLST8 (mammalian lethal with Sec13 protein 8), raptor (regulatory associated protein of mTOR), proline-rich PKB/Akt substrate 40-kDa (PRAS40) and DEPTOR (Esclatine *et al*. 2009; Jung *et al*. 2010). The activity of mTORC1 is regulated by many factors and molecules, including growth factors such as insulin, nutrients, energy availability and cell stressors, such as osmotic stress, hypoxia, viral infections and reactive oxygen species (Corradetti et al. 2006) (Fig. 2). The predominant signalling pathway activating mTORC1 include Akt/PKB, MAPK/ERK, and Wnt pathways. Activated mTORC1 is a major inhibitor of autophagy in part by preventing the interaction between autophagy related protein 13 (Atg13) with the ULK1 kinase complex thus preventing initiation and formation of the IM (Alers *et al.* 2002; Pyo *et al.* 2012). This complex modulates autophagy in a nutrient, energy and stress-dependent way, acting as a sensor (Pyo *et al*. 2012). However, the complete molecular mechanism remains to be fully unraveled. Paradoxically, mTORC1 also activates cell growth and protein synthesis, through phosphorylation of many translational machinery components and regulation of ribosome biogenesis and mRNA translation (Mayer *et al.* 2006; Proud 2007). Because mTORC1 can inhibit autophagy and at the same time activate protein synthesis and cell growth, mTORC1 activation can lead to accumulation of damage proteins and organelles, contributing to damage at the cellular level and ultimately can lead to cell death (Proud 2007).

Animal models with targeted inhibition of mTORC1 by rapamycin have shown to decrease the incidence of age-related diseases, such as cancer, motor dysfunction, immune disruption, insulin resistance and weight gain, prolonging the viability of mice (Anisimov et al, 2010; Harrison et al. 2009). In keeping with these findings, global deletion of the mTORC1 effector protein, ribosomal protein S6 kinase 1 (S6K1) has been shown to extend the lifespan of aged mice (up to 20%) and protect against the age-dependent loss of cancellous bone (Piekarski and Munro 1997), thus highlighting the importance of mTORC-signaling in skeletal ageing.

1.5.2.2 mTORC2

Distinguished from its related signalling complex mTORC1, the rapamycin-insensitive mTORC2 also consists of 5 proteins: mTOR, mLST8, rictor (rapamycin-insensitive companion of mTOR), mammalian stress-activated protein kinase-interacting protein 1 (mSin1) and Protor (protein associated with rictor) (Esclatine *et al*. 2009; Jung *et al*. 2010). In comparison to mTORC1, much less is known about the function and regulation of mTORC2 and its activity is largely insensitive to nutrients or energy conditions (Alessi *et al*. 2009). However, mTORC2 has been shown to serve as a regulator of actin cytoskeletal organization (Corradetti et al. 2006) (Jacinto *et al*. 2004) (Nakashima *et al*. 2011, Xiong et al. 2011). The stability and integrity of the mTORC2 complex is dependent on the presence of rictor, which functions as a scaffold protein for substrate binding to mTORC2 (Nakashima *et al.* 2011). The activity of rictor is controlled by phosphatidylinositol 3-kinase (PI3K). mTORC2 functions as the elusive phosphoinositide-dependent kinase (PDK) that phosphorylate Akt and is required for full Akt activation (Tatsumi *et al.* 2007; Cowin *et al.* 1991; Huiskes *et al.* 2000). The mTORC2-Akt pathway is considered an upstream activator of mTORC1, but its role in autophagy is not well understood.

Current evidence suggests that mTORC2 confers both inhibitory and activating roles during autophagy via two complex crosstalk mechanisms: (i) the mTORC2-Akt activation of mTORC1 and (ii) the mTORC2-Akt inhibition of FoxO, forkhead O family proteins (Tatsumi *et al.* 2007, Winkler *et al*. 2003). The FoxO family of transcription factors activates transcription of autophagy related genes including LC3 (Tatsumi *et al.* 2007; Winkler *et al*. 2003). Recent studies have shown, at least in HeLa cells, a negative feedback regulatory mechanism, in which mTORC1 stimulation inactivates mTORC2 through the inhibitory phosphorylation of the mTORC2 component rictor and Sin1 (Julien *et al*. 2010; Poole *et al.* 2005; Li *et al.* 2005) (Fig. 3). Thus mTORC2 may exhibit dual functionality by regulating the cytoskeleton, and as an upstream regulator of mTORC1 along the Akt/PKB pathway, or function independently in autophagy via AKT/Foxo3 pathway.

Although it is widely accepted that the mTORC complexes regulate autophagy, how GC regulate mTORC signalling and autophagy has yet to be established. We have identified two potential GC responsive proteins that function upstream of mTORC1

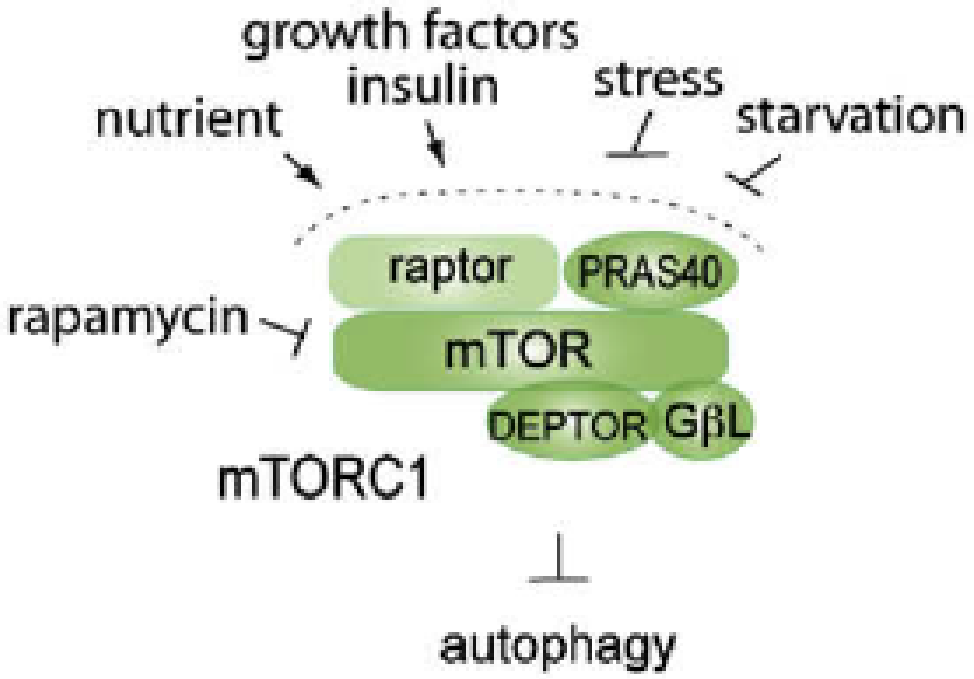

Figure 1.2. Upstream Regulators of mTORC1 (Image taken from Jung et al., 2010). The rapamycin sensitive complex of TOR, mTORC1, consists of 5 distinct proteins: mTOR the serine/threonine protein that belongs to the phosphatidylinositol kinase-related kinase (PIKK) family, GβL/mLST8 (mammalian lethal with Sec13 protein 8), raptor (regulatory associated protein of mTOR), proline-rich PKB/Akt substrate 40-kDa (PRAS40) and DEPTOR. Being a major negative regulator of autophagy, mTORC1 is modulated by a complex combination of factors and molecules, including growth factors, insulin, nutrient and amino acids which activates its activity and thus inhibit autophagy. Conversely, stress and starvation conditions, as well as inhibitors such as rapamycin inhibit mTORC1 and initiate the autophagic program.

signaling and thus may participate in GC-induced autophagy. These genes and the encoded proteins are mitogen-activated protein kinase phosphatase-1 (MKP1) and regulated in development and DNA damage responses-1 (REDD1) (Figure. 1.3).

1.6 Intercellular Communication – The Role of Exosomes

Being entombed in the bone matrix for its entire lifespan, it has been recognised that osteocytes communicate via their dendritic process. However, how osteocytes can exert regulatory influences beyond the boundaries of the bone such as in phosphate metabolism remains to be investigated. An alternative form of communication that could be utilized by osteocytes for intercellular communication is via the release of extracellular microvesicles or exosomes (50-100nm) into the local microenvironment and circulation (Kamioka *et al*. 2001). Secreted exosomes could enable osteocytes to interact with and influence other cellular bodies beyond the bone by exchanging bioactive material and information in the form of proteins, membrane receptors, microRNA, messenger RNA, carbohydrates and even organelles (e.g., mitochondria) (Ratajczak *et al*. 2006; De Maio *et al*. 2011). Exosomes have been shown to play a role in areas such as immune response, tumour microenvironment, and stem cell biology, but have never been described in osteocytes. Interesingly, it has been reported that autophagy and exosome production share a common pathway and that an inverse relationship exists between the two processes (Fader and Colombo, 2008; Fader *et al*., 2008; Simons and Raposo, 2009; Baixauli *et al*., 2014). However, the effects of GC-induced autophagy on osteocytic exosome release have yet to be investigated.

Exosome production and secretion is mediated by a complex intracellular pathway highly integrated with endosome formation and maturation. Exosomes are characterized in their biogenesis by formation of intraluminal vesicles (ILVs), through the inward budding of endosomes to form multvesicular bodies (MVB) or multivesicular endosome (MVE) (Buschow *et al*. 2005; Raposo and Stoorvogel, 2013). Endosomes are first formed by inward budding of the cell membrane by endocytosis which leads to the inversion of the lipid membrane (Figure 1.4A). In this process some extracellular material is engulfed into the intraluminal side of the endosome. A second inward budding of the endosomal membrane results in a positive orientation of the ILVs lipid membrane and similarly, entrapment of a volume of the cell's cytoplasm and

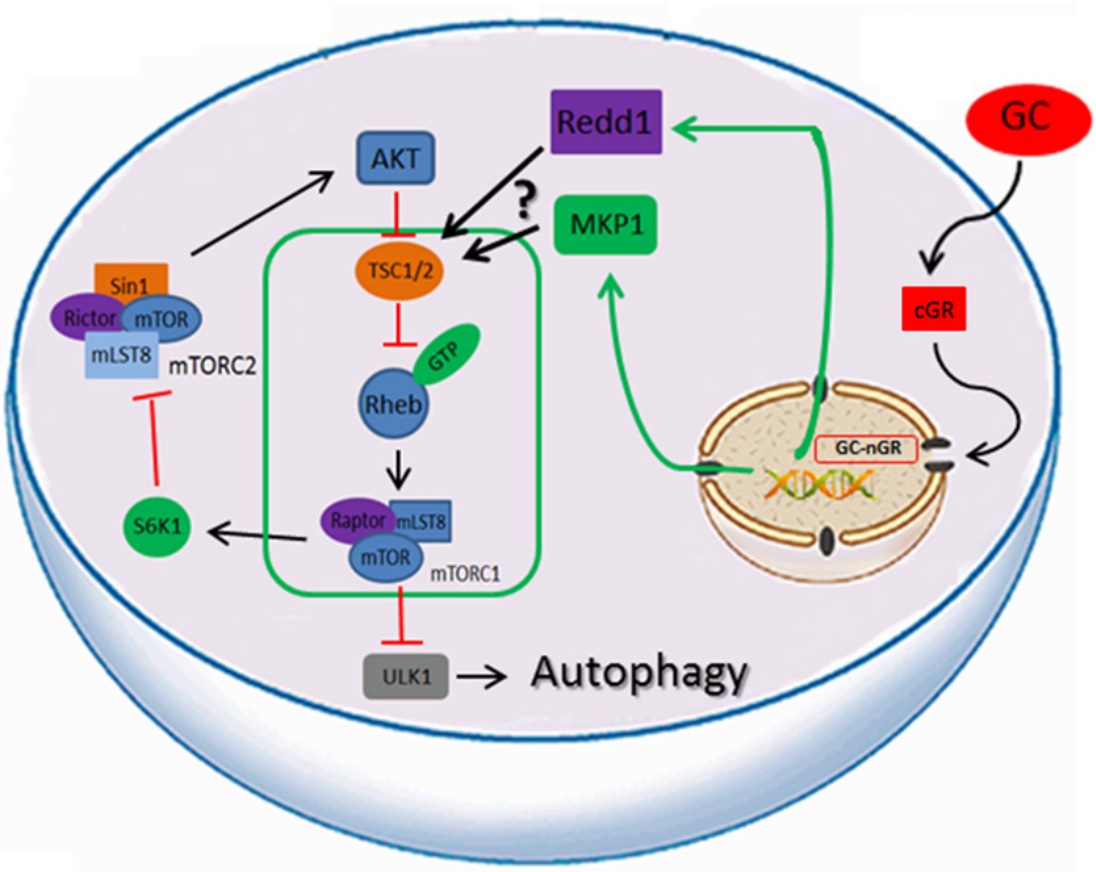

Figure 1.3. Proposed Model of the Signalling Cascade for GC-induced autophagy. Binding of glucocorticoids (GC) to their inactive cytoplasmic receptor, the Glucocorticoid receptor (cGR), causes receptor activation and shuttling into the nucleus. The activated GC-nGR complex binds to GC responsive elements on DNA initiating the transcription and expression of GC-induced genes. Two potential GC responsive genes, REDD1 and MKP1, will be investigated for their effect on the mTORC signalling pathway to activate autophagy.

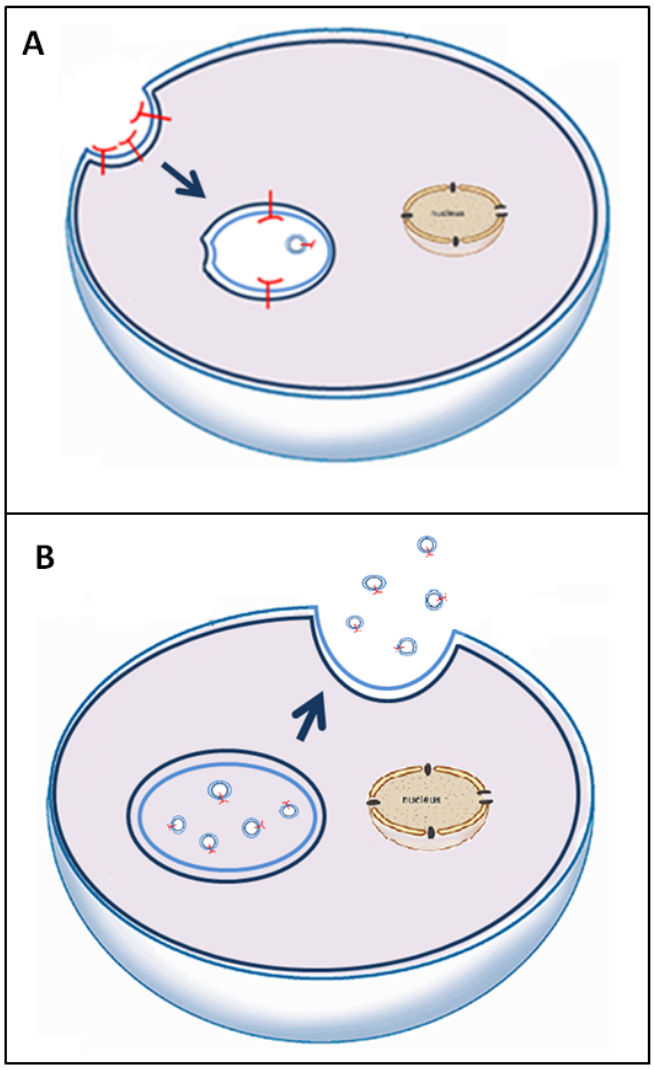

Figure 1.4. Simplified Model of Exosome Biogenesis and Release. **A.** Exosome biogenesis and release is mediated by a complex pathway integrating with the endosomal machinery. The multivesicular body (MVB) is the endosomal compartment that houses the exosomes. The formation of the MVB involves firstly, the inward budding of the cells plasma membrane forming an early endosome. This inward budding of the plasma membrane result in the inversion of the lipid structure as well as engulfment of some extracellular material. Following the formation of the endosome, a second inward budding of the endosomal membrane occurs leading to the formation of intraluminal vesicles (ILVs) within the endosomal vesicle and this compartment is termed the MVB. This second inward budding corrects the orientation of the lipid structure of the ILVs and entrapment of some of the cells cytoplasmic content. **B.** The matured MVB containing ILVs can subsequently merge via vesicular trafficking events, with the cell membrane, releasing the ILVs into the extracellular space or circulation. The released ILVs are termed exosomes. As a result of how the exosomes are formed, they can contain contents of cytoplasmic nature including cytosolic proteins, RNAs, miRNAs, and organelles, as well as expressing specific transmembrane proteins and receptors found on the cell they were derived from.

cytoplasmic contents, to form MVBs. It has been hypothesized that proteins could also be transported directly to endosomal membranes via chaperones such as Hsp70, following their synthesis, and then incorporated into ILV during the second inward budding process. The resulting MVBs can then fuse with the plasma membrane to release their cargo of ILVs (now termed exosomes) to the extracellular environment (Figure 1.4B).

Although the released exosomes have the same orientation as the cell membrane and may exhibit similar surface markers, ILV formation is an active process and thus, exosomal suface proteins are not a simple one-to-one representation of the surface markers from the cell of origin. As a consequence of their origin, exosomes contain a complex lipidic and protein composition. Some proteins are present in all exosomes such as endosome-associated proteins, some of which are involved in MVB biogenesis, and proteins that show cell-type specificity (Wendler *et al*. 2013). Some common exosomal markers used for the idenfication of isolated exosomes include tetraspanins such as CD81, CD9 and CD63, and heatshock proteins (HSP)-70.

After exosomes are released into the extracellular space, these microvesicles can communicate with target cells by various means. Exosomal membrane proteins can interact with cell surface protein receptors, leading to activation of the respective signaling response of the target cell (Figure 1.5A). Conversely, proteins on the exosomal membrane can also be cleaved by extracellular proteases and the resulting fragment can interact with a protein receptor in the cell surface, for example EGF ligand. Hence, the resulting cleaved fragment from the exosome acts as a ligand for the target cell receptor (Figure 1.5B). Another means of communication by exosomes is the direct fusion of exosomes with the target cell, resulting in the non-selective transfer of exosome constituents (proteins, RNA, lipids) to the target cell (Figure 1.5C). This transfer of exosomal contents can initiate a variety of cellular response which may or may not be beneficial to the target cell.

1.7 Autophagy and Exosome Biogenesis and Secretion - The convergence point

Besides fusing with the plasma membrane to release its contents as exosomes, MVBs can also be targeted to lysosomes for degradation. In contrast to the hypothesis that the autophagosomes directly merge to lysosomes, several studies have demonstrated a probable convergence between the autophagic and endosomal pathways

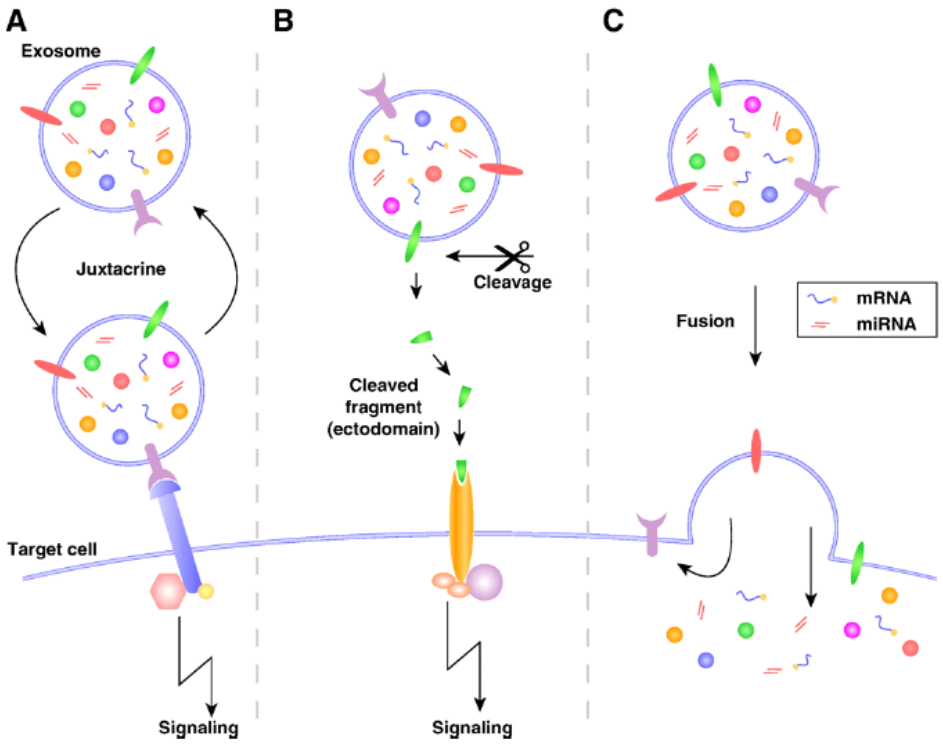

Figure 1.5. Mechanims of Action of Released Exosomes (Image taken from Mathivanan et al., 2010). After exosomes are released into extracellular space, they may interact with the target cell via 3 mechanisms. **A.** Exosomal membrane proteins can interact with specific protein receptors on the target cell surface resulting in the activation of the respective signalling response. **B.** Alternatively, proteins on the exosomal membrane can be cleaved by extracellular proteases and the resulting fragment can interact with a protein receptor on the target cell surface, for example EGF ligand. Hence, the resulting cleaved fragment from the exosome protein acts as a ligand for the target cell receptor. **C.** Exosomes can merge direcly with the target cell, resulting in a non-selective transfer of exosome constituents (proteins, RNA, lipids) into the target cell and subsequent activation/inhibition of downstream signalling cascades.

before the formation of autolysosomes (Gordon *et al.* 1988). It has been shown that autophagosomes may fuse with a late endosome or MVB leading to the formation of a prelysosomal compartment called amphisome. This is the point in which both the autophagic and endocytic pathways converge (Berg *et al.* 1998). In line with this, Fader and colleagues (2008) have shown that induction of autophagy increases the fusion of MVB with autophagosomes. Thus, during this process, the late endosome or MVB merge with the autophagosome, forming the amphisome, whose content is degraded after fusion with lysosome, in the autolysosome (Fader *et al.* 2009).

Although it is not completely understood what differentiates degradative from secretory MVB, it has been demonstrated that inducers of autophagy such as rapamycin and vinblastine increase fusion of MVBs with autophagosomes (Wendler *et al*. 2013; Fader *et al*. 2008). Furthermore it was reported that under conditions that favour autophagy, MVBs are diverted towards the lysosomal degradative pathways and consequently, significantly decrease the release of exosomes (Fader *et al.* 2008). The molecular mechanism and the proteins involved in regulating this switch from secretory MVB to degradative MVB have yet to be determined. Given that these processes will require some sort of trafficking rerouting, various trafficking proteins such as small Rab GTPases are likely to be involved (Villarroya-Beltri *et al.* 2014) and thus may serve as useful tools for investigating the interplay between autophagy and exosome release. Furthermore, it would be interesting to determine whether GC treatment which favours autophagy in osteocytes results in decrease osteocytic exosome release. Thus this study will also investigate the interplay between GC-induced osteocyte autophagy and osteocytic exosome release.

1.8 Summary

Osteoporosis is a common and serious complication of GC therapy, resulting in increased risk of fragility fractures (1). Increased osteocyte lacunar size with a loss of perilacunar mineral along with the osteocytic autophagy were observed during GC treatment, suggesting that the osteocytes are metabolically stressed or compromised (2). Additionally, we propose that osteocytes can release extracellular vesicles or exosomes as an alternative mechanism for intercellular communication. Interestingly, it has been shown that an inverse relationship exists between the autophagic and exosomal pathways. Thus it would be interesting to determine whether GC treatment which

favours autophagy in osteocytes results in decrease osteocytic exosome released. In addition to the molecular deciphering of the signalling events leading to GC-induced osteocyte autophagy, the potential interplay between autophagy and osteocyte exosome secretion will be the subject of investigation in this project.

CHAPTER TWO

RESEARCH PROPOSAL

2.1 Research Proposal

Osteoporosis is a common and serious complication of glucocorticoid (GC) characterised by a systemic impairment of bone mass and microarchitecture resulting in fragility fractures (Weinstein 2001, 2012). Increased osteocyte lacunar size with a loss of perilacunar mineral along with increased osteocytic autophagy have been observed during GC treatment, suggesting that the osteocyte is metabolically stressed or compromised (Canalis *et al.* 2007; Weinstein *et al*. 1998; O`Brien *et al*. 2004). Osteocytes are terminally differentiated from osteoblasts (OBs) that are entombed below the bone surface and maintain intercellular connections with adjacent OYs and the bone surface through dendritic processes that emanate from the cell bodies and extend through discrete canaliculi. The dendrite-housed canalicular system functions as a mechanosensory hub that enables osteocytes to sense and respond to mechanical damage and load by relaying signals to other bone cells required for bone repair and/or remodeling (Aarden *et al*. 1994, Sugawara *et al*. 2004).

Recent studies have demonstrated that GC treatment induces autophagy (self catabolism) in primary osteocytes and osteocytic cell-lines *in vitro* and *in vivo* (Xia et al., 2010; Jia et al. 2011). Osteocyte autophagy may represent a firstline adaptive self-preservation mechanism utilized by osteocytes to adapt to cellular and metabolic stress from agents such as GCs. Thus, osteocytic autophagy may provide a promising new target in the prevention of GC-induced bone fragility however, further investigation into the detailed molecular mechanism that regulates the development and progression of autophagy in osteocytes in response to GC treatment is required. The mTORC1 signaling cascade is a major suppressive pathway of autophagy and thus likely be involved in GC-induced autophagy.

Being eternally in the bone matrix, it has long been recognized that osteocytes communicate locally with their neighbouring osteocytes and cells on the bone surface via its dendritic process. However, how osteocytes exert regulatory influences beyond the boundaries of the bone such as in phosphate metabolism remains largely unknown. Exosome are small extracellular microvesicles secreted by various cells to functions as an alternative mechanism for intercellular communication. We propose that osteocytes secrete exosomes into the local microenvironment and circulation as an alternative form of communication to exert influence on other cellular bodies within the local environment of the bone and beyond. Interestingly, it has been shown that inducers of

autophagy, such as rapamycin and vinblastine, significantly decrease the release of exosomes (Fader et al. 2008; Wendler et al., 2013), demonstrating an intricate interplay between the processes of autophagy and exosome secretion.

2.2 Hypothesis

Therefore, we hypothesize that a fine counterbalance exists between the induction of autophagy and/or the release of exosomes from osteocytes which may account, in part, for the osteolytic complications accompanying GC therapy.

2.3 Aims

1) To investigate the molecular mechanism and signaling pathwy of GC-induced autophagy in MLO-Y4 osteocyte-like cells.

2) To isolate, characterise and profile of MLO-Y4 cells-derived exosomes.

3) To explore the interplay between GC-induced autophagy and exosome release.

It is anticipated that this research will provide further insights into the molecular mechanism regulating the development and progression of GC-induced autophagy in osteocytes and be the first to demonstrate that osteocytes secrete exosomes.

CHAPTER THREE

MATERIALS AND METHODS

3.1 Materials

3.1.1 Chemical Reagents

All experiments performed in this thesis used chemical reagents that were purchased from the following manufacturers:

Name	Supplier
30% Acrylamide/BIS	Sigma-Aldrich, USA
Agar Powder	Promega Corp, USA
Ammonium Persulfate (APS)	Bio-Rad Laboratories, USA
β-Mercaptoethanol	Sigma Chemical Co., St Louis, Mo., USA
Bovine Serum Albumin (BSA) Acetylated 10mg/ml	Sigma-Aldrich, USA
Bio-Rad Protein Assay Dye Reagent Concentrate	Bio-Rad Laboratories, USA
Dimethyl Sulphoxide (DMSO)	Merck, Germany
Ethanol (100%)	Sigma-Aldrich, USA
Ethylene Diamine Tetra-acetic Acid (EDTA)	BDH Laboratories, UK
Paraformaldehyde (PFA)	Merck, Germany
Phenylmethylsulfonyl fluoride (PMSF)	Boehringer Mannheim Corp., Indpl, IN., USA
Phosphate Buffered Saline (PBS)	Sigma-Aldrich, USA
1B 205 Ponceau 2R	Chroma-Gesellschaft Scmid GmbH & Co., Germany
Prolong® Gold Antifade Mounting Media	Life Technologies, USA
Protease Inhibitor	Roche, Germany
Skim milk powder	Diploma, Australia
Sodium Chloride (NaCl)	VWR International Ltd, UK

Sodium dodecyl sulphate (SDS)	Sigma-Aldrich, USA
Sodium Hydroxide (NaOH)	Sigma-Aldrich, USA
Sodium Hypochlorite (4%)	Brighton Professional™, Australia
Sodium Orthovanadate	Sigma-Aldrich, USA
TEMED (N, N, N', N' -tetra-methyl-ethylenediamine)	Bio-Rad Laboratories, Hercules, CA., USA
Tris-HCl	Sigma-Aldrich, USA
Triton-X-100	Pachard Instrument, USA
Tween-20 (molecular grade)	MP Biomedicals, USA

3.1.2 Molecular Products

Name	Supplier
5x MMLV-RT buffer	Promega Corp, USA
6x DNA blue loading dye	Promega Corp, USA
dATP, dTTP, dCTP, and dGTP nucleotides	Promega Corp, USA
DNase I	Sigma-Aldrich, USA
DNA Ladder 100bp (250µl)	Promega Corp., Madison, Wi., USA
DNA Ladder 1kb (250µl)	Promega Corp., Madison, Wi., USA
Moloney Murine Leukaemia Virus Reverse Transcriptase (MMLV-RT)	Promega Corp, USA
Oligo (dT) primer	Promega Corp, USA
Precision Plus Protein™ Standards	Bio-Rad Laboratories,USA
RNasin® RNAase inhibitor	Promega Corp, USA

3.1.3 Commercially Purchased Kits

Name	Supplier
2x GoTaq® Master Mix	Promega Corp, USA
AllPrep® RNA/Protein Kit (50)	QIAGEN Gmbh, Australia
Cyto-ID® Autophagy Detection Kit	Enzo Life Sciences, USA
Exo-Glow™ Exosome Labeling Kits	System Biosciences (SBI), USA
Exosome Antibodies & ELISA Kits	System Biosciences (SBI), USA
FavorPrep™ Blood/ Cultured Cell Total RNA Purification Mini Kit	Favorgen® Biotech Corp, USA
Lipofectamine® 3000 Transfection kit	Invitrogen, USA
Lipofectamine® LTX and PLUS™ Reagent	Invitrogen, USA
Taq DNA polymerase kit	QIAGEN Gmbh, Australia
TrueORF™ cDNA Clone and PrecisionShuttle™ Vector System	OriGene, USA
Western Lightning™ Ultra Sensitivity	Perkin-Elmer, USA
X-tremeGENE HP DNA Transfection Reagent	Roche Diagnostics GmbH, Germany

3.1.4 Oligonucleotide Primers

PCR and sequencing oligonucleotide primers were purchased from the GeneWorks. After receipt in freeze-dried form, the oligonucleotide primers were resuspended in suggested volumes of nuclease-free water and stored at -20°C.

Target Gene	Forward/Reverse primer sequences 5'-3'	
B-actin	Forward	AGCCATGTACGTAGCCATCC
	Reverse	CTCTCAGCTGTGGTGGTGAA
MKP1	Forward	AAG CTT GAA TTC ATG GTG ATG GAG GTG GGC A
	Reverse	GGA TCC TCT AGA TCA GCA GCT TGG AGA GGT GG

Redd1	Forward	AAG CTT GAA TTC ATG CCT AGC CTC TGG GAT CG
	Reverse	GGA TCC TCT AGA TCA ACA CTC TTC AAT GAG CAG CTG
Glucocorticoid-Receptor	Forward	AGGCCGCTCAGTGTTTTCTA
	Reverse	TACAGCTTCCACACGTCAGC
18S	Forward	CTTAGAGGGACAAGTGGCG
	Reverse	ACGCTGAGCCAGTCAGTGTA
GAPDH	Forward	AACTTTGGCATTGTGGAAGG
	Reverse	ACACATTGGGGGTAGGAACA
HBMS	Forward	CAGTGATGAAAGATGGGCAAC
	Reverse	AACAGGGACCTGGATGGTG

3.1.5 Western Blot/Immunoblot Antibodies

Antibody	**Supplier**	**Dilution**
Rabbit monoclonal Anti-Hamartin/TSC1 (129 kDa)	Cell Signaling Technology®	1:1000
Rabbit monoclonal Anti-mTOR (289 kDa)	Cell Signaling Technology®	1:1000
Rabbit monoclonal Anti-p70 S6 Kinase (54 kDa)	Cell Signaling Technology®	1:1000
Rabbit monoclonal Anti-p-mTOR (S2448) (289 kDa)	Cell Signaling Technology®	1:1000
Rabbit monoclonal Anti-p-p70 S6 Kinase (T389) (54 kDa)	Cell Signaling Technology®	1:1000
Rabbit monoclonal Anti-p-Tuberin/TSC2 (S1254) (202 kDa)	Cell Signaling Technology®	1:1000
Rabbit monoclonal Anti-p-Tuberin/TSC2 (S1387) (202 kDa) (202kDa)	Cell Signaling Technology®	1:1000
Rabbit monoclonal Anti-p-Tuberin/TSC2 (S939) (202	Cell Signaling Technology®	1:1000

kDa)		
Rabbit monoclonal Anti-p-Tuberin/TSC2 (T1462) (202 kDa) (202 kDa)	Cell Signaling Technology®	1:1000
Rabbit monoclonal Anti-p-Tuberin/TSC2 (Y1571) (202 kDa)	Cell Signaling Technology®	1:1000
Rabbit monoclonal Anti-p-ULK1 (S757) (112 kDa)	Cell Signaling Technology®	1:1000
Rabbit monoclonal Anti-Tuberin/TSC2 (D67A9) (202 kDa)	Cell Signaling Technology®	1:1000
Rabbit monoclonal Anti-ULK1 (112 kDa)	Cell Signaling Technology®	1:1000
Mouse Monoclonal anti-β-actin JLA20 (~42 kDa)	Developmental Studies Hybridoma Bank (DSHB)	1:5000
Mouse monoclonal Anti-Cathepsin K (26 and 37 kDa)	Santa Cruz Biotechnology® Inc., USA	1:500
Rabbit polyclonal Anti-GFP (~25 kDa)	Santa Cruz Biotechnology® Inc., USA	1:1000
Rabbit polyclonal Anti-MKP1 (39 kDa)	Santa Cruz Biotechnology® Inc., USA	1:1000
Mouse monoclonal Anti-p-Erk (43 kDa)	Santa Cruz Biotechnology® Inc., USA	1:1000
Rabbit polyclonal Anti-Redd1 (25 kDa)	Santa Cruz Biotechnology® Inc., USA	1:1000
Rabbit polyclonal Anti-Total Erk (43 kDa)	Santa Cruz Biotechnology® Inc., USA	1:1000
Mouse monoclonal Anti-V-ATPase B1/2 (57 kDa)	Santa Cruz Biotechnology® Inc., USA	1:1000
Mouse monoclonal Anti-V-ATPase α1 (93 kDa)	Santa Cruz Biotechnology® Inc., USA	1:1000
Rabbit polyclonal Anti-TNFSF11 (RANKL) (48	Sigma Aldrich®, USA	1:1000

kDa)		
Rabbit polyclonal Anti-Sclerostin (23 kDa)	Sigma Aldrich®, USA	1:1000
Mouse monoclonal Anti-GAPDH (36 kDa)	Sigma Aldrich®, USA	1:5000
Rabbit polyclonal Anti-CD63 (53 kDa)	System Biosciences (SBI), USA	1:1000
Rabbit polyclonal Anti-CD81 (26 kDa)	System Biosciences (SBI), USA	1:1000
Rabbit polyclonal Anti-CD9 (25kDa)	System Biosciences (SBI), USA	1:1000
Rabbit polyclonal Anti-HSP70 (70kDa)	System Biosciences (SBI), USA	1:1000
Anti-PINK1 (63 kDa)	Abcam, USA	1:1000

3.1.6 Secondary Antibodies

Antibody	Supplier	Dilution
Anti-Mouse IgG (Fab specific) – Peroxidase antibody produced in goat	Sigma Aldrich®, USA	1:5000
Anti-Rabbit IgG (whole molecule) – Peroxidase antibody produced in goat	Sigma Aldrich®, USA	1:5000

3.1.7 Antibodies, Markers and Dyes Immunofluorescence Microscopy

3.1.7.1 Primary Antibodies

Name	Supplier	Dilution
Hoechst 33258	Invintrogen Molecular Probes, USA	1:5000
(Mouse) Anti-CD63	Developmental Studies Hybridoma Bank	1:100
Atg 16L1	Cell Signaling Techlogy®	1:200
LC3	Cell Signaling Techlogy®	1:200
LC3 A/B	Cell Signaling Techlogy®	1:200

3.1.6.2 Secondary Antibodies

Name	Supplier	Dilution
Alexa Fluor® 546 Phalloidin (F-actin)	Invitrogen Melocular Probes, USA	1:300
Alexa Fluor® 647 Phalloidin (F-actin)	Invitrogen Melocular Probes, USA	1:300

3.1.8 Other Materials and Equipments

Material and Equipment	Manufacturer
10x10 cm2 and 7x10 cm2 UV transparent gel tray; 8 and 15 well comb	Bio-rad, Hercules, CA., USA
A 1 Si Confocal Microscope	Nykon Corporation, Japan
Acrodisc® 25 mm Syringe Filters w/ 0.2 µm Supor® Membrane	Pall Corporation, USA
Avanti™ J-25 I Centrifuge	Beckman Instruments, USA
Baxter ddH2O	Baxter, Australia
Bio-Rad Mini Trans-Blot® Electrophoresis Transfer Cell	Bio-Rad Laboratories, Australia
Bio-Rad PROTEAN® III Cel Electrophoresis System	Bio-Rad Laboratories, Australia
Bio-Rad PowerPac™ Basic Power Supply	Bio-Rad Laboratories, Australia
Cell culture T-75 flasks	Corning, USA
Cell culture T-175 flaks	Corning, USA
Centricon® Plus-70 Centrifugal Concentrator	Merck KgaA, Darmstadt, Germany
Centrifuge 5810 R	Eppendorf, Germany
CFX Connect® Real Time System Thermal Cycler	Bio-Rad Laboratories, Australia
Costar® 48-well cell culture plates	Corning, USA
Costar® 6-well cell culture plates	Corning, USA

Coverslips (fitted for 48-well plate)	ProSiTech, Australia
EK-300i Balance	A&D® Weighing, Australia
Filter Paper	Whatmans International, England
Grant W-14 water bath	Selby Scientific and Medical, USA
Hettich® ROTOFIX 32A Centrifuge	Sigma-Aldrich®, USA
Protran Pure Nitrocellulose Tranfer and immobilization Membrane	Whatman International, England
LAS-3000 Mini Imager	FujiFilm Medical Systems, USA
LabCHEM Microprocessor pH Meter	Rowe Scientific Pty Ltd, Australia
Microplate reader, Model 680	Bio-Rad Laboratories, Australia
Plain Microscope Slides	LabServ®, Philippines
Milliq H2O	Generated in our laboratory
MilliQ Reagent Water System	Millipore Corp, USA
MiniSpin® centrifuge	Eppendorf AG, Germany
Nanodrop 2000 Spectrophotometer	Thermo Fisher Scientific, USA
Optima™ MAX – TL Ultracentrifuge	Beckman Coulter, USA
Orbital Mixing Incubator	RATEK Instruments, Australia
P1210 Weighing Balance	Metler, Zurich, Switzerland
Parafilm® Laboratory film	Bemis Flexible Packaging, Neenah, Wi, USA
PCR tubes – 0.2mL	Sarstedt, Germany
Pipet Tips	Axigen Scientific®, USA
Research Pipettes	Eppendorf, Germany
Rocking Plataform Mixer	Ratek Instruments Pty Ltd, Australia
Safe ImagerTM 2.0 Blue-Light transilluminator	InvitrogenTM, USA

Thermomixer Comfort	Eppendorf, Germany
TLA110 Ultracentrifuge Rotor	Beckman Coulter, USA
Transfer Pippete – 1mL	Sarstedt, Germany
Ultra Pipettes 0.2-2µL, 2-20µL, 20-200µL, 200-1000µL	Eppendorf, Germany
Veriti 96 Well Thermal Cycler	Applied Biosystems, Australia
Ratek Vortex Mixer	Rowe Scientific, Australia
Water Jacket CO2 Incubator	Thermo ScientificTM, USA
WNB14 Water bath	Memmert GmbH, Germany

3.1.9. Softwares

Name	Supplier
Micro plate Manager 5.2	Bio Rad Laboratories, Australia
Fiji Image J 1.49i	Wayne Raspband National Institutes of Health, USA
Image Reader LAS-3000	Fujifilm Medical Systems, USA
Bio-Rad CFX Manager	Bio-Rad Laboratories, Australia
Microsoft® Office Excel 2013	Microsoft Corporation
Microsoft® Office Word 2013	Microsoft Corporation
Microsoft® Office PowerPoint 2013	Microsoft Corporation
NIS-Elements AR 4.13.01 64-bit (Imaging Software)	Nikon Corporation, Japan

3.1.10 Solutions and Buffers

All buffers and solutions used were prepared using sterilized (autoclaved), highly purified MilliQue (MQ) doubled distilled water. pH adjustments were performed using a pH-2 Scan pH meter (Whatmans), calibrated with appropriate pH standards (pH 4.0 or 7.0). Chemicals were weighted on a calibrated Mettler p1210 balance.

Solution/Buffer	Ingredients	Weight/Volume
0.2% BSA-PBS	BSA (Bovine Serum Albumin) 1xPBS	0.4g 200mL Filtered through 0.2-0.8 µL Acrodisc syringe filter and stored at 4°C
3% BSA-PBS	BSA (Bovine Serum Albumin) 1xPBS	0.15g 5mL Filtered through 0.2-0.8 µL Acrodisc syringe filter and stored at 4°C
Cell Lysis Buffer	300mM NaCl 50mM Tris (pH=7.4) 0.5% Triton-X Autoclaved MilliQ ddH2O	4.2g 6,06g 2,5mL Made up to 500mL Protein Extraction Buffer was added
Coomassie Blue Stain	Coomassie® brilliant Blue R250 Glacial Acetic Acid Methanol MQ ddH2O	5g 50mL 200mL Made up to 500mL
0.5M EDTA	EDTA disodium salt Sodium Hydroxide (NaOH) Autoclaved MQ ddH2O Solutions autoclaved before use	18.61g 2g Made up to 1L pH = 8.0 (adjusted with HCl) Stored at 4°C
Freezing Medium (92% FBS, 8% DMSO)	FBS DMSO	1960µL 40µL
4% Paraformaldehyde	Paraformaldehyde Autoclaved MQ ddH2O	2g Made up to 50mL

		Filtered, aliquoted and Stored at -20°C
10 x Phosphate Buffered Saline (PBS)	NaH2PO4 Na2HPO4 NaCl MilliQ ddH2O Solutions autoclaved before use	9.9g 3.6g 76g Made up to 1L
1x Phosphate Buffered Saline (PBS)	10x PBS MilliQ ddH2O	100mL Made up to 1L Filtered, autoclaved and stored at room temperature
8.8mg/ml PMSF stock	Phenylmethyl sulfonyl fluoride Isopropanol 1ml aliquots stored at -20°C	0.088g Made up to 10mL
0.1% Ponceau S Staining Solution	Ponceau S Acetic Acid MilliQ ddH2O	1g 50mL Made up to 1L Stored at room temperature
5% Ponceau S Distaining Solution	100% Acetic Acid (Glacial) MilliQ ddH2O	50mL 950mL
RIPA Lysis Buffer	1M Tris-HCl (pH=7.5) 5M NaCl Nonidet P-40 (NP40) SDS 1% Sodium deoxycholate MilliQ ddH2O	25mL 15mL 5mL 0.5g 2.5g Top up to 500mL Autoclaved and stored at 4°C
Protein extraction buffer (Added to RIPA	 PMSF	Quantity per mL of Lysis buffer: 5.7µL 40µL

Lysis Buffer and Cell Lysis Buffer)	Protease inhibitor Sodium Orthovanadate DNase I	10µL 10µL
Rat Tail Colagen 1 (RTC)	Acetic Acid (0.02N) Colágeno (4.0 mg/mL) Autoclaved MilliQ ddH2O	10mL 1,2mL 28,8mL Stored at 4°C
3M Sodium Acetate	Sodium Acetate Autoclaved MQ ddH2O Solutions autoclaved before use	40.83g Made up to 100ml
50X TAE buffer	Tris-Base Glacial Acetic Acid 0.5M EDTA (pH = 8.0) Autoclaved MQ ddH2O	242g 57.1ml 100ml Made up to 1L
1X TAE buffer	50X TAE buffer MQ ddH2O	40ml 1960ml
10X TBS (pH = 7.4)	Tris-HCl ph=7.4 NaCl MilliQ water	60.5g 85g Top up to 1L
1X TBS (Tris Buffered Saline)	10X TBS MilliQ water	50ml Top up to 500ml
1X TBS-Tween	1X TBS Tween	500mL 0.5mL
0.1% Triton X-100	Triton X-100 (100%) 1 x PBS	50µl Made up to 50ml
Trypsin-EDTA	Trypsin-EDTA 1 x PBS filtered in fumehood or under sterile conditions	100ml Made up to 1L
Western Blot Stripping Buffer	Tris HCl, pH = 6.7 SDS (Sodium dodecyl sulphate) 2-beta Mercaptoethanol	3.79g 10g 3.5mL

	(BME) MilliQ ddH2O	 Made up to 500mL
	Dissolve fully and adjust pH, then add BME and adjust to 500 mL	
2% X-gal	X-gal Autoclaved ddH_2O	0.2g Made up to 10mL

3.1.11 Cells

	Description	Supplier
MLO-Y4 cell line	Mouse osteocyte-like cells	Kindly provided by Dr. Lynda Bonewald, University of Missouri-Kansas City, School of Dentistry, Department of Oral Biology.
Primary calvarial osteoblast	Mouse (C57BL/6) calvaria	ARC, Murdoch
Primary bone marrow monocytes	Mouse (C57BL/6) long bones	ARC, Murdoch

3.1.12 Cell Culture Medium and Reagents

All reagents and cell culture mediums were warmed in 37°C water bath and sprayed with 70% ethanol before use, in order to maintain sterility.

Dulbecco's modified Eagle's medium (DMEM)	Gibco® BRL, Life Technologies, Melbourne, Australia
Fetal Bovine Serum (FBS)	TRACE, Sydney, NSW, Australia
Fetal Calf Serum (FCS)	TRACE, Sydney, NSW, Australia
L-Glutamine	Gibo BRL, Life Technologies, Melbourne, Australia
Minimum Essential Medium Alpha (MEM Alpha)	Gibco® BRL, Life Technologies, Melbourne, Australia
Penicilin/Streptomycin (P/S)	Gibo BRL, Life Technologies, Melbourne, Australia

Rat Tail Collagen Type I (4.01 mg/mL)	BD Biosciences, Bedford, USA
Opti-MEM	Gibco® BRL, Life Technologies, Melbourne, Australia
Dexamethasone	Sigma-Aldrich®, USA
Rapamycin	Sigma-Aldrich®, USA

3.2 Cell Culture

3.2.1 Culturing of MLO-Y4 Cells

To maintain the dendritic characteristic of MLO-Y4 cells, petri dishes, culture flasks, plates and coverslips used for culturing MLO-Y4 cells were coated with rat tail type-1 collagen (RTC). Stock RTC was dilute to 0.15mg/ml in filter sterilized 0.02N acetic acid. Sufficient quantity of 0.15mg/ml RTC solution was added to coat the culture vessels. The following quantity of diluted collagen was added to each dish:

Petri dishes and Flasks	Volume of diluted collagen
96 well plate	100 µL
48 well plate	300 µL
12 well plate	700 µL
6 well plate	2 mL
T75 flask	10 mL
T175 flask	15mL

Coating was carried out at room temperature, inside a tissue culture hood, for 1 to 2 hours. The diluted collagen was then removed and stored at 4°C (can be used up to five times). The dish was then rinsed three times with autoclaved 1xPBS and air dried for 1 hour at room temperature. RTC coated culture vessels could be used immediately or stored at 4°C for future use.

MLO-Y4 cells were maintained in Alpha Minimum Essential Medium (α-MEM) supplemented with pre-warmed 2.5% Fetal Bovine Serum (FBS), 2.5% Fetal Calf Serum (FCS), 2mmol/L of L-glutamine, 100U/mL penicillin, and 100µg/mL streptomycin. Cells were incubated in a 37°C incubator humidified with 5% CO_2. The medium were changed every 48 hours and cells were sub-cultured (1:5 ratio) when cell reached 70-80% confluency. Calf serum and bovine serum maintains the proliferation and differentiation of MLO-Y4 cells respectively.

3.2.2 Culturing of Primaru Calvarial Osteoblasts

Primary calvarial osteoblasts were cultured in T75 culture flasks and maintained in α-MEM, supplemented with 10% FBS, 2mmol/L of L-glutamine, 100IU/mL of penicillin, and 100µg/mL of streptomycin in a humidified (5% CO_2) 37°C incubator (*Forma Scientific*). Upon reaching confluency, cells were trypsinized with Trypsin-EDTA and plated onto tissue culture plates at the required plating density of the experimental assay.

3.2.3 Culturing of Primary Bone Marrow Monocytes and Osteoclasts

The femur and tibia were removed from C57BL/6 mice and flushed for bone marrow in a sterile tissue culture hood. Cells were cultured in T75 flasks in complete α-MEM supplemented with supplemented with 10% FBS, 100IU/mL of Penicillin, 100µg/mL of Streptomycin and 2mmol/L of L-glutamine and 50ng/ml MCSF to ensure survival of cells. The medium was changed every second day. To generate multinucleated osteoclasts from MCSF-dependent BMM precursors, cells were stimulated with 100ng/ml RANKL or isolated exosomes for 5 to 7 days changing media every second day. Cells were fixed and stained for TRAP activity according to the procedure in the lab.

3.3 Protein Analysis

3.3.1 Total Cellular Protein (TCP) Extraction

Total cellular protein was extracted from cultured cells using either Cell lysis or RIPARIPA lysis buffer supplemented with 5.7 µL/mL of 17.6mg/mL PMSF, 40 µL/mL of 25X Protease Inhibitor (Roche), 10 µL/mL of 100mM sodium orthovanadate (Na_3VO_4) and 50 µL/mL of 10mg/mL DNase I. Cells were left to lyse on ice for 20 minutes, lysate collected and centrifuged at 14,000 rpm for 20 minutes at 4°C to pellet unlysed cells and cellular debri. Cleared supernatant containing TCP was carefully transferred to fresh labelled tubes and stored at -20°C for future use.

3.3.2 Protein Concentration Quantitation

The protein concentration in each sample was quantified on a Model 680 Micro-Plate Spectrophotometer (BIO-RAD) using the Bradford Protein Assay. Bradford Dye was diluted (1 part dye:4 part water) and filtered through a Whatman #1 filter, in order to remove particulates. Five dilutions of BSA protein standard, with known concentrations, were prepared from a 10mg/ml BSA stock. The concentrations prepared

were 0.05mg/ml, 0.1mg/ml, 0.2mg/ml, 0.3mg/ml, 0.4mg/ml and 0.5mg/ml. 200µL of Bradford Dye was added to each well in a 96-well plate. Then, 10µL of each BSA standard and protein sample were added to each well in duplicates and mixed by pipetting up and down. Measurements of absorbance were performed using the microplate spectrophotometer at wavelength 595nm, following a 10sec low mixing speed.

3.3.3 SDS Polyacrylamide Gel (SDS-PAGE) Analysis of Protein Profile

Proteins were separated on SDS-PAGE gel using the Mini-PROTEAN® 3 Cell Electrophoresis System (BIO-RAD) according to manufacturer's guidelines. A 10% SDS-PAGE gel which allowed separation of proteins with sizes from 15-100kDa was prepared using the following recipe:

Separating Gel

MilliQ water	2.97mL
1.5 M Tris-HCl, pH = 8.8	1.875mL
10% SDS	75µL
30% Acrylamide / BIS solution	2.5mL
10% Ammonium Persulfate (APS)	75µL
TEMED	6µL
Total Volume	7.5mL

Following the preparation of the separating solution, it was immediately cast into a pre-assembled glass plate sandwich, composed of a short and a long glass plate, which is aligned with the bottom of the casting frame assembly. Once the separating solution was cast, 20% ethanol was added to overlay the separating gel, in order to remove any bubbles that had formed and make the surface, to which the stacking gel is to be set, horizontal. The separating solution was allowed to set at room temperature for approximately 30 minutes, with the polymerization evident by separation of the ethanol from the gel. Once set, the stacking gel was prepared using the following recipe:

Stacking Gel

MiliQ H_2O	2.1mL
30% Acrylamide / BIS solution	500µL

1.0 M Tris (pH 6.8)	380µL
10% SDS	30µL
10% ammonium persulfate	30µL
TEMED	3µL
Total Volume	3mL

Firstly, the 20% ethanol was completely discarded and rinsed off. Once prepared, the stacking solution was cast on top of the separating gel. A 15-well teeth comb was immediately inserted and the solution was allowed to set at room temperature for 30 minutes. Once the stacking gel has polymerized, the comb was carefully removed, and SDS-PAGE gel, inside the glass plate sandwich, was assembled into the Mini-PROTEAN® 3 Cell Electrophoresis System as shown in Figure 3.1. The mini tank was filled with 1xSDS-PAGE running buffer.

All protein samples used in western blotting was diluted in 4xSDS Loading Buffer containing 2% β-mercaptoethanol (β-ME), in a proportion of 75% of protein sample and 25% of loading buffer. Protein samples were boiled at 100°C for 5 minutes in a thermomixer to denature the proteins. After 5 minutes, all samples were removed from the thermomixer and briefly centrifuged at max speed. 20µg of protein samples were loaded into each well, in accordance with experimental assay. The gel was electrophoresed at 90 to 120 volts (V) for 90 to 130 minutes. The electrophoresis machine was stopped and switch off as soon as the dye front of the loading buffer had reached the bottom of the gel.

3.3.4 Protein Transfer to Nitrocellulose Membrane for Western Blotting

Follow electrophoresis, separated proteins were transferred from the gel to a nitrocellulose membrane, using the Mini Trans-Blot® Electrophoretic Transfer Cell System (BioRAD). Before assembling the protein transfer sandwich, two sponge pads, a PROTRAN (nitrocellulose) membrane (Whatman) and 6 Whatman 3MM paper were pre-soaked in western blot transfer buffer. The protein transfer cassette was then placed on the bench oriented with the black (negative) facing up and the white (positive) facing down. The protein transfer sandwich components was then laid on top of the white side according to the following sequence: 1x sponge pad, 3x pieces of Whatman 3MM paper, 1x PROTRAN nitrocellulose membrane, SDS-PAGE Gel, 3x pieces of Whatman

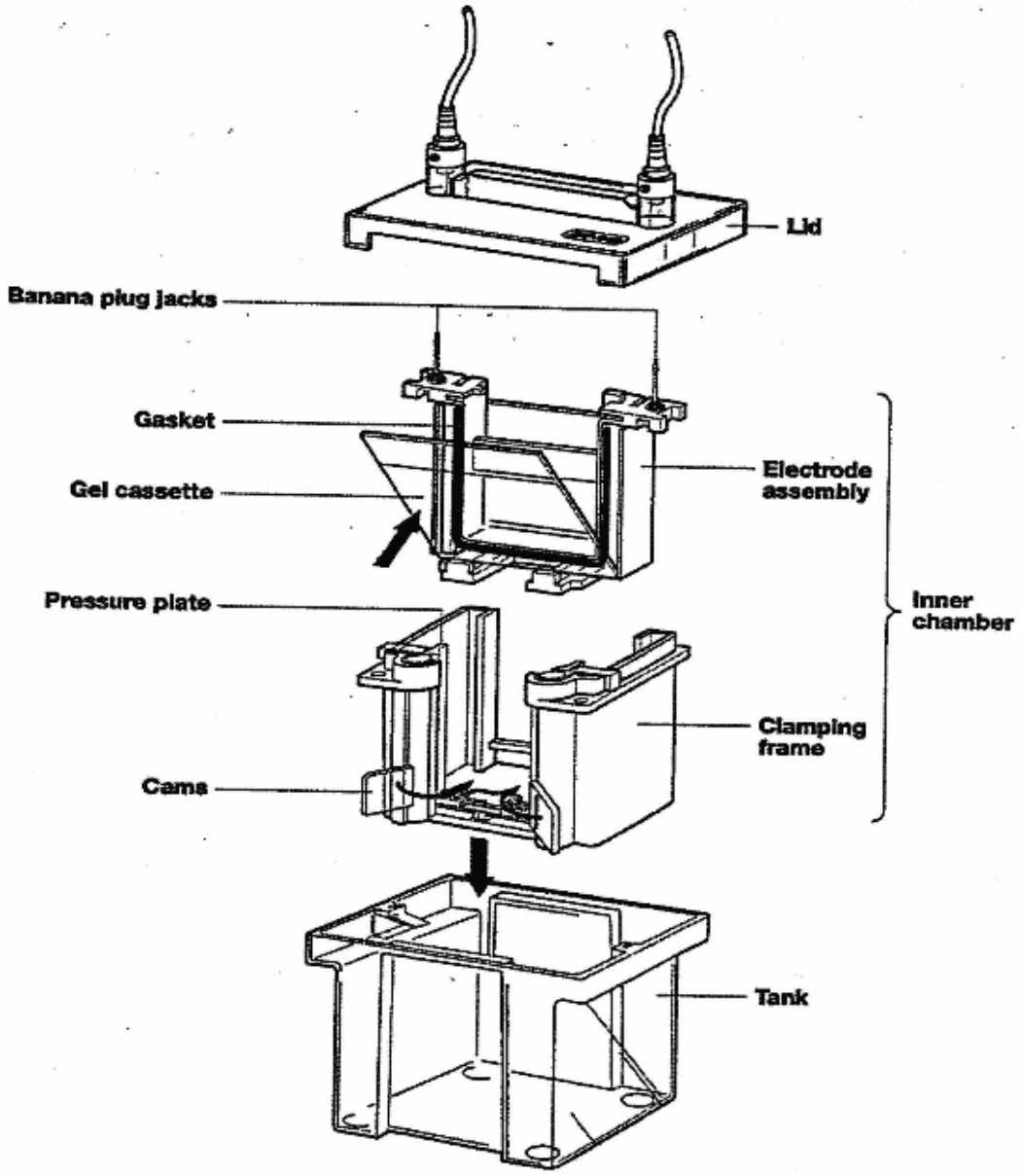

Figure 3.1. Assembly of the Mini-Protean 3 Cell Electrophoresis System.

3MM paper and 1x sponge pad. Air bubble between the nitrocellulose membrane and the gel were carefully removed, by pressing the sandwich or rolling a 50mL tube over the sandwich. At last, the cassette was closed and placed in a holding transfer chamber. The transfer chamber was placed within a buffer tank, alongside an ice block, and then filled with western blot transfer buffer. Protein transfer was performed at a constant amps of 30mA overnight. The next day, the transfer was stopped, and the nitrocellulose membrane with transferred protein (indicated by the protein marker) was stained with Ponceau Red S Stain to determine transfer efficiency.

3.3.5 Ponceau Red S Staining

Ponceau Red S Stain is a rapid and reversible method used to determine protein bands on nitrocellulose membrane following protein transfer. It was widely used in this thesis to dictate the cutting of the nitrocellulose membrane into strips when necessary, since it does not have any deleterious effect on the detection of blotted polypeptides. The nitrocellulose membrane was immersed in a sufficient quantity of Ponceau Red S Stain solution and stained for 5 minutes, at room temperature, with rocking in a Ratek® plataform mixer. Membrane was then destained by immersion in an aqueous solution containing 5% acetic acid (v/v), for another 5 minutes, at room temperature, with rocking in a plataform mixer (Ratek®). Following destaining, the protein bands become visible enable the alignment of the membrane for cutting strips for multiple protein blots. The membrane was then washed several times with 1xTBS-Tween (TBST) or until the stained bands started to fade. All traces of Ponceau Red S stain was removed before proceeding with blocking step.

3.3.6 Western Blot/Immunoblot Analysis

Non-specific background binding of primary and secondary antibodies to the nitrocellulose membrane was reduced by blocking the membranes in 5% (w/v) skim milk in TBST for 1 hour, at room temperature with gentle rocking on a plataform mixer. The blocked membranes were then washed for 5 minutes with TBS Tween, and incubated with the diluted (in 1% skin milk) primary antibody (see topic 3.1.5), for 2 hours at room temperature or overnight at 4°C. After incubation, the used primary antibody solution were collected and stored at -20°C for future use (can be re-used up to 3 times). The membranes were washed three times with TBST and then immersed in the corresponding secondary antibody solution in TBST according to the primary antibody used, for 45 minutes to 1 hour, at room temperature. After secondary antibody

incubation, the membrane was washed twice with TBST, for 5 minutes each, and then washed twice in TBS, for 5 minutes each.

In order to visualize the bound antibody, it was used the Western Lightening™ Ultra Sensitivity, in accordance to manufacturer instructions. The detection reagent was directly added to the nitrocellulose membrane and allowed to incubate in the dark, for 1 minutes, at room temperature. The protein bands were then visualized using the LAS-3000 Mini Chemiluminescent Imaging System (FujiFilm).

3.3.7 Stripping and Reprobing of Membranes

When necessary, the nitrocellulose membrane was stripped, in order to remove the previously bound antibodies and then reprobed with different antibodies for different proteins. Membranes were immersed in pre-warmed stripping buffer and incubated at 55°C, for 30 minutes with gentle agitation in a Ratek Orbital Mixer Incubator. After incubation, the stripping buffer was discarded and the membrane was extensively washed with several rounds of TBST for 5 minute each to remove residual stripping buffer. Once stripped, the membranes can be reblocked with 5% skim milk and reprobed with primary antibodies as outlined above. Membranes were stripped and reprobed a maximum of two times before loss of proteins from membrane.

3.4 Isolation and Purification of MLO-Y4-derived Exosomes

The most commonly used protocol for the purification of exosomes from cell culture conditioned medium involves several steps of centrifugation, filtration, concentration and finally ultracentrifugation. The general idea of exosome purification is depicted in Figure 3.2. Exosomes-conditioned medium (ECM) from MLO-Y4 cells were prepared using a serum free α-MEM supplemented with Penicillin/Streptomycin and L-glutamine. Cells were incubated in this media for 72 hours prior to collection of ECM for isolation and purification of exosomes. For this thesis, each batch of exosomes were isolated from ECM pooled from 4-6x T175 flasks of MLO-Y4 cells. ECM were immediately centrifuged at 300 x g at 4°C for 5 minutes to eliminate dead cells. Pre-cleared ECM were collected and stored at 4°C if subsequent purification was to be carried out within the next week otherwise stored at -80°C. MLO-Y4 total cell lysate corresponding to each ECM was also harvested according to protocol above.

For subsequent purification, pre-cleared ECM were centrifuged at 2000 x g at

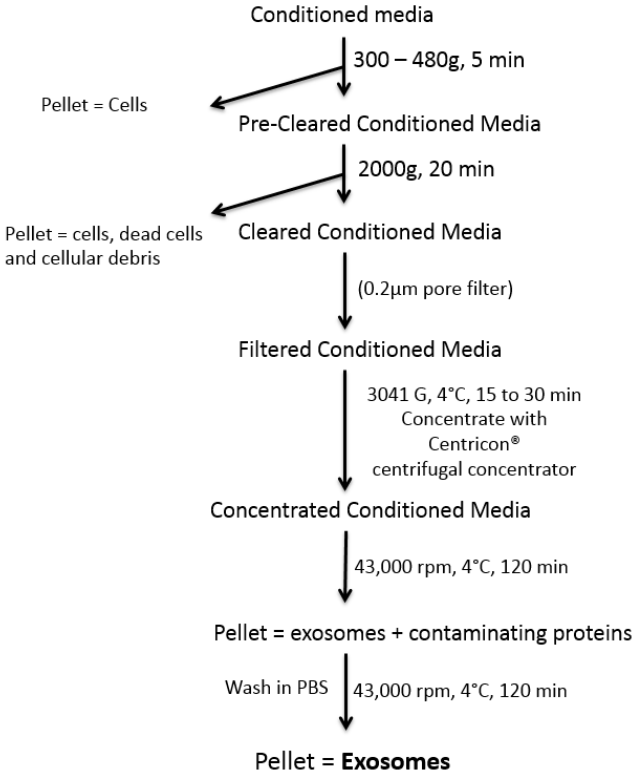

Figure 3.2. Flow chart for the exosome purification procedure based on differential ultracentrifugation

4°C for 20 minutes, to eliminate cells, dead cells and cellular debris. The resulting cleared ECM were then filtered through a 0.22µm pore filter (Supor®) into a Centricon Plus-70 centrifugal filter device (Millipore) with a 10,000 NMWL. This step was carried out to concentrate the cleared ECM down to a smaller volume for processing on a Beckman Coulter tabletop ultracentrifuge (Optima MAX-TL) equipped with a TLA110 rotor (max volume of 3mls per tube). To concentrate, the filtered ECM were in the Centricon Plus-70 were centrifuged at 3000 x g at 4°C for 15-30 minutes, until all filtered ECM has been processed and concentrated down to the required volume. The concentrated ECM were then transferred to a 3.2 ml polycarbonate thick wall tube, appropriate for the TLA110 ultracentrifugation rotor (Beckman Coulter®).

Ultracentrifugation was carried out at 100,000 x g (43,000 rpm) at 4°C for 2 hours. Supernatant was carefully decanted and the resulting pellet, which contains exosomes and contaminating membranes, was resuspended in sterile PBS (wash) and then ultracentrifuged again, at 100,000 x g (43,000 rpm) at 4°C for 2 hours. The resulting supernatant was carefully decanted and the pellet containing the purified exosomes were resuspended in 50-100µL of sterile PBS and stored at -80°C until use. For the fluorescent labeling of isolated exosomes, the Exo-GLOW Exosome Labeling Kit (SBI System Biosciences) was used according to manufacturers protocol.

3.5 RNA Extraction and Quantification

3.5.1 General Handling Procedures

All solutions, buffers, ultrapure water, micropipette tips, microfuge tubes and any equipment were previously sterilized by filtration or autoclaving. In addition, general aseptic techniques were employed during samples and RNA manipulation. RNAs were stored in sterile RNase-free water, provided by FAVORGEN Total RNA Purification Mini Kit, at -80°C. When RNA samples were required, they were removed from the freezer and allowed to thaw on ice. In order to prevent RNA degradation, RNA was not unnecessarily kept on ice for long periods of time.

3.5.2 Extraction of Total RNA

Total cellular RNA was extracted from MLO-Y4 cells and primary calvarial osteoblasts culture using FavorPrep Total RNA Purification Mini Kit (FAVORGEN), in accordance with manufacturer's protocol. All the procedure was conducted at room temperature. Firstly, 10µL of β-ME was added to each mL of FARB buffer required.

Culture medium was removed and 350µL of FARB buffer containing β-ME was added to each well of a 6-well plate. The plates were incubated at room temperature, over a platform mixer for 5 minutes. Lysates were then transferred to a filter column, placed in a collection tube provided by the kit, and centrifuged at 14,000 rpm for 2 minutes. One volume (350µL) of 70% molecular grade ethanol was added to the resulting clarified supernatant and mixed by pipetting. The total volume (700µL) of sample, including any precipitate, was transferred to the FARB Mini Column, placed in a collection tube, and centrifuged at 14,000 rpm for 1 minute. The flow-through was discarded and 500µL of Wash Buffer 1 was added to FARB Mini Column. Samples were centrifuged at 14,000 rpm for 1 minute. The flow-through was again discarded and the FARB Mini Column was washed twice with 700µL of Wash Buffer 2 by centrifuging at 14,000 rpm for 1 minute between each wash. The final flow-through was discarded and the FARB Mini Column was centrifuged at 14,000 rpm, for 3 minutes to dry the column and avoid residual liquid which can inhibit subsequent enzymatic reactions. The FARB Mini Column was placed in an elution tube, supplied by the kit to which 50µL of RNase free water was carefully added to the membrane center of the FARB Mini Column and centrifuged at 14,000 rpm for 2 minutes to elute the RNA. Purified RNA sample was kept on ice if used immediately or stored at -80°C for future use.

3.5.3 Quantification of RNA Concentration

The RNA concentration was quantified spectrophotometrically using the Nanodrop® 2000 UV Spectrophotometer (Thermo Scientific). Each RNA sample was measured against RNase-free water as blank. 1µL of the blank and RNA samples were loaded on the lower measurement pedestal and measurements carried out at 260nm and 280nm. The quality of the RNA samples were determined by the ratio of the readings at 260nm and 280nm (A_{260}/A_{280}). This value provides an estimate of the purity of the RNA in regards to the presence of contaminants that absorb in UV wavelength, such as proteins. Pure RNA has an A_{260}/A_{280} ratio of approximately or close 2.0. All purified RNA samples used in this thesis had A_{260}/A_{280} ratios between 1.5 -2.0.

3.6 Reverse Transcription – Generation of cDNAs

Reverse transcription was performed using RNA extracted and quantified above. All procedures were carried out on ice, unless stated otherwise. Two master mixes were prepared and placed in RNase-free tubes. Master mix 1 contained 2µL of 5mM dNTP mix and 0.25µL of 100µM Oligo(dT) first strand primers. Master mix 2 contained 4µL

of 5X RT buffer, 0.5µL of MMLV-RT enzyme and 0.5µL of Recombinant RNasin® Ribonuclease Inhibitor. The volume of all reagents in both master mixes was multiplied by the number of samples that were subjected to reverse transcription.

In order to create equal amount of total cDNA in each sample, the reverse transcription was performed using the same quantity of RNA. Therefore, taking into consideration the calculated RNA concentrations of each sample, different volumes of previously extracted RNA were required in each PCR tube.

RT1 Mix	Volume x 1 Reaction
Mater mix 1	2.25 µL
ddH_2O – DEPC-treated	X µL
RNA template (quantity?)	Y µL*
Total Volume	15 µL

*Volume required to reach the previously determined quantity of RNA. X µL of DEPC-treated water was added to each RT1 mix to make up to total reaction volume of 15 µL.

Once the RT1 Mix was ready, the tubes were mixed by flicking and briefly centrifuged, in order to collect all solution at the bottom of the tube. The tubes were then heated to 75°C for 3 minutes, in a 96-well Veriti Thermal Cycler (Applied Biosystems), to disrupt secondary structures. All PCR tubes were immediately returned on ice in order to promote the annealing and then 5µL of master mix 2 was added to the solution to give a final volume of 20µL per sample. Samples were again mixed by flicking and brief centrifugation before being placed in the thermal cycler. Samples were incubated at 42°C for 1 hour (cDNA transcription) and then heated at 92°C for 10 minutes (MMLV-RT inactivation). The newly synthesized cDNA was used immediately for PCR reactions or stored at -20°C for future experiments.

3.7 DNA Amplification of Target Genes by Semi-Quantitative PCR

Polymerase chain reaction (PCR) is an *in vitro* molecular biology technique used to amplify a specific gene of interest. The reaction process is characterized by several cycles of denaturation, annealing and extension of the gene of interested by a thermostable DNA polymerase – Thermus aquaticus (Taq) Polymerase. During these

cycles, a target sequence is bounded by a pair of previously designed primers which are complementary to the 3' and 5' ends of the target DNA sequence. PCR carried out in this thesis used GoTaq® Green Master Mix, a premixed solution of Taq DNA polymerase, $MgCl_2$, dNTPs and blue and yellow loading dyes.

Reagents and solutions for PCR reactions were added to PCR tubes on ice as follows:

PCR Mix		Volume 1X Reaction
2X GoTaq® Green Master Mix		12.5µL
Sterile ddH_2O		9.5 µL
Primers (20µM)	Forward	1 µL
	Reverse	1 µL
cDNA		1 µL
Total Volume		25 µL

Each PCR tube was mixed by flicking and briefly centrifuged before placing into the thermal cycler. The thermal cycler was set for initially denaturation of the samples by heating at 95°C for 2 minutes. Depending on the primers used, repeated cycles of the following conditions were used.

Primers	Denaturation; Annealing; Extension	Number of cycles
18S	95°C, 40 sec; 60°C, 40 sec; 72°C 60 sec	30
β-actin	95°C, 40 sec; 60°C, 40 sec; 72°C 60 sec	30
CD63	95°C, 40 sec; 65°C, 40 sec; 72°C 60 sec	30
MKP1	95°C, 40 sec; 60°C, 40 sec; 72°C 60 sec	30
Redd1	95°C, 40 sec; 60°C, 40 sec; 72°C 60 sec	30
SGK1	95°C, 40 sec; 60°C, 40 sec; 72°C 60 sec	30

The last extension was set at 72°C for 10 minutes, with an indefinite holding temperature of 4°C at the end of the reaction. The samples were stored at -20°C for future analysis by agarose gel electrophoresis.

3.8 DNA Agarose Gel Electrophoresis

Agarose gel electrophoresis is a routine molecular biology tool for the separation

of DNA fragments based on their sizes. Depending on the sizes of DNA fragments that needed to be electrophoresed, agarose gel was set by melting, in a microwave oven, different quantities of agarose powder (Promega) (% w/v) in 100mL 1xTAE buffer. Larger DNA fragments would require a smaller percentage of agar powder, while smaller fragments would require a gel with higher concentration of agarose. All PCR products analysed in this thesis were electrophoresed on 1.5% agarose gels prepared as indicated below. Once the agarose was molten, 1:20000 dilution of GelGreen Nucleic Acid Gel Stain (Biotium) was added. The mixture was gently swirled and then poured into UV Perspex gel tray with one or two 20-well comb inserted. The gel was left to set at room temperature for about 20 minutes.

1.5% (w/v) Agarose gel	Medium Gel (15X7cm^2)	Large Gel (15X10cm^2)
Agarose Powder	1.2g	1.5g
1xTAE buffer	80mL	100mL
GelGreen Nuclei Acid Stain	4µL	5µL

The gels as well as the tray were placed in a Wide Mini-Sub Cell GT Cell (Bio-rad) apparatus containing 1xTAE running buffer. 10 µL of each PCR product was directly loaded into each well. In a separate well with 2µL of 1 kb DNA ladder mix, which was prepared using 1µL of 6x Loading Buffer (Promega) and 1µL of either 1kb or 100bp DNA ladder (Promega). The electrophoresis was carried out at 90V for about 30 minutes. The DNA bands were visualized on a Blue-Light trans-illuminator (Life Technologies) and photographed using a Nikon Coolpix S4 digital camera.

3.9 Quantitative Real Time PCR (qPCR)

Quantifying gene expression levels is increasingly relevant in molecular biological research. Quantifying the expression of a particular gene of interest is possible by measuring the amount of cellular RNA. For several genes, the expression level varies dramatically from gene to gene, during different experimental conditions, such as exposure to chemical substance or drug, or during a pathological state. Real time PCR, also known as quantitative PCR (qPCR), is a powerful, sensitive and precise tool to quantify gene expression. Unlike conventional PCR, which analyses the amount of DNA at the end all repeated cycles, qPCR technology measures the amount of amplicons in the reaction as it is amplified during each PCR cycle.

Real-time qPCR was conducted using the SensiMix™, using Bio-Rad CFX Connect™ Real-Time System for fluorescence detection. The reactions were performed in 96-well PCR plate (Figure 3.3). For every single well of the qPCR plate, 2X SensiMix(dT) (1X), Universal ProbeLibrary Probe (200nM), forward primer (400nM), reverse primer (400nM), $MgCl_2$ (5mM), RNase-free water (4.25µL) and cDNA (5µL) were added (note: final concentration and volumes are given in brackets). Each cDNA sample was added in triplicates for the gene interest and in duplicates for the reference gene, in the 96-well PCR plate. Plates were run at 95°C for 15 minutes and then amplified at 95°C for 15 seconds, 60°C for 60 seconds and 72°C for 15 seconds for 40 cycles.

3.10 Transient Transfection of MLO-Y4 cells

3.10.1 Transformation of pCMV6-AC-Redd1-GFP plasmid

Full-length Redd1 gene/transcript (NCBI Accession NM_029083) was cloned into SgfI and MluI restriction sites, upstream of the green fluorescent protein (GFP) tag (Figure 3.4), in the pCMV6-AC-GFP expression vector (Figure Y), according to the manufacturer (OriGene). 10µg of lyophilized plasmid was supplied by OriGene and was reconstituted with 100µL ddH_2O. Retransformation to replicate additional amounts of the plasmid was carried out using 100µL TOP10F competent cells and 1µL of plasmid. Cells were incubated on ice for 3mins, followed by heatshock and coldshock at 42°C for 45secs and on ice for 2mins respectively. 1mL of LB was then added to the cells and incubated at 37°C with shaking at 225rpm for 1hr. Following incubation, cells were pelleted by centrifugation at 14,000 rpm for 1min at room temperature and resulting supernatant was carefully removed and discarded. Cell pellet was resuspended in 50µL of fresh LB and plated out onto LB/Ampicillin agar plates. Cells were allowed to grow on the agar plate at 37°C overnight. The next day, a single colony of cells were carefully removed with a pipette tip and inoculated into 100ml of LB containing 100uL of 100mg/ml Ampicillin and allowed to grow at 37°C with shaking at 225rpm for 18-24hrs. Following incubation, cells were pelleted by centrifugation at 4000rpm for 30mins at 4°C. Cells were lysed and plasmid DNA was extracted using the PureLink HiPure Plasmid Filter Extraction Kit (Invitrogen) according to the manufacturer's protocol. Plasmid DNA was eluted with 300µL of nuclease-free ddH_2O, concentration quantified using the Nanodrop® 2000 UV Spectrophotometer and stored at -20°C until further use.

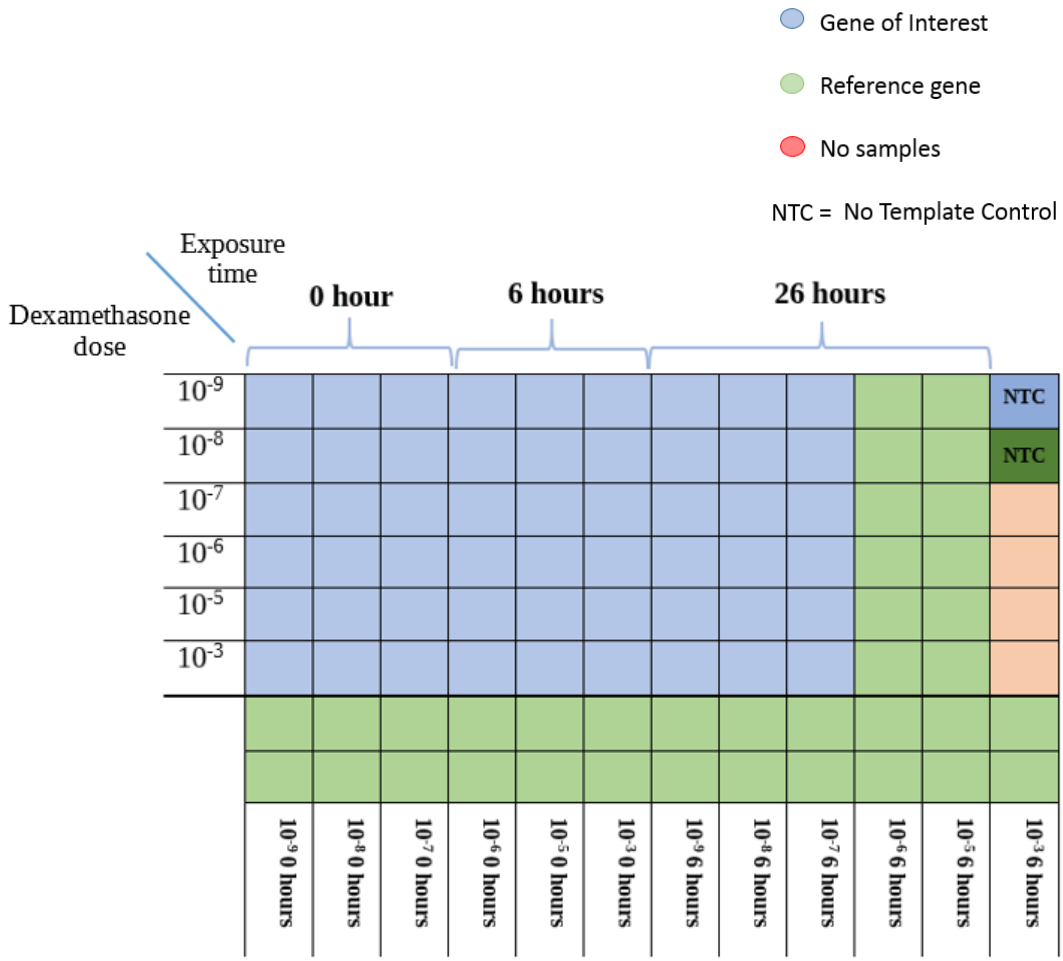

Figure 3.3. Quantitative real-time qPCR plate layout

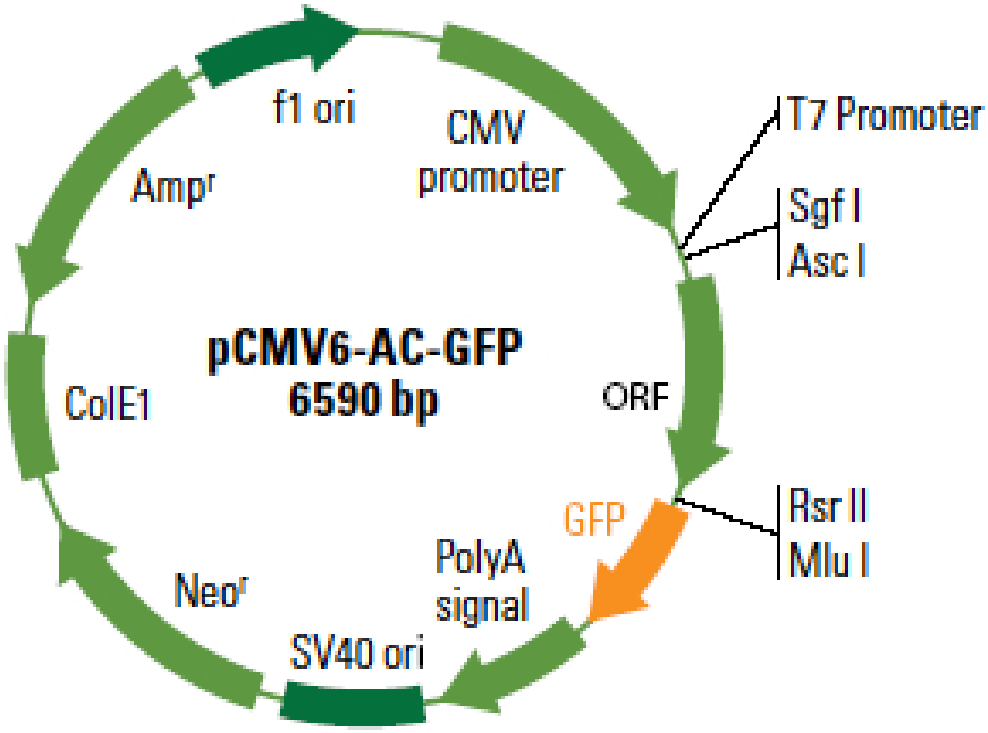

pCMV6-AC-GFP

Kozak Consensus

EcoR I BamH I Kpn I RBS Sgf I Asc I

CTATAGGGCGGCCGGGAATTCGTCGACTGGATCCGGTACCGAGGAGATCTGCCGCCGCGATCGCCGGCGCGCCAGATCT

Hind III Rsr II Mlu I Not I Xho I GFP Tag

CAAGCTTAACTAGTTAGCGGACCG ACG CGT ACG CGG CCG CTC GAG ATG GAG AGC GAC --- --- ---

T R T R P L E M E S D - - -

Pme I

--- --- GAA GAA AGA GTT TAA ACGGCCGGCCGCGG

- - E E R V Stop

Figure 3.4. pCMV6-AC-GFP vector map and multiple cloning sites

3.10.2 Overexpression of pCMV6-AC-Redd1-GFP in MLO-Y4 cells

All overexpression transfections were carried out using Lipofectamine® 3000 Transfection Reagent in either 6-well plates (for protein extraction and western blot analyses) or 48/96-well plates with collagen coated coverslips (for immunofluorescence microscopy). Cells transfected with GFP only was used as control. MLO-Y4 were seeded at a density of ~$5x10^3$ cells/cm^2 24 hours prior to transfection. Transfection reaction was performed in accordance with manufacturer's protocol. Parameters (for 1-well) for the transient transfection of MLO-Y4 cells using Lipofectamine 3000 are:

Plate	Cell Density	Plating Volume (mL)	DNA per well (µg)	P3000 reagent per well (µL)	Lipofectamine 3000 reagent per well (µL)	Volume of Opti-Mem (µL)
6-well	~$5x10^4$	2	2.5	5	3.75	250
48-well	~$3\text{-}4x10^3$	0.25	0.5	1	0.75	30
96-well	~$1\text{-}2x10^3$	0.1	0.1	0.2	0.15	10

The required volume of plasmid DNA, P3000, and Lipofectamine 3000 reagent was diluted in the appropriate amount of Opti-Mem serum free media. Contents were mixed by gentle flicking and allowed to incubate at room temperature for 5 minutes. The DNA-lipid complexes were then added dropwise to the cells. The plate was swirled gentle to ensure even distribution of complexes. Cells were incubated at 37°C in a humidified incubator (5% CO_2) for 6-12 hrs. After incubation time, the media containing transfection complex was removed and replaced with fresh complete media and incubated for further 12-18hrs. Cells were either lysed for protein extraction (6-well plate) or processed and fixed for immunofluorescence staining (48/96-well plate with coverslips).

3.10.3 REDD1 Silencing in MLO-Y4 Cells

All siRNA silencing transfections were carried out using Lipofectamine LTX Transfection Reagent in 48/96-well plates with collagen coated coverslips (for immunofluorescence microscopy). Cells were transfected with siGFP as control. MLO-Y4 were seeded at a density of ~$5x10^3$ cells/cm^2 24 hours prior to transfection. Transfection reaction was performed in accordance with manufacturer's protocol.

3.11 Immunofluorescence Staining

To examine autophagy under the various experimental conditions (dexamethasone treatment, REDD1 overexpression or REDD1 silencing), cells grown on coverslips were stained with Cyto-ID Green Autophagy Detection Kit (Enzo) prior to cell fixation. Cyto-ID is a fluorescence based assay that labels autophagic vacuoles (autophagosomes) and is also suitable for the monitoring of autophagic flux in live cells. The staining solution was prepared by adding 4μL of Cyto-ID to 1ml of complete α-MEM. Staining solution was added to cover the monolayer of MLO-Y4 cells and incubated for 20 to 30 minutes at 37°C in a humidified incubator (protected from light). After incubation, cells were gently washed with assay buffer to remove excess stains. For optimal preservation of actin structures cells were fixed in pre-warmed 4% paraformaldehyde for 20 minutes at 37°C. Cells were then washed twice with 1xPBS and stored at 4°C for future use or immediately processed for subsequent staining.

For subsequent immunofluorescence staining, fixed cells were permeabilized with 0.1% Triton X-100 for 5 minutes, at room temperature. Cells were washed twice in 0.2% BSA-PBS and then incubated with 3% BSA-PBS, for 30 minutes, at room temperature, to block non-specific binding of antibodies and consequently reduce background staining. After blocking with 3% BSA-PBS, primary antibodies (summarized in section 3.1.6.1) together with rhodamine-conjugated phalloidin (to visualize the actin cytoskeleton) diluted in 0.2% BSA-PBS were added to fixed cells, and incubated at room temperature for 2hrs in the dark. Following incubation with primary antibodies, cells were extensively washed in 0.2% BSA-PBS (4 times), PBS (4 times) and again with 0.2% BSA-PBS (4 times). Secondary antibodies (summarized in section 3.1.6.2) were then added and incubated for 45 minutes at room temperature in the dark. After secondary antibody incubation, cells were again extensively washed with 0.2% BSA-PBS (4 times), PBS (4 times) and 0.2% BSA-PBS (4 times). To visualize nuclei, all samples were incubated with Hoechst 33256 (diluted 1:5000 in PBS) for 15 minutes, at room temperature, in the dark. Cells were then washed three times with PBS. Glass slides were prepared and individually labeled with cell type, antibodies used, initials, date and experimental parameter (e.g. dexamethasone treated/dose, REDD1 overexpression and REDD1 silencing). Cells were then mounted onto glass coverslips using Prolong Gold Anti-fade mounting mounting media and stored in the dark on a flat surface to allow for curing and setting overnight.

3.11.1 Confocal Microscopy

The detection of fluorochromes was carried out using a Nikon Ti-E inverted motorized microscopy with Nikon A1Si spectral detector confocal system running NIS-C Elements Advance software (Nikon). For the detection of Cyto-ID and immunostainings from MLO-Y4 cells, a 60x oil immersion objective lends. Serial optical sections or z-stacks were acquired and analysed using ImageJ.

CHAPTER FOUR

MOLECULAR MECHANISM OF GLUCOCORTICOID-INDUCED AUTOPHAGY IN MLO-Y4 OSTEOCYTIC-LIKE CELLS

4.1 Introduction

Glucocorticoids (GCs) are extensively used for the treatment of chronic inflammatory and autoimmune diseases. However, prolonged use of glucocorticoids results in reduction of bone mineral density (BMD) and increased risk of bone fragility (Weinstein 2012). Histomorphometric analyses of patients with GC-induced osteoporosis consistently show fewer osteoblasts and an increased prevalence of osteocyte apoptosis, as compared with normal controls (Canalis *et al.* 2007; Weinstein *et al*. 1998; O`Brien *et al*. 2004). However, more recent studies have interestingly demonstrated that low dose GC treatment in mice (1.4 mg/kg/d for 28 days) induces a self-preservation mechanism known as autophagy (self-catabolism) in osteocytes both *in vitro* and *in vivo* (Jia *et al.* 2011). Similarly, Xia and colleagues (2010) have also reported induction of autophagy by GC in MLO-Y4 cells, a murine osteocyte-like cell line often used for the study of osteocyte function *in vitro* (Xia *et al.* 2010). Furthermore, ablation of the autophagic response in osteocytes by the osteocyte-specific deletion of autophagy related gene 7 (Atg7) results bone structural changes typically observed in skeletal aging and GC-induced osteoporosis (Onal *et al*. 2013). Six month old knockout mice exhibit low bone mass characterized by decreased cancellous bone volume and cortical thickness, and increased cortical porosity. Together, these observations offer novel insights into the possibility that osteocytic autophagy may serve as an initial major self-protective mechanism to guard against metabolic stress conditions induced by GC treatment.

Autophagy is a cell adaptive mechanism, characterized by degradation of cellular components and organelles, in response to cellular damage, metabolic requirements and/or during stressing conditions. However, autophagic flux is a “double-edged sword”, in that excessive and unregulated autophagy can cause exhaustion of cellular compnents which can ultimately lead to the process of autophagy-induced cell death. Thus, autophagy is tightly regulated by a highly integrated signaling cascade, in which mTORC1 (mammalian target of rapamycin complex 1) functioning as the master negative regulator of autophagy (Ravikumar *et al*. 2010). Despite the significant progress in the field of autophagy and osteocyte biology, the molecular mechanism by which GC induces autophagy in osteocytes has yet to be investigated. Therefore, the major aim of this chapter was to investigate the molecular mechanism by which GC induces autophagy in MLO-Y4 osteocyte-like cells.

4.2 Results

4.2.1 Effect of GC (Dex) on Autophagy in MLO-Y4 Osteocyte-like Cells

Previous study by Xia and colleagues has demonstrated that GC treatment resulted in an increase in the expression of autophagic genes and the accumulation of autophagosome vacuoles *in vitro* (Xia et al. 2010). In order to confirm and validate their results, as well as to establish an *in vitro* osteocyte autophagy model in the lab, we treated the osteocyte-like cell line, MLO-Y4 with various concentrations of dexamethasone (Dex; 10^{-9} M, 10^{-6} M, 10^{-3} M) and examined the induction of autophagy using the autophagic marker Cyto-ID Green by immunofluorescence confocal microscopy.

As shown in Figure 4.1A, untreated control MLO-Y4 cells exhibit very minimal basal levels of autophagic flux. However, treatment Dex lead to a robust and dose-dependent increase in autophagic vacuole formation indicated by the green fluorescent staining (CytoID Green) of autophagosomes (Figure 4.1A). Rapamycin (final concentration of 1μM) a well-established inducer of autophagy was used as a positive control. Cells were also counterstained with Hoechst to visualize the nucleus. The numbers of autophagosomes was quantified and again show a dose-dependent increase in autophagic flux following stimulation with Dex (Figure 4.1B). Interestingly, autophagic vacuoles were observed to be localized mainly in perinuclear region of the cell, rather than the periphery. This could be likely due to the site of formation of the autophagic vacuoles. The double membranes of the autophagic vacuoles have been proposed to be donated by various subcellular organelles including mitochondria, endoplasmic reticulum and the golgi (Tooze and Yoshimori, 2010; Hamasaki *et al*, 2013) whose general subcellular localization is at the perinuclear region of the cell.

To further monitor autophagy we examined LC3 lipidation by immunoblotting following Dex treatment. LC3 lipidation from LC3I to LC3II correlates with the onset of autophagy and with the number of autophagosomes. Immunoblotting was carried out on total cellular protein (TCP) extracted from MLO-Y4 cells treated with 10^{-6}M Dex for 2, 6, 14 or 26hrs. As shown in Figure 4.1C, LC3-I was progressively lipidated to LC3-II as the time progressed in the presence of Dex. Again rapamycin a positive inducer of autophagy

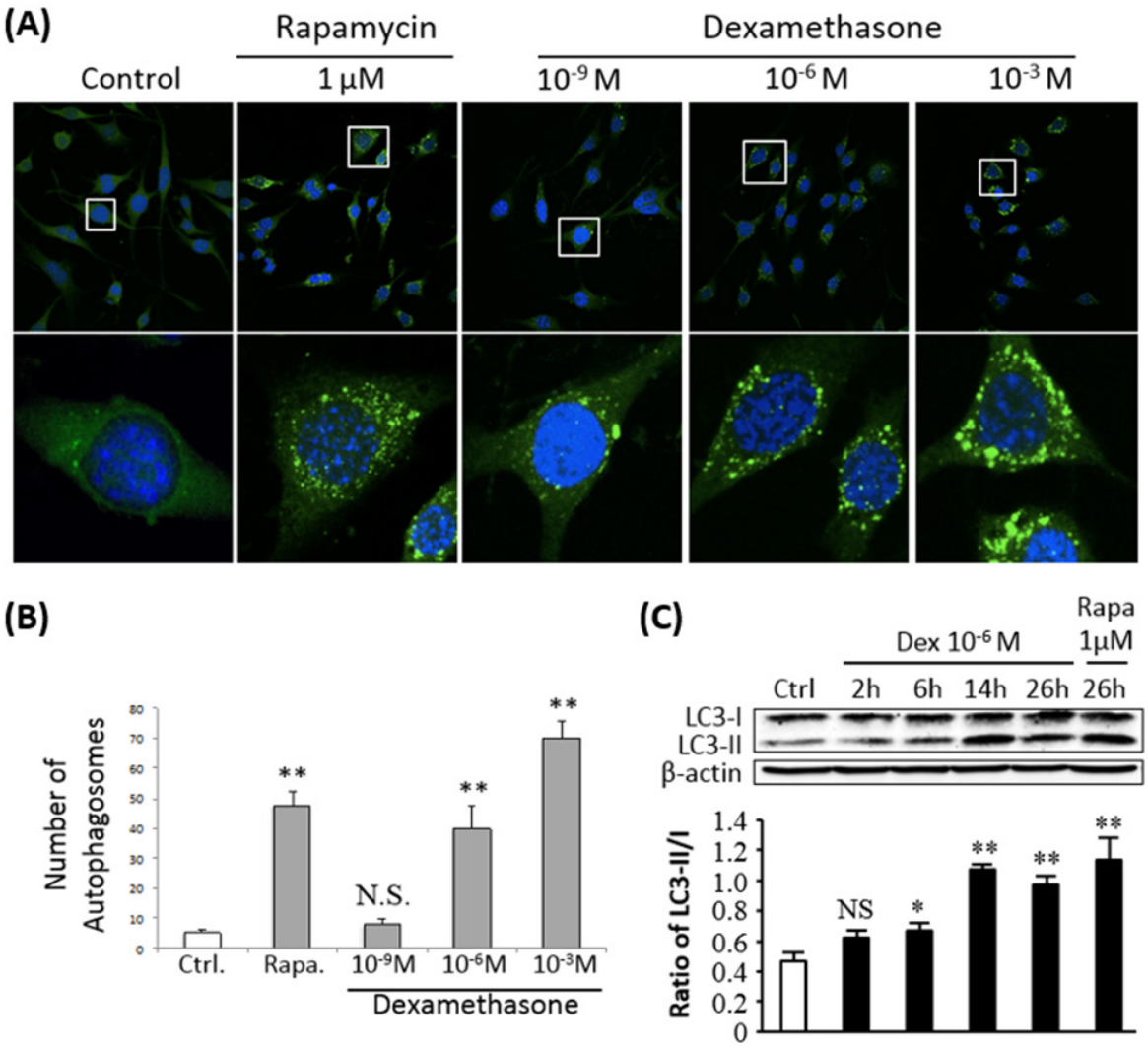

Figure 4.1. Dexamethasone-induced autophagy in MLO-Y4 osteocyte-like cells. MLO-Y4 cells cultured in 48-well plate were stimulated with various doses of dexamethasone (10^{-9} M, 10^{-6} M, 10^{-3} M) or 1µM Rapamycin for 24hours followed by incubation with CytoID Green for 30 minutes. Following incubation cells were fixed with 4% paraformaldehyde, stained with Hoechst (nuclei; blue) and mounted on glass slides with Prolong Gold Anti-fade mounting medium. **(A)** Immunofluorescence images were acquired on a Nikon confocal microscope equipped with a 60x oil emersion lens. MLO-Y4 cells staining positive for autophagasomes (CytoID Green) following treatment with Dex and rapamycin. **(B)** Number of autophagosomes were quantified and shown to be significantly increased in MLO-Y4 cells following dex treatment. **(C)** Immunoblot analysis and densitometric quantitation of LC3 lipidation. * $P < 0.05$, ** $P < 0.01$ when compared to control.

demonstrates similar levels of LC3I to LC3-II lipidation as Dex treatment at 26hrs. Collectively, these data demonstrates that a Dex treatment can induce the activation of the autophagic program in MLO-Y4 osteocyte-like cells *in vitro*.

4.2.2 Effect of GC (Dex) on *redd1* and *mkp1* Gene Expression

When GC binds to its receptor (GC receptor; GR), the activated GC-GR complex is translocated to the nucleus to transcriptionally activate expression of GC-responsive genes. We conducted an immunblot analysis to determine the translocation of the GR to the nucleus following Dex treatment. TCP isolated from MLO-Y4 cells treated with or without Dex were separated into cytoplasmic (Cyto) and nuclei (Nuc) fractions and immunoblotted for the presence of GR. As depicted in Figure 4.2A, without Dex treatment, GR resides mainly in the cytoplasm (upper blots) with very little GR in the nucleus (lower blots). Within 2hrs stimulation with Dex, GR is translocated from the cytoplasm into the nucleus. GR remains in the nucleus even after 24hrs treatment with Dex indicated that the GR is maintained in an activated state in the nucleus to carry out transcriptional functions. The translocation of GR into the nucleus was further verified by immunofluorescence staining (Figure 4.2B). Dex treatment of cells resulted in the accumulation of GR (green) in the nucleus (blue) as compared to untreated controls.

Having now established that Dex treatment results in the activation and translocation of GR into the nucleus in MLO-Y4 cells, we next sought to investigate subsequent transcriptional events that can lead to the induction of autophagy. As mTORC1 and its signaling cascade are considered the master regulatory pathway of autophagy we focused our research on how GC-responsive genes that affects mTORC1 activity. Through literature searches we have identified two potential GC-responsive genes that have been shown to function upstream of mTORC1 signaling cascade (Kassel *et al*., 2001; Wang *et al*., 2003) and thus we hypothesize that they partake in the regulation of GC-induced autophagy in MLO-Y4 osteocyte-like cells. The two GC-responsive genes are mitogen-activated protein kinase phosphatase-1 (*mkp1*) and regulated in development and DNA damage responses-1 (*redd1*).

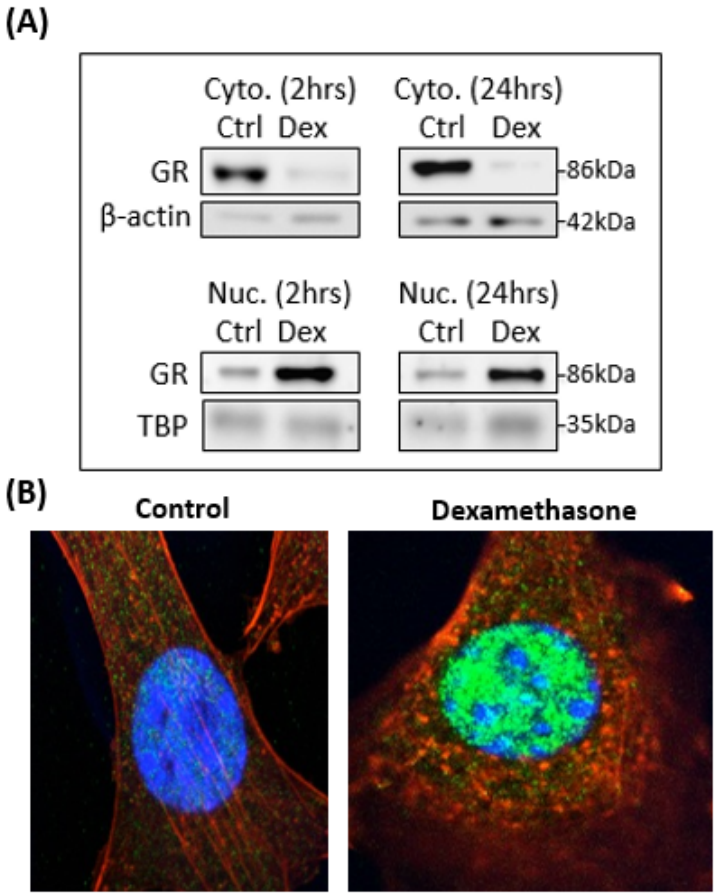

Figure 4.2. Nuclear localization of glucocorticoid receptor (GR) in MLO-Y4 cells following Dex treatment. (A) MLO-Y4 cells cultured in 6-well collagen coated plates were stimulated with with Dex for 2 or 24hrs. Following stimulation, cells were lysed and total cellular protein (TCP) were separated into cytoplasmic (Cyto.) and nuclear (Nuc.) fractions by centrifugation. Immunoblot analyses of GR nuclear translocation was carried out using specific antibodies to GR. GR was detected in the nuclear fraction within 2hrs of dex stimulation and persisted for 24hrs. GR is normally localized to the cytoplasm when unstimulated. β-actin and TBP were used as loading controls for cytoplasmic and nuclear fractions respectively. **(B)** MLO-Y4 cells cultured on glass coverslips and treated with or without Dex for 24hrs were fixed in 4% paraformaldehyde and immunostained with antibody specific to the GR (green), actin (rhodamine phalloidin; red) and Hoechst (nuclei; blue). Coverslips were mounted on glass slides with Prolong Gold Anti-fade mounting medium and analysed by immunofluorescence on Nikon confocal microscope with 60x oil emersion lens. As shown in the confocal image, 24hrs following stimulation with Dex, GR is translocated from the cytoplasm to the nucleus of the cell. Unstimulated cells show no nuclear localization of GR.

Thus we used semi-quantitative RT-PCR to initially investigate the gene expression of the two potential GC-reponsive genes, *redd1* and *mkp1*, following Dex treatment. Total RNA was isolated from MLO-Y4 cells and primary osteoblasts that had been treated with various concentrations of Dex for 24 hours. RT-PCR was then performed using specific primers to *redd1* and *mkp1*. The expression of housekeeping genes, such as *β-actin* and *Glucocorticoid Receptor*, were used as internal controls to ensure equal volume of loading and amplification products. As shown in Figure 4.3, a significant and dose-dependent increase in *redd1* and *mkp1* gene expression following Dex treatment in both osteoblasts and MLO-Y4 osteocyte-like cells was observed.

However, as RT-PCR is a method which analyses the amount of DNA at the end of all repeated cycles and, therefore only semi-quantitative, we further analyzed *redd1* and *mkp1* gene expression quantitatively using real-time qPCR. As an initial attempt to carry out the qPCR assay, we firstly examined the gene expression of *mkp1* in MLO-Y4 cells that have been treated with six doses of Dex (10^{-9} M, 10^{-8} M, 10^{-7} M, 10^{-6} M, 10^{-5} M and 10^{-3} M), that is, the dose-dependent effect. As shown in Figure 4.4, and consistent with the RT-PCR results, we observed a dose-dependent increase in gene expression of *mkp1* in response to Dex stimulation.

A more complete qPCR assay was then performed using RNA samples from both a dose- and time-dependent Dex treatment experiments. Real-time qPCR was performed on cDNAs that were reverse transcribed from RNA extracted from MLO-Y4 cells treated with 10^{-9}, 10^{-8}, 10^{-7}, 10^{-6}, 10^{-5} or 10^{-3}M Dex for 6 or 26 hours. Two housekeeping genes were used to normalized the gene expression, *hbms* and *gapdh*. As shown in Figure 4.4 *mkp1* gene expression was significantly increased following stimulation with higher concentrations of Dex, specifically when treated with 10^{-6}, 10^{-5}, and 10^{-3}M. The highest expression of *mkp1* gene was observed at 6hrs following treatment and decreases at 26hrs.. This trend was the same regardless of normalization against *hbms* (Figure 4.5A) or against *gapdh* (Figure 4.5B). Interestingly, at lower doses of Dex treatment (10^{-9}, 10^{-8}, and 10^{-9}M) the expression of *mkp1* was significantly lower than untreated controls at both 6hrs and 26hrs of Dex treatment.

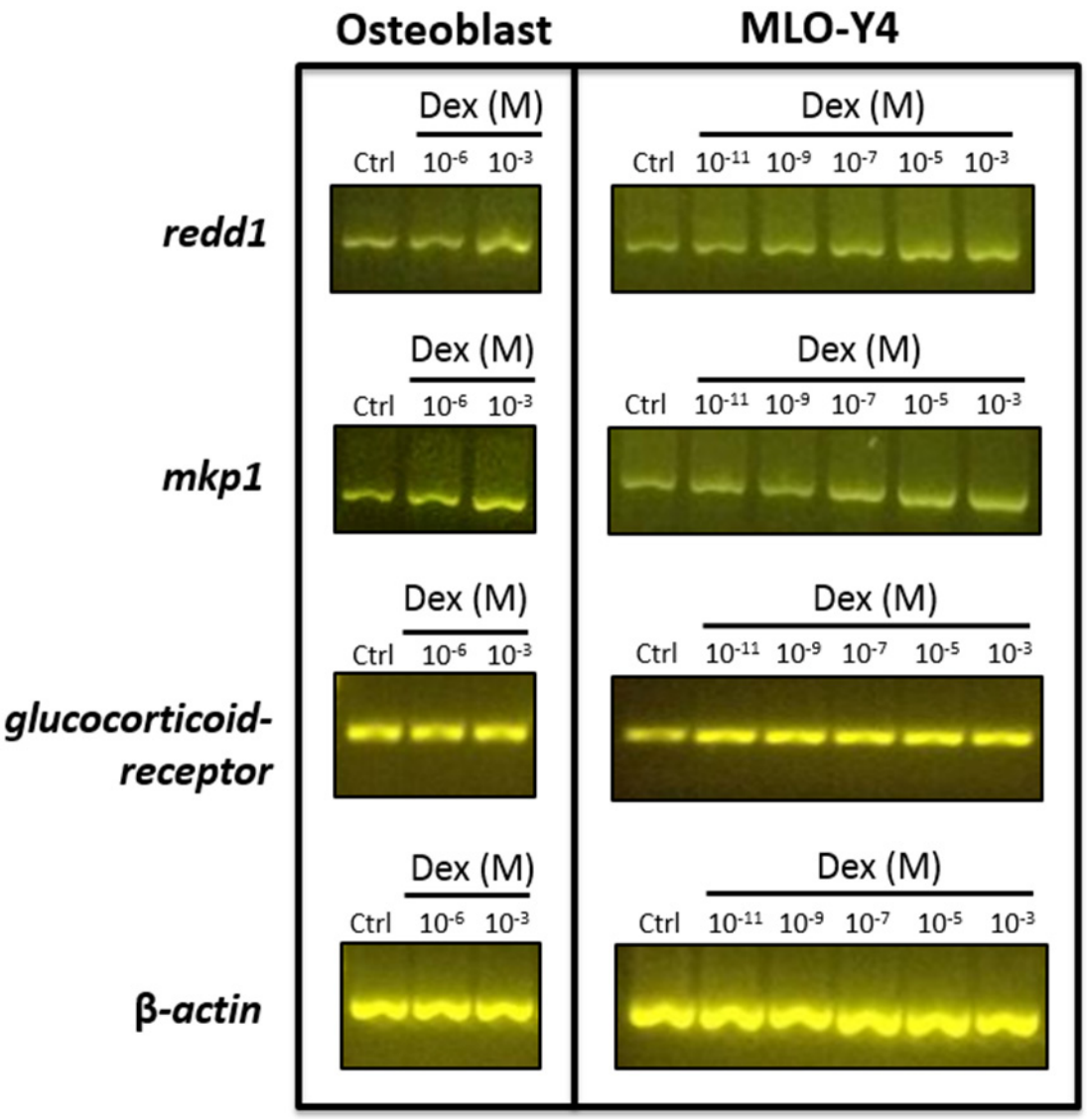

Figure 4.3. Semi-quantitative RT-PCR analysis of *mkp1* and *redd1* gene expression. PCR analysis was carried using cDNA reverse transcribed from RNA extracted from primary calvarial osteoblasts and MLO-Y4 osteocyte-like cells that have been treated with various concentrations of Dex. PCR products were resolved on a 1.5% agarose gel and visualized on a blue light emitting transilluminator. RT-PCR shows that the gene expression of *redd1* and *mkp1* in osteoblasts and MLO-Y4 cells were dose-dependently upregulated following treatment with Dex. Gene expression of *β-actin* and *glucocorticoid-receptor*, used as house-keeping genes, remain unchanged.

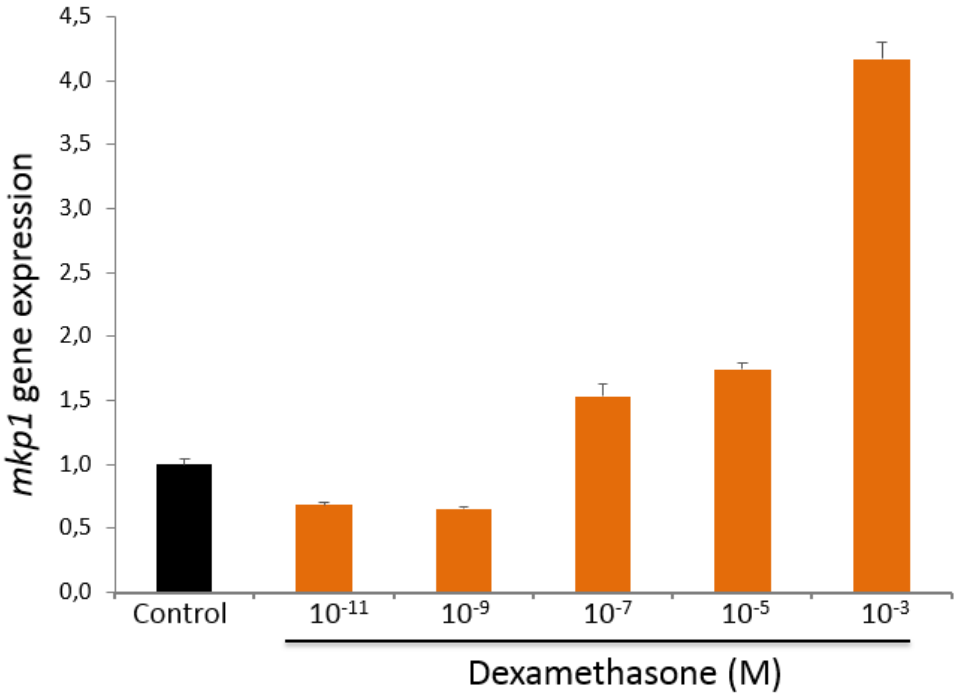

Figure 4.4. Quantitative real-time qPCR analysis of *mkp1* gene expression (dose-dependent Effect). Real-time qPCR analysis was carried using cDNA reverse transcribed from RNA extracted from MLO-Y4 osteocyte-like cells treated with various concentrations of Dex (10^{-11}, 10^{-9}, 10^{-7}, 10^{-5}, and 10^{-3}M) for 26hrs. Gene expression of *mkp1* was normalized to *gapdh* housekeeping control and expressed as fold change against control (untreated cells). qPCR analysis demonstrates that *mkp1* gene expression significantly increased in response to higher concentrations of Dex. The expression *mkp1* gene were up to four fold higher when cells were treated with 10^{-3}M Dex.

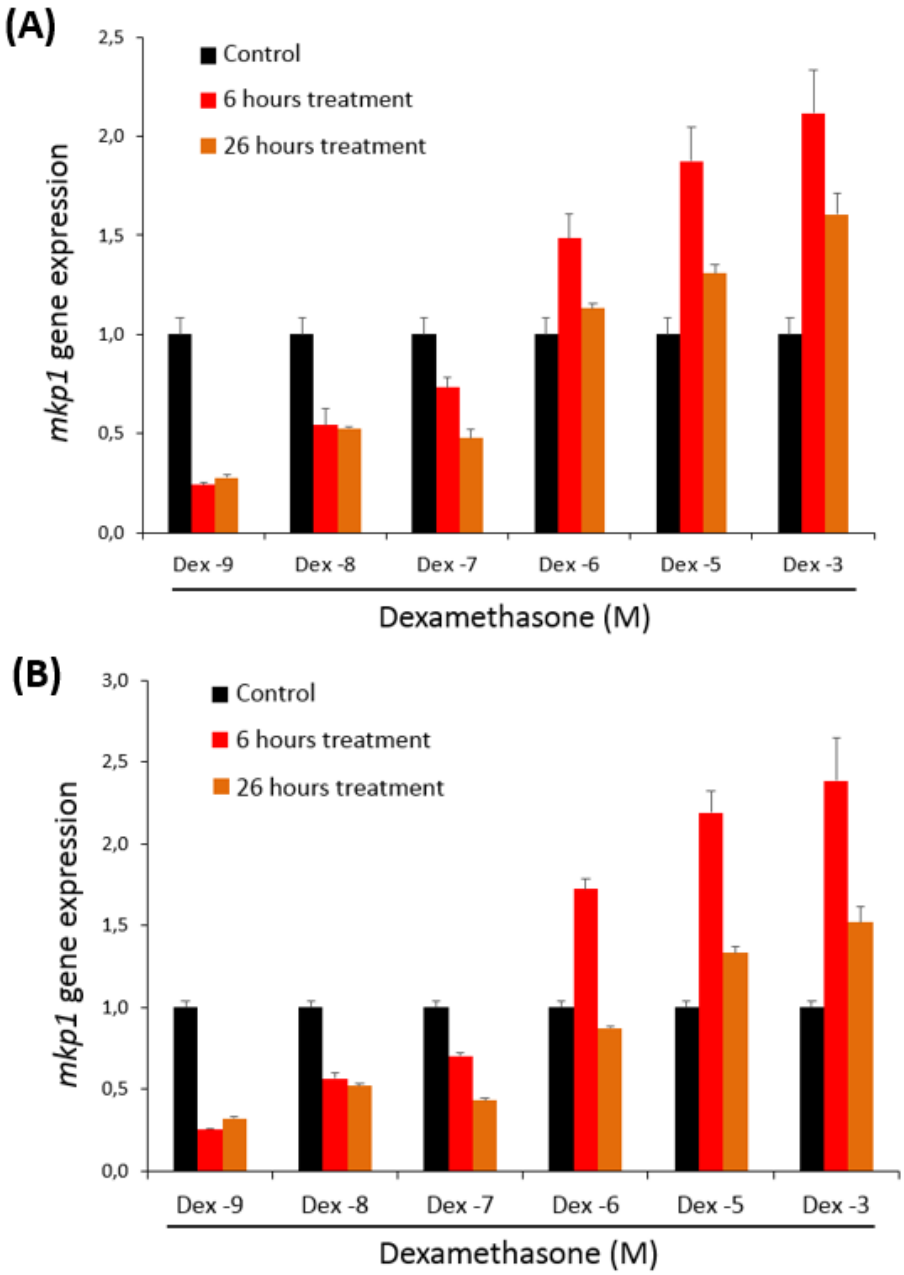

Figure 4.5. Quantitative real-time qPCR analysis of *mkp1* gene expression (dose- and time-dependent effect). Real-time qPCR analysis was carried using cDNA reverse transcribed from RNA extracted from MLO-Y4 osteocyte-like cells treated with various concentrations of Dex (10^{-9}, 10^{-8}, 10^{-7}, 10^{-6}, 10^{-5}, and 10^{-3}M) for 6 and 26hrs. Gene expression of *mkp1* was normalized to *hbms* **(A)** and *gapdh* **(B)** housekeeping genes and expressed as fold change against control (untreated cells). Normalization against either housekeeping genes demonstrate a dose-dependent increase in the expression of *mkp1* at 6hrs and with expression falling by 26hrs. The maximal fold increase in *mkp1* gene expression was ~2.5-folds.

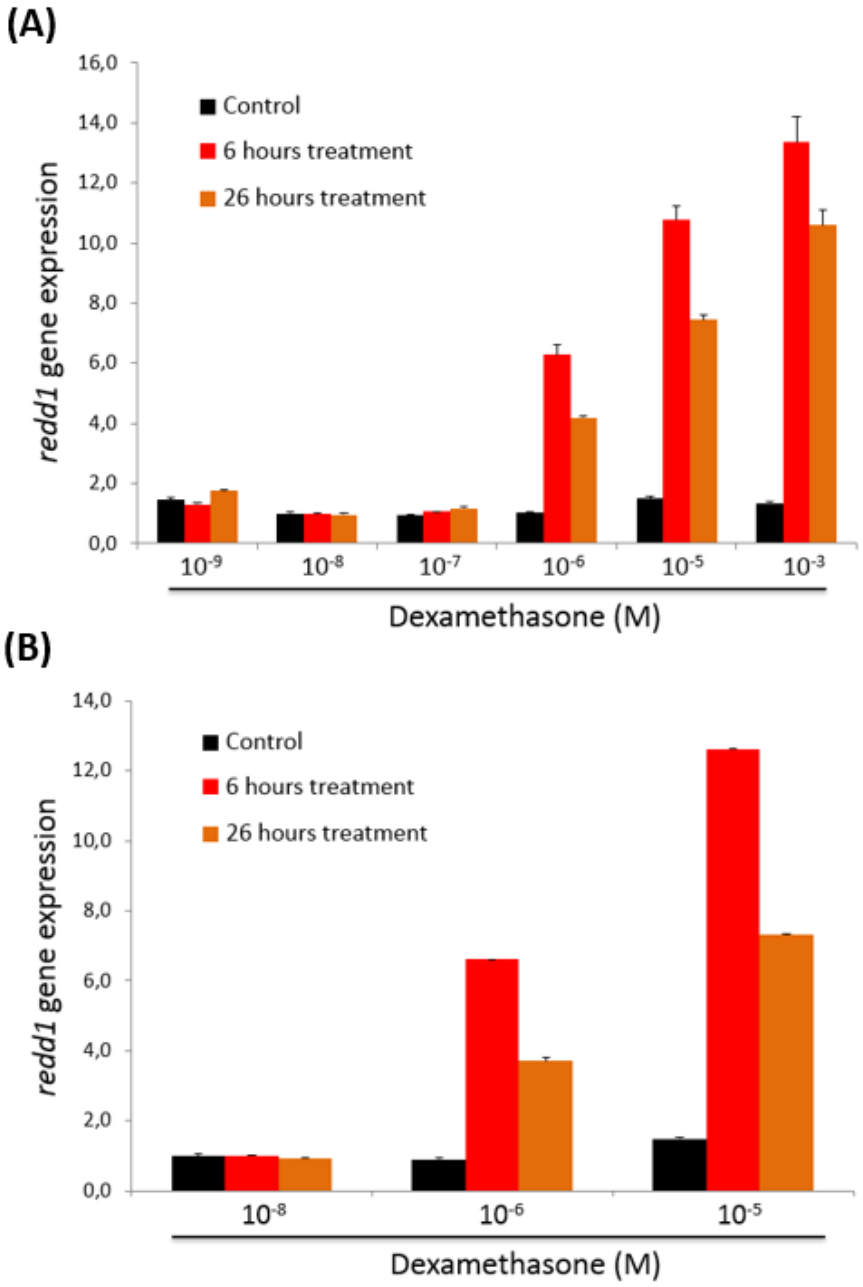

Figure 4.6. Quantitative real-time qPCR analysis of *redd1* gene expression (dose- and time-dependent effect). Real-time qPCR analysis was carried using cDNA reverse transcribed from RNA extracted from MLO-Y4 osteocyte-like cells treated with various concentrations of Dex (10^{-9}, 10^{-8}, 10^{-7}, 10^{-6}, 10^{-5}, and 10^{-3}M) for 6 and 26hrs. Gene expression of *mkp1* was normalized to *hbms* **(A)** and *gapdh* **(B)** housekeeping genes and expressed as fold change against control (untreated cells). Normalization against either housekeeping genes demonstrate a dose-dependent increase in the expression of *redd1* at 6hrs and with expression falling by 26hrs. The maximal fold increase in *redd1* expression was ~14-folds.

A similar trend was observed for *redd1* gene expression following Dex treatment both in a dose- and time-dependent manner (Figure 4.6). The gene expression of *redd1* was markedly upregulated following high doses of Dex peaking at 6hrs with lower but still highly significant increase at 26hrs. Again the trend of increase was not affected by normalization against either HBMS or GAPDH (Figures 4.6A and 4.6B respectively). Unlike *mkp1*, the gene expression of *redd1* at lower Dex concentrations (10^{-9}, 10^{-8}, and 10^{-7}M) did not decrease but remain the same as basal control levels. More interestingly is that the increased gene expression of *redd1* following treatment with Dex was around 6 to 7 folds greater than the increase seen in *mkp1* gene which may indicate that REDD1 plays a more significant role in GC-induced effects than does MKP1.

4.2.3 Effect of GC (Dex) on MKP1 and REDD1 Protein Expression

Although having shown that Dex can transcriptionally induce the gene expression of REDD1 and MKP1, this does not necessary mean that the genes are translated into functional proteins. Thus, we next examined the protein expression of REDD1 and MKP1 by immunoblotting using specific antibodies to both proteins. TCP were extracted from MLO-Y4 cells at 2, 6, 14 or 26 hours after treatment with various doses of Dex. TCP were resolved on 10% SDS-PAGE and transferred to nitrocellulose membranes for analysis by immunoblotting. Figure 4.7 shows that REDD1 expression was markedly upregulated in a time (Figure 4.7A) and dose-dependent (Figure 4.7B) manner following treatment with Dex correlating well with the qPCR results. On the contrary, the protein level only increase a little after 2, 6, and 26 hrs treatment with 10^{-6}M of Dex (Figure 4.8). This indicates that although MKP1 is transcriptionally induced by Dex, the gene is not actively translated into functional proteins. Together with the qPCR results, it can be concluded that REDD1 is more likely the candidate protein that execute the cellular effects of Dex. Thus we focused our attention onf REDD1 for functional analysis.

4.2.4 Effect of REDD1 Overexpression on mTORC1 Signaling Pathway

Initially, we wanted to determine whether overexpression of REDD1 could mimic GC-induce autophagy in MLO-Y4 cells in the absence of Dex treatment by monitoring autophagosome formation as performed in section in 4.2.1 using Cyto-ID Green. However,

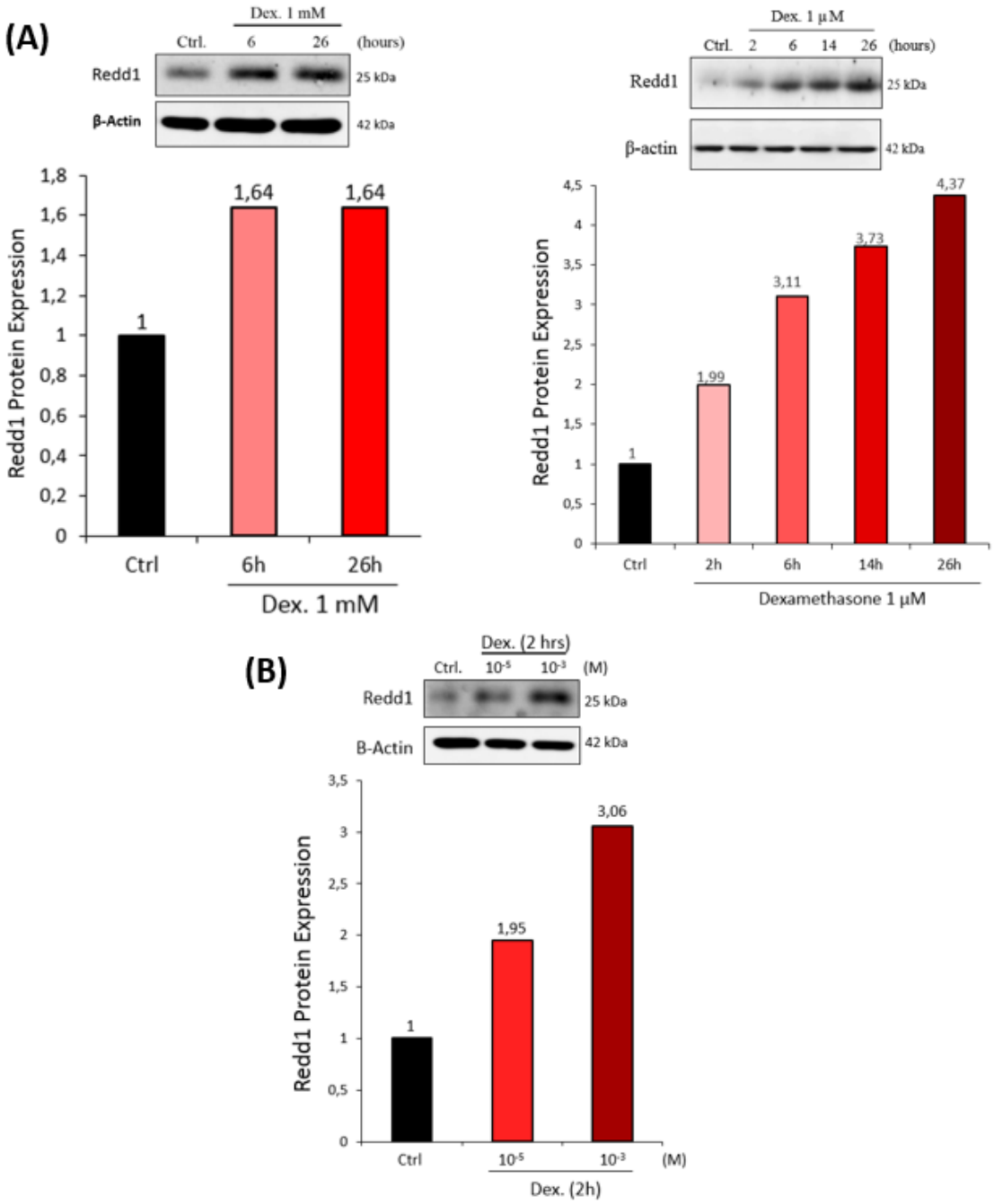

Figure 4.7. Immunoblot analysis of REDD1 protein expression following Dex treatment. (A) MLO-Y4 cells treated with 10^{-3} and 10^{-6}M Dex were lysed and TCP were harvested and resolved on a 10% SDS-Page gel for immunoblotting using specific antibody against REDD1. Protein levels of REDD1 showed a time-dependent increase at both 10^{-3} and 10^{-6}M Dex treatement. **(B)** Dose-dependent increase in REDD1 protein levels following treatment with Dex for 2hrs. All densitometric quantitation of protein expression were obtained using Fiji ImageJ v1.49i. Expressions were normalized against untreated control and expressed as fold changes.

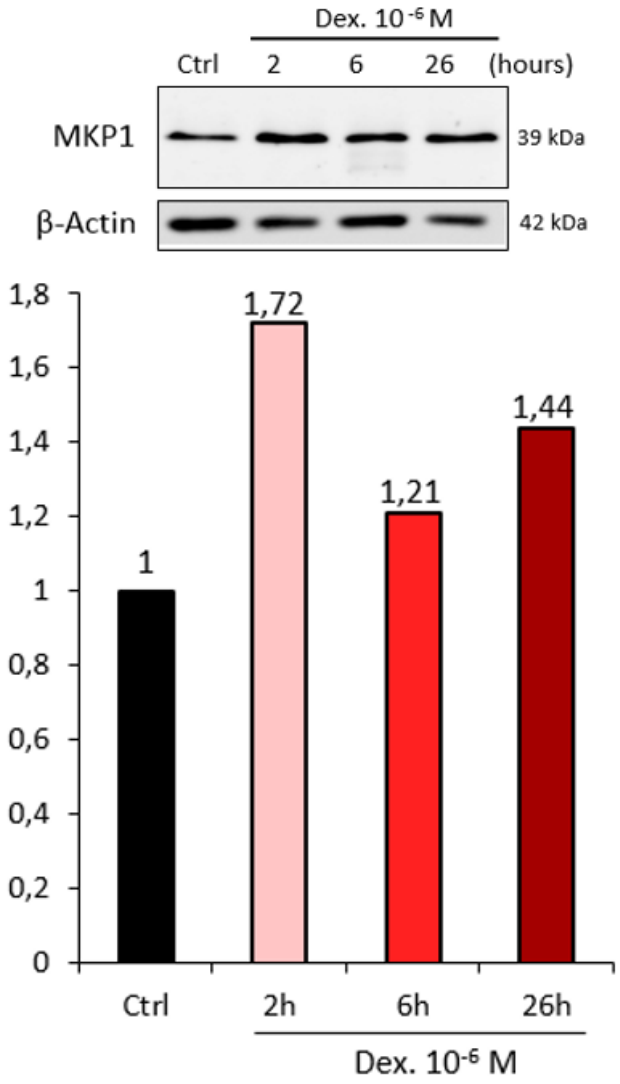

Figure 4.8. Immunoblot analysis of MKP1 protein expression following Dex treatment. MLO-Y4 cells treated with 10^{-6}M Dex were lysed and TCP were harvested and resolved on a 10% SDS-Page gel for immunoblotting using specific antibody against MKP1. Protein levels of MKP1 only showed a slight increase during Dex treatment periods at 10^{-6}M concentration. An increase on MKP1 protein expression, in response to longer Dex stimulation did not occur. All densitometric quantitation of protein expression were obtained using Fiji ImageJ v1.49i. Expressions were normalized against untreated control and expressed as fold changes.

both the overexpression construct pCMV6-AC-REDD1-GFP (REDD1-GFP) and Cyto-ID Green shares similar excitation wavelength under immunofluorescence so this was not possible. Previous studies have shown that REDD1 functions upstream of the mTORC1 signaling cascade. Given that mTORC1 is a negative regulator of autophagy and GC-induces autophagy and REDD1 expression, we thus investigated how REDD1 overexpression affects mTORC1 signaling. To this end, we investigated the effects of overexpressing REDD1-GFP on the various signaling components of the mTORC1 signaling cascade. The REDD1-GFP construct was transfected into MLO-Y4 cells using Lipofectamine 3000. To assess transfection efficiency, cells were fixed and analysed by confocal microscopy for GFP fluorescence. As shown in Figure 4.9A, cells were successfully transfected with REDD1-GFP depicted by the green fluorescence in transfected. Cells were additionally stained for actin (red) and nucleus (blue) to enable visualization of the cell. In addition to immunofluorescence, immunoblotting for REDD1-GFP with specific antibodies to REDD1 and cells whereas non-transfected cells display no green fluorescence. The presence of green fluorescence validated and confirmed that the transfection was successful. Cells were also GFP was also used to validate and confirm transfection efficiency (Figure 4.9B). Both REDD1 and GFP antibodies detected a band at around 52kDa which corresponds to the predicted molecular weight (MW) of the REDD1-GFP fusion protein (MW of REDD1 and GFP is 25 and 27kDa respectively). Control cells transfected with GFP alone only had a band at 27kDa.

Once confirmed that REDD1-GFP transfection was successful, the effects of REDD1 overexpression on mTORC1 signaling pathway was then investigated. Figure 4.10 illustrates immunoblots of proteins and their phosphorylation status involved in regulating mTORC1 activity. The immunoblots demonstrate a general increase in all proteins from TCP extracted from REDD1-GFP transfected cells. Although apparent equal quantities of TCP were loaded (20μg) for analysis, this was not the case as supported by the higher amount of GAPDH and β-actin detected in the REDD1-GFP TCP sample (Figure 4.10). Densitometry of the bands quantified by Fiji ImageJ (Figure 4.11) reinforced what was observed on immunoblot images, showing that the various proteins of interest were apparently up-regulated following overexpression of Redd1-GFP including GAPDH. Thus to overcome the unequal loading issue and to determine whether REDD1 overexpression

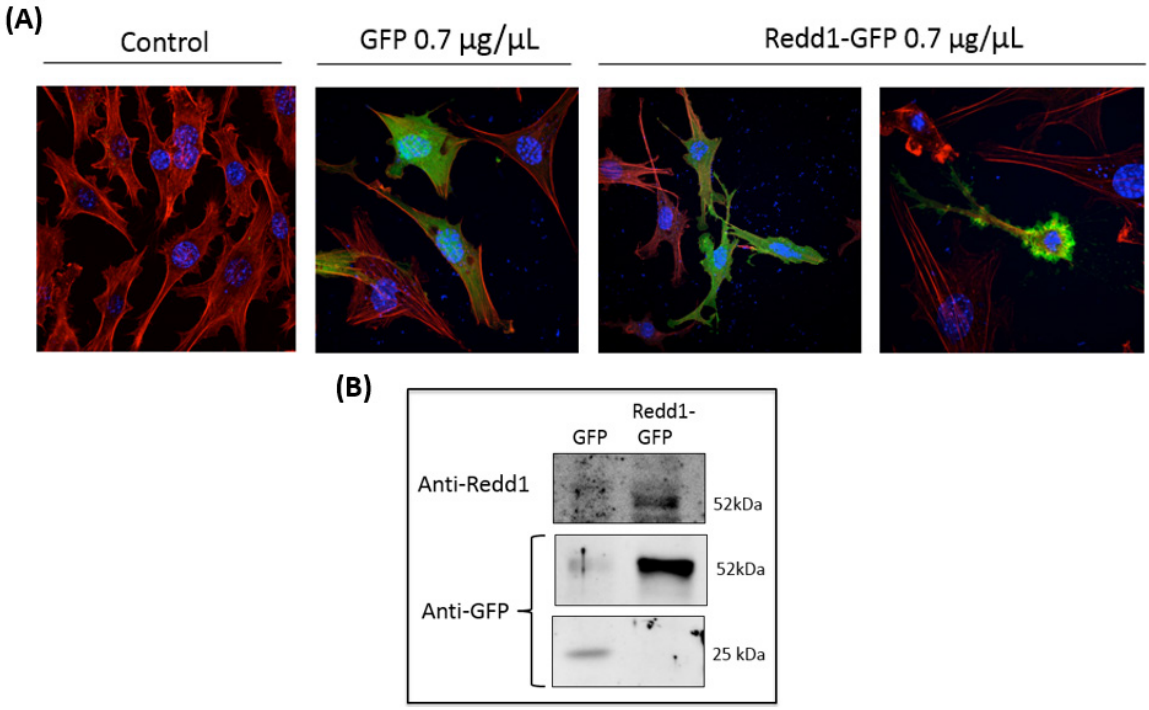

Figure 4.9. Confirmation of Redd1-GFP transfection into MLO-Y4. **(A)** MLO-Y4 cells cultured on collagen-coated coverslips, were transfected with GFP or REDD1-GFP using Lipofectamine 3000 for 24hrs. Cells were fixed with 4% paraformaldehyde, immunostained with rhodamine phalloidin (actin; red) and Hoechst (nucleus; blue) and mounted on glass slides. Immunofluorescence images were acquired using Nikon confocal microscope setup with 60X oil emersion lens. Cells were successfully transfected with REDD1-GFP construct as indicated by the green fluorescence which corresponds to the green fluorescent protein (GFP) tag. **(B)** Immunoblot confirmation of REDD1-GFP transfection. TCP isolated from MLO-Y4 cells transfected with either GFP or REDD1-GFP for 24hrs were resolved on 10% SDS-PAGE gel and immunoblotted using antibodies specific to REDD1 and GFP. Molecular weight of REDD1-GFP fusion protein and GFP alone is 52kDa and 25 kDa respectively.

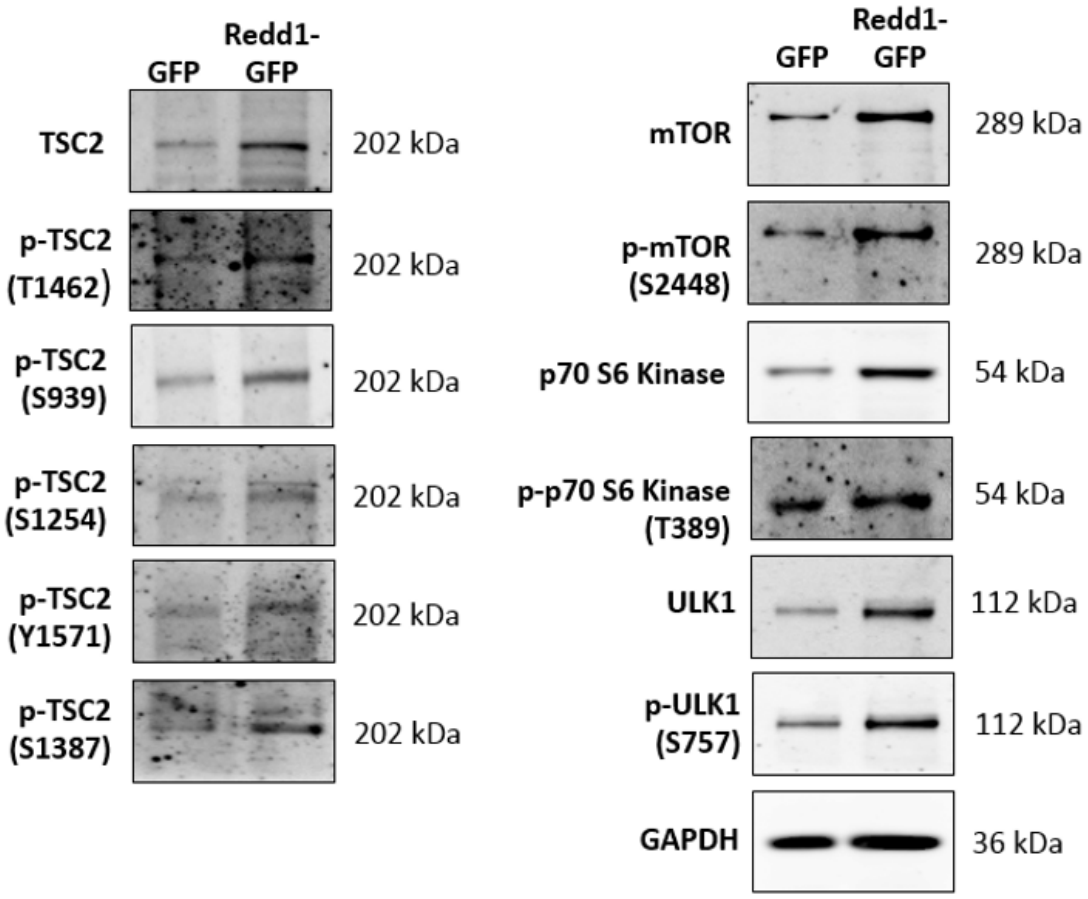

Figure 4.10. Immunoblot analysis of the effect of REDD1-GFP overexpression on mTORC1 signaling cascade. MLO-Y4 cells transfected with either GFP alone or with REDD1-GFP were lysed and TCP harvested and resolved on a 10% SDS-Page gel for immunoblot analyses. TCP were probed using specific antibodies to the following proteins in the mTORC1 signaling cascade: total TSC2 and its phosphorylation sites (Ser939, Ser1254, Ser1387, Thr1462, and Tyr1571), mTOR and its phosphorylation site (Ser2448), S6K and its phosphorylation site (Thr389), and ULK1 and its phosphorylation site (Ser757). GAPDH was used as internal loading control. Increased expression was observed in all investigated proteins, however, GAPDH loading control was also increased in REDD1 overexpression suggesting unequal loading of the quantity of proteins for analysis.

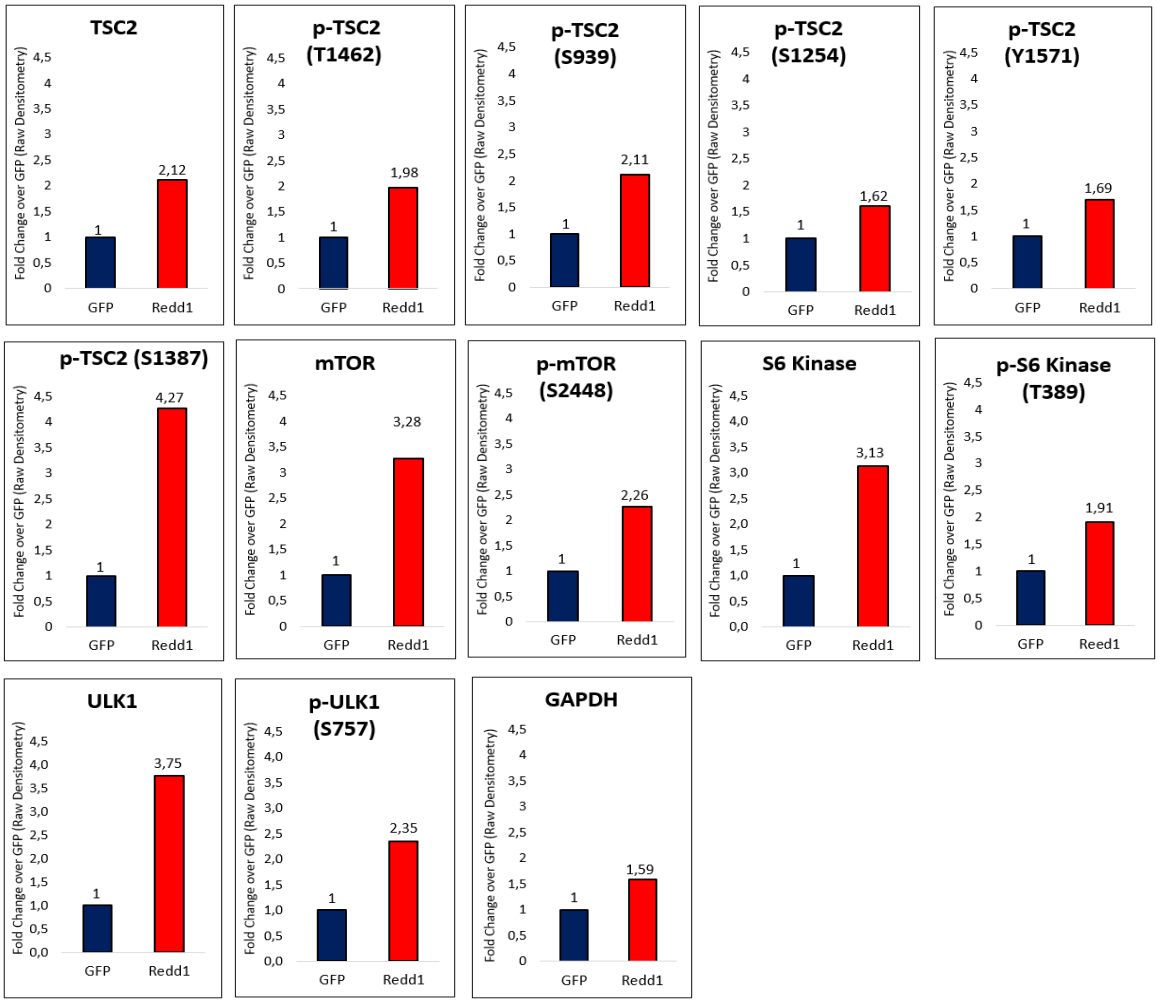

Figure 4.11. Raw densitometric quantitation of protein expression following REDD1 overexpression. Immunoblots images from Figure 4.10 were subjected to densitometric quantitation using Fiji ImageJ v1.49i. Values represented the raw densitometric measurement of each band of interest expressed as a fold change against GFP control.

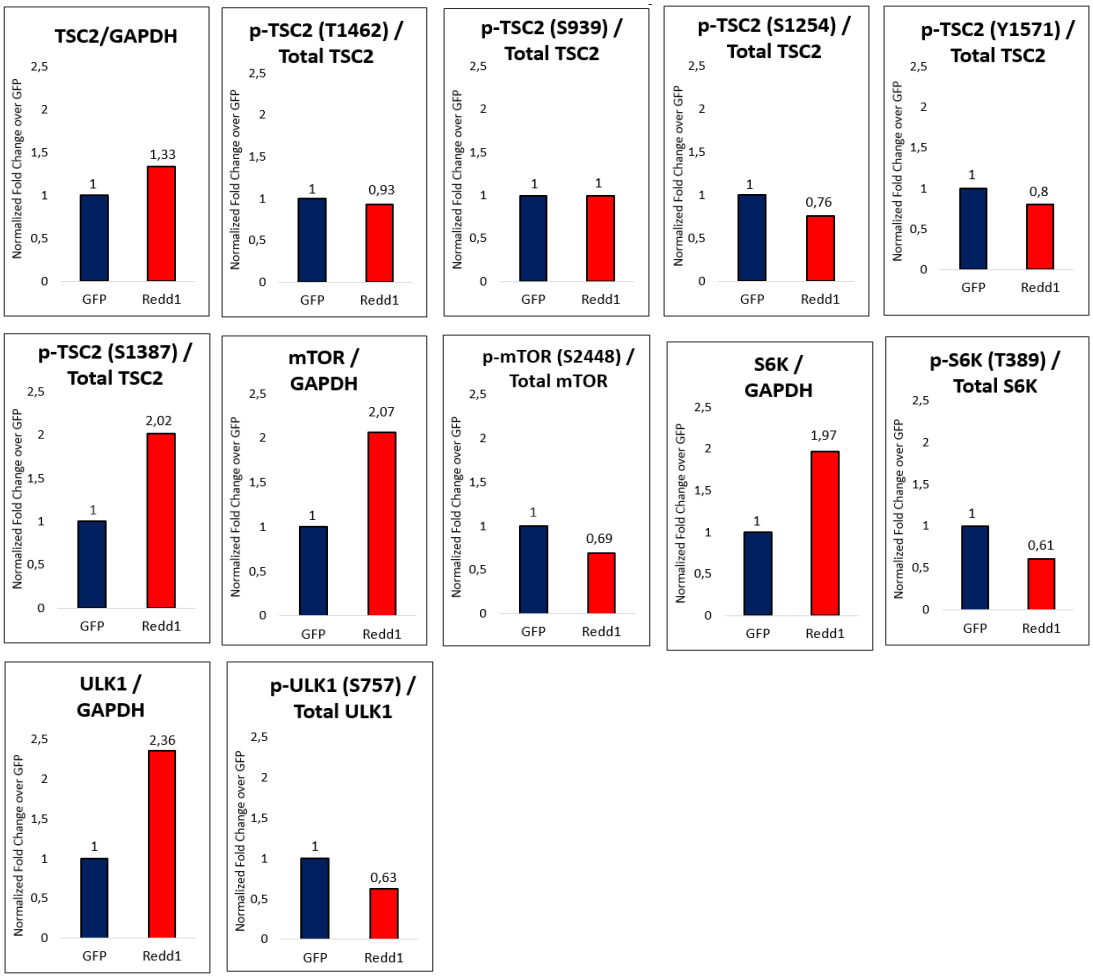

Figure 4.12. Normalized densitometric quantitation of protein expression following REDD1 overexpression. Raw densitometric measurements were normalized against loading control protein GAPDH. Total protein expression were expressed as normalized fold change against GFP control. Phosphorylated forms of the proteins were also normalized against its respective total protein before being expressed as fold changes against GFP control. Following normalization, TSC2 was found to be phosphorylated at Ser1387 which is important for the GAP activity of TSC2. Despite increased total mTOR protein levels, activation phosphorylation at Ser2448 was not observed suggesting that mTORC1 was not active. Consistent with inhibited mTORC1 activity, S6K and ULK phosphorylation at Thr389 and Ser757 respectively by mTORC1 was not decreased.

truly had an effect on the various proteins, the raw densitometry values of each band were normalized to GAPDH (Figure 4.12). Furthermore, in addition to normalization to GAPDH, the phosphorylated proteins (e.g. p-TSC2) were normalized to their respective total protein (e.g. TSC2) (Figure 4.12).

As highlighted in Figure 1.3, TSC2 (tuberin) is in a complex with TSC1 (hamartin) which functions upstream of mTORC1. TSC2 is a GTPase activating protein (GAP) that converts active Rheb-GTP to inactive Rheb-GDP thereby inhibiting mTORC1 activity. TSC2 GAP activity is modulated by both activating (Ser1387 and Tyr1571) and inhibitory phosphorylation (Ser939, Ser1254 and Thr1462) events. As shown in the immunoblots (Figure 4.10) and raw densitometry charts (Figure 4.11), TSC2 seems to be phosphorylated at all residues (Ser939, Ser1254, Ser1387, Thr1462, and Tyr1571). However following normalization, it was very interesting to see that only activating phosphorylation at Ser1387 was observed (Figure 4.12) indicating that following REDD1 overexpression, TSC2 activity is activated.

Consistent with an active TSC2, phosphorylation of mTOR at Ser2448 (target of active Rheb-GTP) was decreased despite increased total mTOR protein levels following REDD1 overexpression (Figure 4.12). Phosphorylation of mTOR at Ser2448 is required for binding to adaptor protein raptor in the mTORC1 complex and important for mTORC1 kinase activity. S6K a kinase important for protein synthesis and cell proliferation, and ULK1 a kinase important for initiation of autophagy are direct substrates of mTORC1. mTORC1 activates S6K and imhibits ULK1 by phosphorylation at Thr389 and Ser757 respectively. Consistent with an inhibited mTORC1 activity, both phosphorylation of S6K and ULK was inhibited by REDD1 overexpression (Figure 4.12). Although we did not directly show induction of autophagy but the immunoblotting results demonstrate that overexpression of REDD1 could inhibit mTORC activity via the activation phosphorylation of TSC2. As mTORC1 is a negative regulator of autophagy, its inhibition by REDD1 overexpression prevented the inhibitory phosphorylation of ULK1 a kinase important for the initiation of the autophagic cascade. Thus we indirectly showed that REDD1 overexpression could induce autophagy and thus GC-induced autophagy is via the transcriptional induction of REDD1 to inhibit mTORC1 activity.

4.2.5 Effect of REDD1 Silencing on GC (Dexamethasone)-induced Autophagy

To further verify that REDD1 is involved in GC-induced autophagy, the effects of REDD1 gene knockdown/silencing was investigated. Ideally we would have first determined the specificity and efficiency of siRNA gene knockdown by examining both gene and protein expression following treatment of cells with various concentrations of siRNA oligos. However, due to time constraints and late availability of the siRNA oligo, this was not possible. Thus, using the knowledge of previous siRNA experiments of other proteins conducted by fellow colleagues in the lab, a final concentration of 40nM of siRNA was used for silencing REDD1 in MLO-Y4 cells. MLO-Y4 cells were transfected with REDD1 siRNA oligos for 24hrs followed by treatment with with Dex for another 24hrs. Cells were then incubated with Cyto-ID Green, fixed, counterstained for actin and nuclei, and mounted on glass slides. Autophagy induction by Dex following REDD1 gene knockdown was examined by confocal immunofluorescence microscopy.

As illustrated in Figure 4.13, Dex can dose-dependently (10^{-6} and 10^{-3}M) induced autophagosome formation as indicated by the increase in green fluorescence staining. Interestingly, cells that were transfected with REDD1-siRNA oligos prior to treatment with Dex (10^{-3} M) exhibit markedly lower autophagosomes indicating that the silencing of REDD1 gene expression could diminish the Dex-induced autophagic response in MLO-Y4 osteocyte like cells. However there are still some autophagasomes formation indicating that REDD1 silencing was not 100% efficient, which is consistent with gene knockdown as opposed to complete gene knockdown. If time permits, the effect of REDD1 silencing on mTORC signaling and activation would have been investigated. However, in light of these preliminary results, we can conclude that REDD1 is important in eliciting the molecular signals of GC-inducing autophagy in MLO-Y4 cells.

4.3 Discussion and Conclusion

Under physiological conditions, bone homeostasis is delicately maintained through the balance between bone formation and resorption (Heino *et al*. 2002). Drugs and conditions that lead to pertubations in this balance can cause osteoporosis, an extremely debilitating disease, that causes fragility fractures and significantly increase

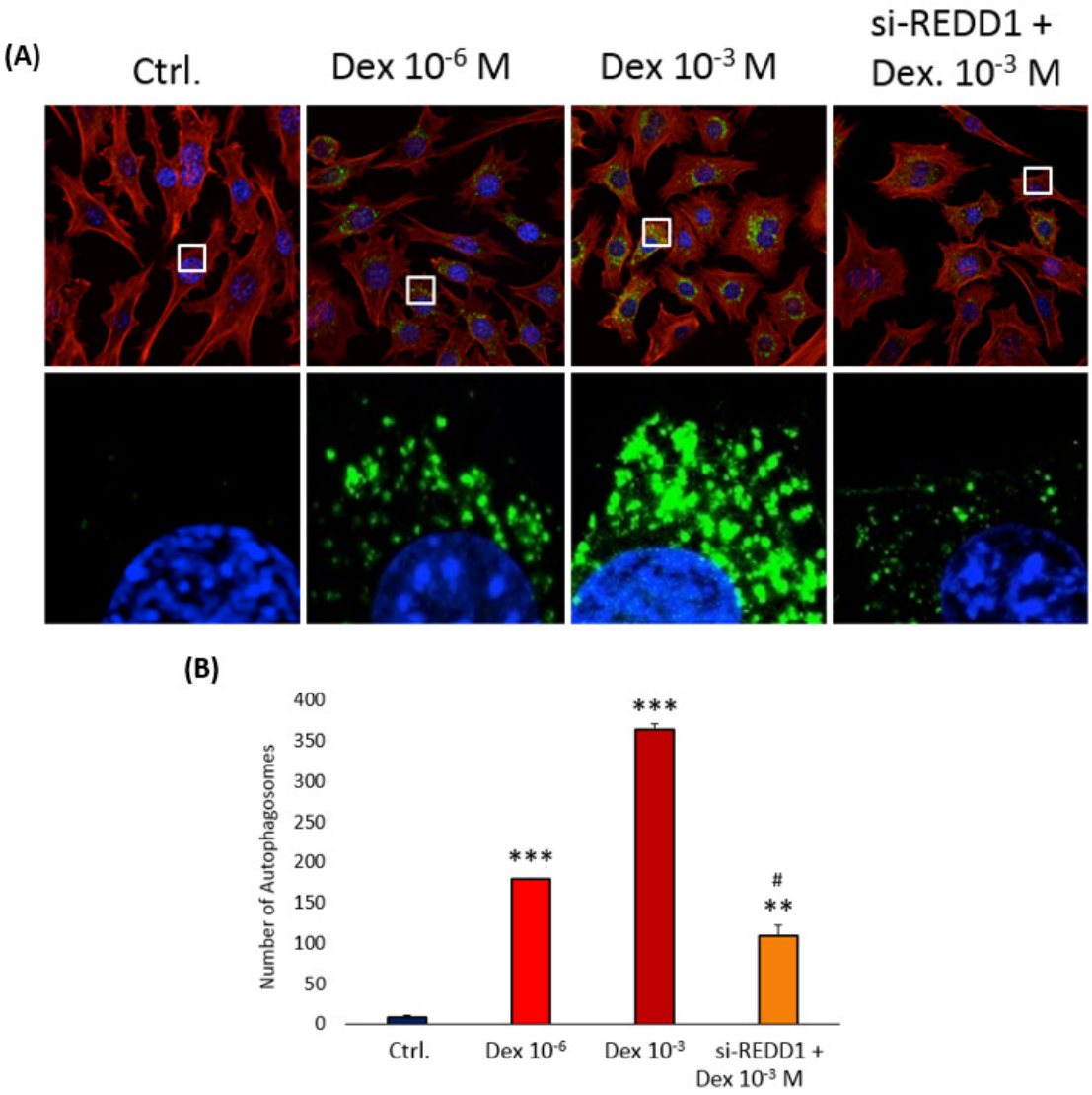

Figure 4.13. REDD1 silencing attenuates GC (Dex)-induced autophagy. (A) MLO-Y4 cells cultured on glass coverslips were transfected with REDD1 40nM siRNA oligos for 24hrs followed by Dex treatment at 10^{-6} and 10^{-3}M for further 24hrs. Cells were incubated with CytoID Green for 30mins prior to fixation with 4% paraformaldehyde. Cells were then immunostained with rhodamine phalloidin (actin; red) and Hoechst (nucleus; blue) and mounted onto glass coverslips for analysis by immunofluorescence on a Nikon confocal microscope setup equipped with a 60x oil emersion lens. Autophagosome formation (green) was markedly reduced following REDD1 gene knockdown suggesting impairment of Dex-induced autophagy. **(B)** Quantitation of the number of CytoID positive autophagosomes under each experimental condition. *P < 0.05; ***P < 0.005 when compared to control. #P < 0.01 when compared to 10^{-3}M.

risk of death in elderly patients (Leboime *et al.* 2010). Glucocorticoid (GC) is the most common cause of drug-related osteoporosis, however the physiopathological mechanism how GC changes the biology of the osteocyte function, remains not completely understood.

Osteocyte autophagy, a crucial adaptative mechanism to cellular stress, has been identified as an important regulator of bone homeostasis and skeletal maintenance (Onal *et al*. 2013). In accordance with previous studies (Jia *et al.*, 2011), our immunofluorescence microscopy of MLO-Y4 osteocyte-like cells showed that Dexamethasone (Dex) can induced the formation and accumulation of autophagic vacuoles suggesting the increased autophagic flux. It was also noted that the site of autophagosome formation and accumulation predominatly occurred within the perinuclear region of the cell. Similarly, the accumulation of LC3-positive autophagosomes in the perinuclear region have been previously described in HeLa cells and mouse embryonic fibroblast, in response to longer serum and amino acids starvation (2-4 hours) (Jager *et al.* 2004). A likely explanantion for this is that the source of the autophagosomal double membranes have been proposed to be "donated" by or originated from various subcellular organelles including the endoplasmic reticulum, Golgi, and mitochondria all of which exhibit somewhat perinuclear residency. Indeed, the biogenesis of autophagasomes, their subcellular distribution and trafficking are current topics of intense investigation in the autophagy field. The purpose of this thesis however, was to investigate the molecular mechanism and signaling pathway governing GC-induced autophagy in osteocytes using the MLO-Y4 osteocyte-like cell line as *in vitro* model.

GC elicit its effects by binding to its cognate receptor GR in the cytoplasm of the cell. The primary action of an activated GC-GR complex is the regulation of gene transcription. Thus how GC-induces autophagy is likely via transcriptional activation of GC-responsive genes that exhibit functional roles in the autophagic cascade. Literature searches identified two potential GC-responsive genes implicated in autophagy, *mkp1* (mitogen-activated protein kinase phosphatase-1) and *redd1* (regulated in development and DNA damage responses 1). Semi-quantitative PCR and real-time qPCR analyses showed that Dex can indeed induced the increased expression of *mkp1* and *redd1* gene in a dose dependent-manner.

MKP1, also known as DUSP-1, is a tyrosine phosphatase that plays important role of immune response to pathogens. It is significantly induced by stress, growth factors and many cytokines, such as TNF-α and TGF-β (Xiao *et al*., 2006; Chen *et al*., 2014). MKP1 plays a critical role in limiting the inflammatory response, thus preventing multi-organ damage and failure caused by an unregulated/exaggerated inflammatory response (Wang *et al.* 2008). Additionally, the immuno-modulatory effect of Dex has been shown to be partially dependent on MKP1 induction, since the anti-inflammatory effect of Dex is attenuated in MKP1-knockout macrophages (Abraham *et al.* 2006). Besides its immune-modulatory function, MKP1 may also participate in the modulation of the autophagic signalling pathway. It was demonstrated that MKP1 can downregulate the activating phosphorylation of ERK-1/2. ERK (extracellular signal regulated kinase) is a MAP kinase that can directly phosphorylates TSC2 at Ser664 and Ser540 residues. Phosphorylation of TSC2 at these serine residues results in the dissociation of TSC1-TSC2 complex, consequently leading to functional inhibition (Ma *et al.,* 2005). Therefore, upregulation of MKP1 can lead to the alleviation of ERK-1/2 inhibitory activity over TSC1-TSC2 complex, consequently upregulating autophagy, through inactivation of mTORC1 activity.

Although Dex induced the expression of *mkp1* gene, the same cannot be said for protein expression. The protein levels of MKP1 did not increase significantly in response to Dex treatment, as suggested by the gene profile. Possibility is that although *mkp1* gene is transcriptionally induced, it was not actively translated into functional proteins. Although showing promising functional roles in downstream autophagy responses and but taking into consideration that protein levels remain unchanged following Dex treatment we focused our subsequent functional investigations on REDD1.

REDD1, also known as DDIT4, RTP801 and dig2, has a widely ubiquitous tissue distribution profile whose low basal expression is significantly increase in response to cellular stress, hypoxia, DNA damage, serum deprivation and glucocorticoid treatments (Wang *et al.* 2003), As with *mkp1* gene, r*edd1* gene expression was significantly increased in MLO-Y4 osteocyte like cells in response to Dex treatment, demonstrated by both semi-quantitative PCR and real-time qPCR. The

induction of *redd1* gene by Dex occurred in a dose-dependent manner and within 6 hrs of treatment. However, as with *mkp1* gene expression, longer periods of stimulation with Dex (26hrs), decreased *redd1* gene expression. Why this was the case, we are unsure but it could be a regulatory mechanism to prevent the unregulated overexpression of *redd1* and *mkp1* gene.

Unlike MKP1 and in accordance to *redd1* gene expression profile, REDD1 protein levels were significantly increased after dose-dependently after Dex treatment in MLO-Y4 cells with protein levels remaining abundantly expressed even at 26hrs. This expression profile suggests that REDD1 may play a more functional important role in GC-induced effects that does MKP1. Consistent with our gene and protein analyses, biochemical studies have shown that Dex-dependent REDD1 induction is mediated by GR, since treatment of cells with the GC antagonist RU486 blocks GC-induced Redd1 gene expression (Wang et al., 2003). In addition, actinomycin D, a protein biosynthesis inhibitor, also prevented REDD1 induction by Dex, suggesting that GCs induce a *de novo* gene transcription of REDD1 (Wang *et al.* 2003). Functionally, preliminary gene silencing data demonstrates a marked reduction in the ability of Dex to induced autophagasome formation in REDD1 knockdown MLO-Y4 cells. The dramatic impact of REDD1 gene silencing on autophagosome formation provide further evidence that REDD1 is functionally required to evoke GC-induced autophagic response. Interestingly, REDD1-dependent induction of autophagy have been reported in lymphocytes treated with Dex (Molitoris *et al.* 2011).

As with MKP1, REDD1 functions upstream of TSC1-TSC2 and Rheb in the mTORC1 signaling cascade (Corradetti *et al*. 2005). However unlike MKP1 REDD1 inhibit mTORC1 activity in a TSC1-TSC2 dependent manner by activating TSC1-TSC2 GAP activity via activating phosphorylation of TSC2. *In vitro* and *in vivo* studies have shown that, under physiological conditions, phosphorylation of TSC2 at serine residues 939, and 981 and threonine residue 1462 by AKT will recruit the cytosolic anchoring protein 14-3-3 to TSC2, disrupting the TSC1-TSC2 complex (Aicher *et al*., 2001; Huang and Manning. 2008; Ma *et al*., 2009; Orlova and Crino, 2010). Furthermore, phosphorylation of TSC2 at Ser1254 by p38-activated kinase MK2 (MAPKAPK-2) augments the interaction between TSC2 and 14-3-3 (Li *et al.*, 2003; Huang and Manning. 2008; Orlova and Crino, 2010). When TSC2 is not in association with TSC1,

the GAP activity of TSC2 is deactivated and can no longer hydrolyze active Rheb-GTP to inactive GDP form, resulting in continued activation of mTORC1 activity (Huang and Manning. 2008; Orlova and Crino, 2010; Mendoza *et al.*, 2011; Beauchamp *et al*., 2012).

Our REDD1 overexpression experiments revealed Ser939, Ser1254 and Thr1462 sites were not phosphorylated suggesting that TSC2 is in its active state bound to TSC1 and not to 14-3-3. Interestingly, REDD1 overexpression induced the activation phosphorylation of TSC2 at Ser1387. This site is phosphorylated by AMPK which leads to the activation of TSC2 GAP activity allowing active Rheb-GTP to by hydrolyzed into inactive Rheb-GDP form. Another activating phosphorylation site of TSC2, Tyr1571 (Aicher *et al*., 2001), was not affected by REDD1 overexpression.

How REDD1 overexpression affects the phosphorylation status of TSC2 is unclear. Instead of phosphorylation, REDD1 activates TSC2 by 14-3-3 protein sequestration through association of REDD1/14-3-3 complex and promoting dissociation of TSC2/14-3-3 complex. REDD1 sequesters 14-3-3 from TSC2 by movement of 14-3-3 proteins bound to the two AKT phosphorylation sites on TSC2 (Ser939 and Thr1462) from these sites to Ser137 on REDD1, thereby allowing TSC2 to associate with TSC1 and activating its GAP activity (Bhasker *et al.*, 2007; DeYoung *et al*., 2008; Huang and Manning. 2008; Orlova and Crino, 2010; Regazzetti *et al*., 2012). Thus it is likely that the overexpression of REDD1 led to the sequestration of 14-3-3 away from TSC2 allowing to form an active complex with TSC1.

Interestingly, previous work in our lab have shown that Dex treatment leads to impaired phosphorylation of AKT at Thr308 and Ser473, both required for the activation of AKT kinase activity to phosphorylate downstream substrates including Ser939 and Thr1462 on TSC2. However, how GC inhibits AKT activation remains to be explored. But taking collectively, Dex treatment can lead to inactivation of AKT activity preventing the inhibitory phosphorylation of TSC at Ser939 and Thr1462 and binding of 14-3-3 proteins. At the same time Dex transcriptionally induces REDD1 which can sequester 14-3-3 proteins by forming REDD1/14-3-3 complexes allowing active TSC1-TSC2 complexes to form. Further activating phosphorylation at Ser1387

activates the GAP activity of TSC2 allowing it to hydrolyze Rheb-GTP to Rheb-GDP to inhibit mTORC1 activity.

In accordance with an active TSC2, activation phosphorylation of mTOR at Ser2448 was attenuated following REDD1 overexpression. Furthermore, the phosphorylation status of downstream substrates of mTORC1, such as S6K and ULK1 (mammalian homologue of yeast Atg1) kinases was also attenuated. The lack of inhibitory phosphorylation of ULK1 by mTORC1 was of particular importance as this kinase is directly implicated in the initiation of autophagy and as a convergence point for multiple signals that control autophagy (Stephan and Herman, 2006; Chan *et al.*, 2007). When activated, ULK1 can bind to several autophagy-related (Atg) proteins, regulating their phosphorylation states and intracellular trafficking (Kamada *et al*., 2000; Young *et al*., 2006; Lee *et al*., 2007; Hara *et al*., 2008). By demonstrating that ULK1 was activated, that is, inhibitory phosphorylation was attenuated when REDD1 was overexpressed, it was direct evidence to support that the upsteam molecular pathway that governs GC-induction of autophagy is dependent on the REDD1.

Collectively, our data provides strong evidence that REDD1 plays an important role in signaling the activation of autophagy in response to GC treatment. If time permits, it would been ideal to further decipher the autophagy signaling cascade downstream of ULK1 activation following REDD1 overexpression. Furthermore, comparison of the signaling effects of REDD1 silencing to REDD1 overexpression would have provided even stronger support for a positive role of REDD1 in GC-induced autophagy.

CHAPTER FIVE

CHARACTERIZATION AND PROFILING OF MLO-Y4 OSTEOCYTIC-LIKE CELLS-DERIVED EXOSOMES

5.1 Introduction

The terminally differentiated osteocyte is a spindle-shaped cell with numerous dendritic projections that penetrates throughout the bone matrix. Being entombed in the bone matrix for its entire lifespan, these dendritic projections are crucial for intercellular communication with neighbouring osteocytes as well as with other cells on the bone surface such as osteoblasts and osteoclasts. However, osteocytes have been shown to exert regulatory influences beyond the boundaries of the bone, such as in phosphate metabolism, but the mechanism by which this occurs remains unclear. It is likely that osteocytes release soluble factors in the form of exosomes to exert influences beyond the local bone environment. Exosomes are small (50-100nm) extracellular vesicles released by cells in to the local microenvironment and circulation (Kamioka et al. 2001). Exosomes have been shown to carry bioactive materials such as proteins, membrane receptors, microRNAs, messenger RNAs, carbohydrates, and organelles, all of which could affect various systemic tissues (Ratajcsak *et al*., 2006; De Maio *et al*., 2011). However, osteocyte-derived exosomes have yet be described. Furthermore, it has been reported that autophagy and exosome production and release share a common pathway that exists in an inverse relationship.

Multivesicular bodies (MVB) are the convergence point that link exosome secretion and autophagy. MVB are intracellular compartments that houses intraluminal vesicles (ILV) (immature exosomes) and via as yet ill-defined regulatory mechasims will fuse with the plasma membrane to release their cargo, now termed exosomes to the extracellular environment (Buschow *et al.*, 2005). Alternatively, when cells undergo autophagy, MVBs are targeted to fuse with autophagasomes to form a prelysosomal vesicle called an amphisome which ultimately fuse with lysosomes to form autolysosome (Gordon *et al.*, 1988; Berg *et al.*, 1998; Fader *et al.*, 2008; Fader and Colombo, 2009). Although a great deal of effort has been placed on understanding exosome biogenesis, the molecular signals and the metabolic clues that coordinate the fate of MVBs between secretory MVB (i.e. exosomes) or their integration with the degradative and recycling pathways (i.e. autophagy) are not completely understood. Therefore, the major aims of this chapter was to determine whether MLO-Y4 osteocyte-like cells release exosomes and how GC-induced autophagy affects exosome released by MLO-Y4 osteocyte-like cells.

5.2 Results

5.2.1 Effect of GC (Dex) on MLO-Y4 Morphology

OYs are cytoskeletally dynamic cells possessing numerous dendritic processes which facilitate intercellular communication and potentially the site of exosome release. An interesting phenomenon observed during Dex-induced autophagy in MLO-Y4 cells was an apparent reorganization of cellular morphology and loss of dendrites (Figure 5.1). Closer examination using immunofluorescence staining revealed that Dex treatment dose-dependently induced a drastic rearrangement of the actin cytoskeleton (red), resulting in a loss of dendritic processes and concomitant increase in stress fibers formation ultimately switching the morphology of MLO-Y4 cells from a spindle-to-polygonal appearance (Figure 5.1A). The length of the dendrite sprouting from each cells was quantified and was found to be decrease in response to increased concentrations of Dex (Figure 5.1B). Although the exact mechanism underlying this phenomenon is presently unclear, it appears to be closely coupled with the onset of autophagy. Indeed, the cytoskeleton is known to be intricately linked to autophagosome formation as well as exosome secretion.

5.2.2 Optimization of Exosomes Isolation Protocol

Exosomes have been isolated successfully from cell culture medium and several body fluids, such as serum, plasma, breast milk and urine (Ashcroft *et al.* 2012; Keller *et al*. 2011). Although there are many different protocols that can be employed for the purification of exosomes from biological solutions, the most commonly used protocol utilize the basic principle of separation through a series of centrifugation, filtration and ultracentrifugation steps (See Materials and Methods Section xxx). First to establish that MLO-Y4 cells release exosomes, a small scale attempt was carried out. MLO-Y4 were cultured in four T175 flasks to 70% confluency, to which the cells were then split into two groups: one group was maintained in 25ml of completed media supplemented with serum (2.5% FBS and 2.5% FCS) and antibiotics, and the other group in 25ml serum-free (SF) media with antibiotics. Both groups were also treated with or without 10^{-3}M Dex for 48hrs. Two groups were established in order to assess the levels of MLO-Y4-derived exosomes (serum-free conditions) compared with contaminating exosomes already present in serum (both FBS and FCS) that are generally used in tissue culture.

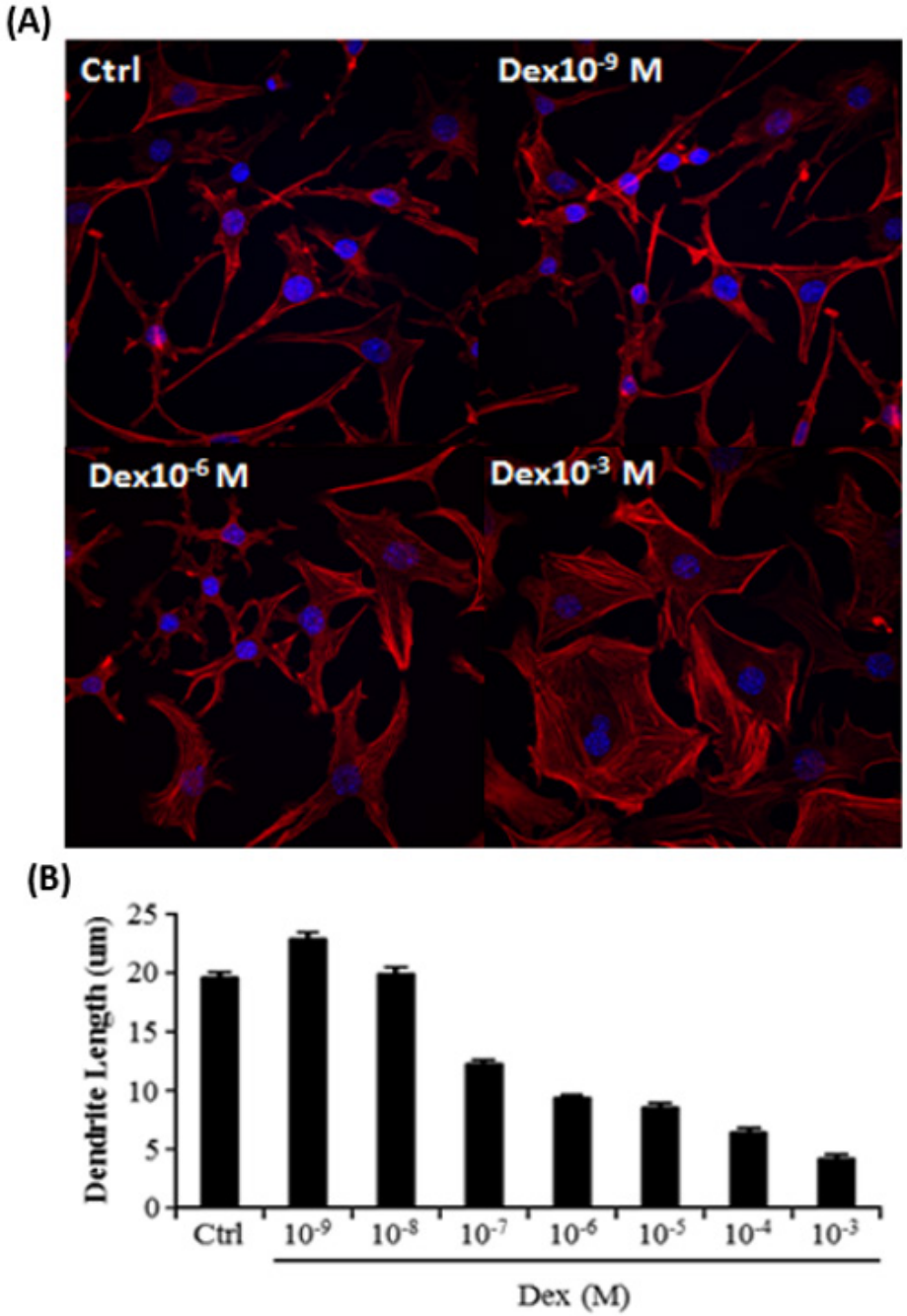

Figure 5.1. Dex-induced retraction of MLO-Y4 cell dendritic processes. MLO-Y4 cultured RTC-coated coverslips were stimulated with various concentrations of Dex (10^{-9}, 10^{-8}, 10^{-7}, 10^{-6}, 10^{-5}, 10^{-4}, 10^{-3} M) for 24 hours. Following incubation, cells were fixed and immunostained with rhodamine phalloidin (actin; red) and Hoechst (nuclei; blue). Immunofluorescence images were acquired on a Nikon confocal microscope equipped with a 60x oil immersion lens. **(A)** Dex results in a dose-dependent retraction and loss of dendritic processes and increased formation of actin stress fibres. **(B)** Quantitation of the average dendritic length following Dex treatment.

Following 48hrs incubation, exosomes-conditioned medium (ECM) in each flask were collected and initially processed as described in Materials and Methods Section XXX, without carrying out the concentration of the conditioned media step and ultracentrifugation in a floor standing ultracentrifuge (Beckman Coulter Optima L-90K). Extracted exosomes (resuspended in 50-100µl of PBS) were then analysed by immunoblotting (10-20ul exosomal sample per well) against known exosomal markers HSP70 and CD9 to determine the success of isolation procedure, the amount obtained and the purity of the exosomes.

Figure 5.2 is an immunoblot of the first batch of isolated exosomes and their respective TCP lysates. The result showed that no exosomes were isolated under SF conditions whereas abundant amounts of exosomes were isolated from conditioned media supplemented with serum. A few outcomes were obtained from this result. Firstly, the exosome isolation procedure works as endogenous amounts of exosomes were isolated from cells maintained in media containing serum. Secondly, the serum used in our media to maintain the cells contains an abundant amount of endogenous exosomes that could contaminate the cell-derived exosomes. Thirdly, MLO-Y4 cells either do not release exosomes or release very small amounts of it and thus the starting volume of ECM used for isolation resulted in amounts that could not be detected by immunoblotting.

Two more attempts were carried out under SF conditions utilizing the same protocol, but increased the starting ECM from 25ml (one T175 flask) to 50ml (two T175 flasks) for 48hrs (batch 2) and another group with 200ml (four T175 flasks) for 72hrs (batch 3), all carried out in the absence or presence of 10^{-3}M Dex. As shown in Figure 5.3, 50ml of starting ECM (from 48hrs culture) still resulted in no exosomes being isolated. However, when 200ml of starting ECM (from 72hrs of culture) was used, we detect a faint HSP70 band (green box) in the exosomes isolated from cells without Dex treatment. These results demonstrate that MLO-Y4 cells do indeed secrete exosomes but the amount released is very small. Alternatively the method used may not be efficient in isolating such small amounts of exosomes.

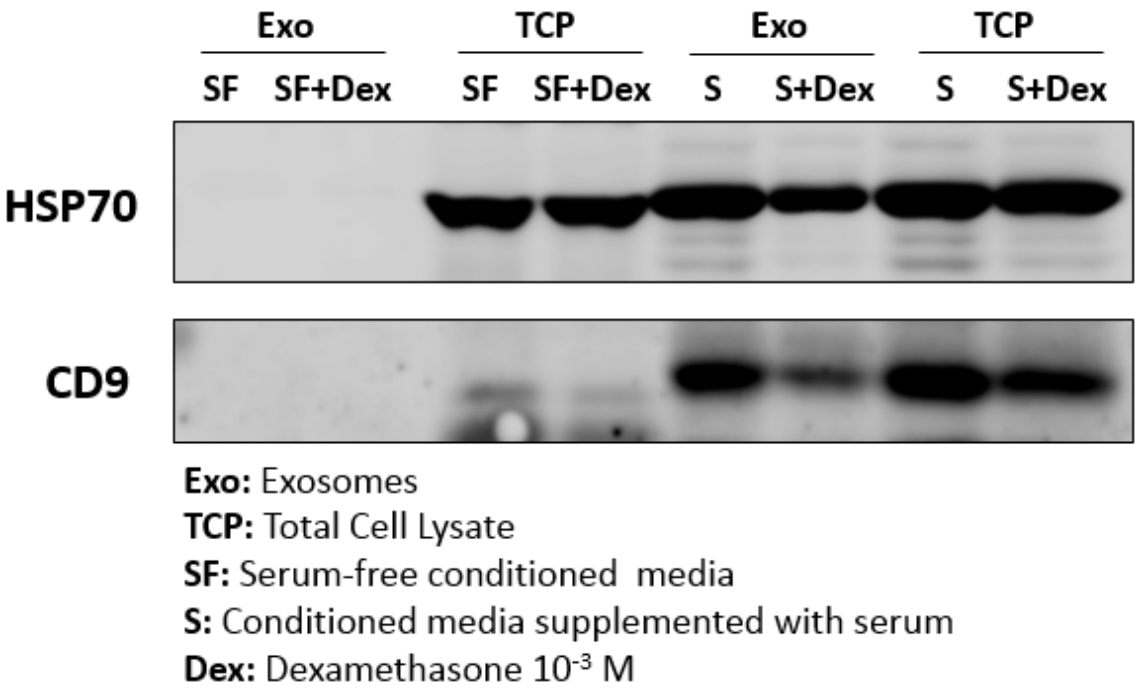

Figure 5.2. Immunoblot analysis of isolated MLO-Y4 exosomes in the presence and absence of serum. MLO-Y4 cells were maintained in 25ml of indicated conditioned media (presence or absence of serum; and with or without dex) for 48hrs. Exosomes were isolated using differentiatial ultracentrifugation procedure with a floor standing ultracentrifuge (Beckman Coulter Optima L-90K). Isolated exosomes and total cellular proteins (TCP) were resolved on a 10% SDS-Page gel and immunoblotted for known exosome markers HSP70 and CD9 using specific antibodies. Immunoblots demonstrates that serum containing conditioned media contains abundant levels of endogenous exosomes and thus serum should be omitted during preparation of exosome-conditioned media (ECM). Unfortunately, no exosomes were isolated from serum-free conditioned media either indicating that MLO-Y4 cells do no secrete exosomes or the amound secreted was too low to be detected (ie. starting volume of ECM was too low).

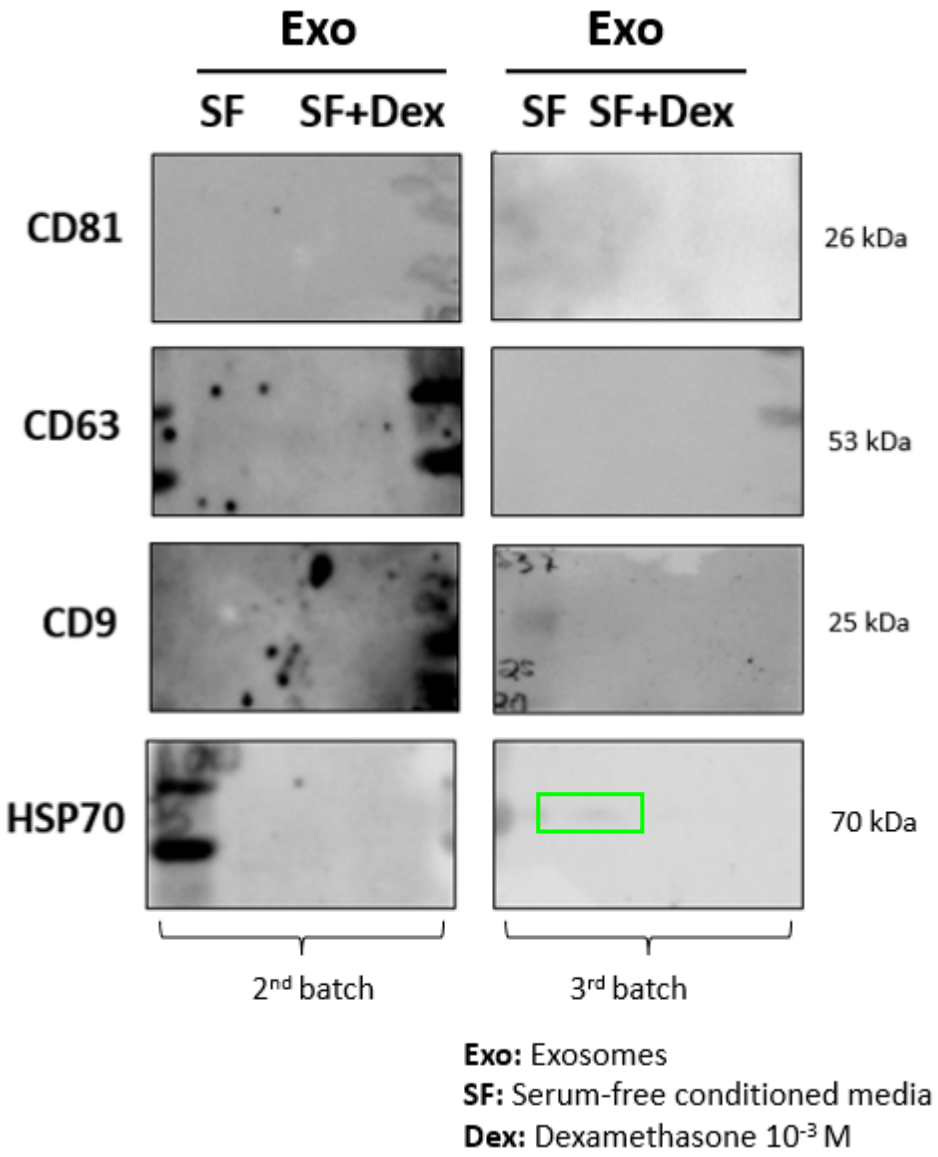

Figure 5.3. Immunoblot analysis of 2nd and 3rd batches of isolated exosomes from MLO-Y4 cells cultured under serum-free conditions. MLO-Y4 cells were maintained in serum-free conditioned media (with or without dex) for 48 (batch 2) or 72hrs (batch 3). ECMs were harvested after incubation (50ml for batch 2 and 200ml for batch 3) and exosomes were isolated using differentiatial ultracentrifugation procedure with a floor standing ultracentrifuge (Beckman Coulter Optima L-90K). Isolated exosomes were resolved on a 10% SDS-Page gel and immunoblotted for known exosome markers HSP70, CD63, CD81 and CD9 using specific antibodies. Immunoblots demonstrates that with 50ml of starting ECM no detectable amounts of exosomes were isolated. Higher volume of ECM (200ml) collected after 72hrs incubation show a very faint HSP70 band in the absence of Dex indicating that there are exosomes being secreted but the levels are too low to be detected or efficiently isolated.

From literature searches, it was proposed that to enhance the efficiency and chance of successfully isolating small amounts of exosomes from large volumes of conditioned media, a concentration step should be added into the procedure prior to ultracentrifugation in a tabletop rather than a floor standing ultracentrifuge to minimize loss of exosomal material. As shown in Figure 5.4A, just by filtering and concentrating the starting ECM through a Centricon PLUS centrifugal concentrator (10,000 NMWL) and carrying out ultracentrifugation on a tabletop ultracentrifuge (Bechman Coulter Optima MAX-TL), we can successfully enrich the amount of exosomes isolated.

5.2.3 Characterization of MLO-Y4-derived Exosomes

The purified exosomes expresses markers proposed to be frequently found in exosomes such as HSP70, CD63, CD81 and CD9, and appears to be enriched in exosomes as compared to their respective TCP (Figure 5.5A). Interestingly, following Dex treatment the amount of exosomes isolated was significantly reduced compared to without Dex treatment (in both batch 4 and batch 5 exosomes). Densitometric analysis of the bands for each of the marker proteins confirmed the decrease amounts of isolated exosomes following Dex treatment (Figure 5.5B). Comparison of the β-actin levels in TCP shows little difference between cells treated with Dex and cells that are untreated indicating that the decrease in exosomes released following Dex treatment is not a result of increased cell death (Figure 5.5A). Furthermore, nitrocellulose membranes stained with Ponceau S Red to show the full exosomal protein profile revealed similar results to immunoblotting where Dex treatment reduced the amount of exosomes secreted (Figure 5.5C). Also noted following Ponceau S Red staining was that the exosomal protein profile was different to TCP, indicating that many of the proteins in or on exosomes are distinct from the proteins from TCP (Figure 5.5C). Concentrations of subsequent batches of isolated exosomes were quantified by Bradford protein quantitation methods and summarized in Table 5.1. Consistent with earlier batches, the amount of isolated exosomes decreased following Dex treatment. This is in line with the hypothesis that induction of autophagy will lead to decrease exosome secretion.

To verify, that the isolated exosomes were not contaminated with other potential organelles such as mitochondria, immunoblotting against PINK1, an inner mitochondrial

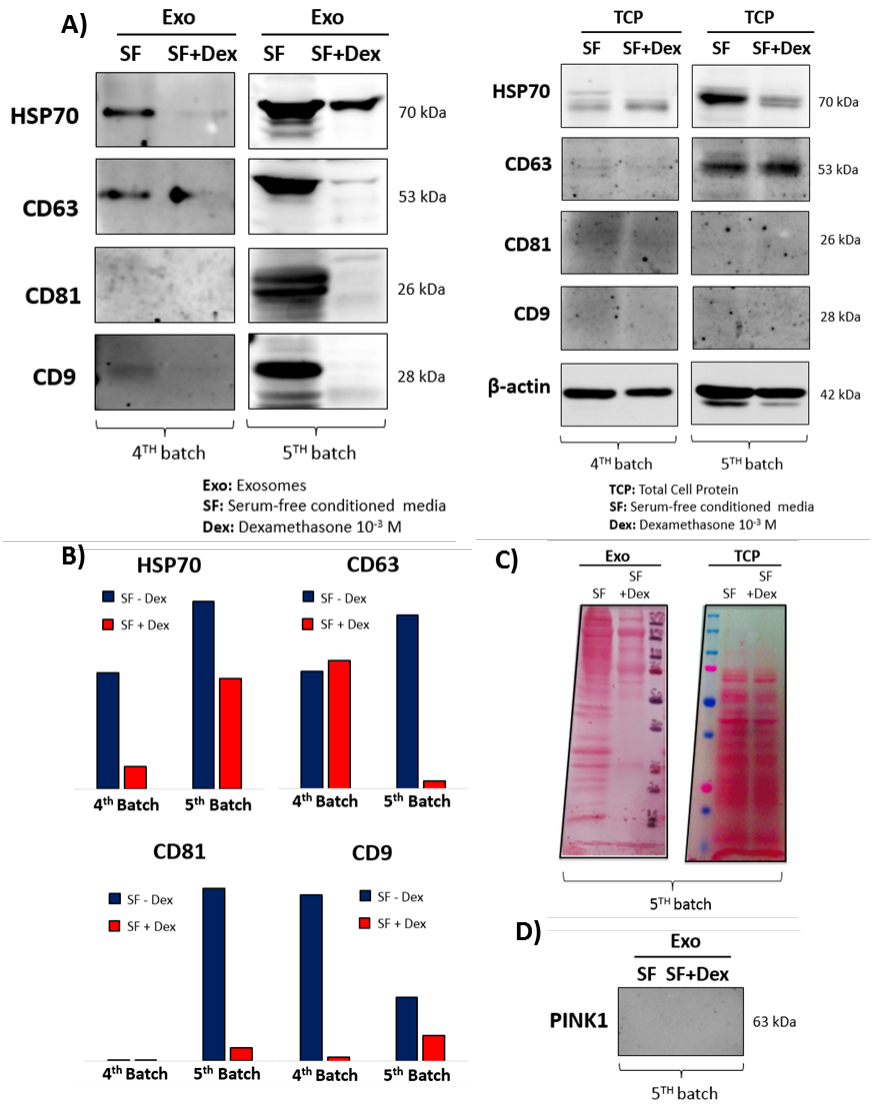

Figure 5.4. Exosome secretion by MLO-Y4 cells is markedly reduced following Dex treatment. MLO-Y4 cells were maintained in 200ml of serum-free conditioned media (with or without dex) for 72hrs. ECM was harvested after incubation, was concentrated down to a smaller volume using Centricon PLUS centrifugal concentrator (10,000 NMWL) prior to differentiatial ultracentrifugation with a tabletop ultracentrifuge (Beckman Coulter Optima MAX-TL) according to a modified protocol. Isolated exosomes and TCP were resolved on a 10% SDS-Page gel and immunoblotted for known exosome markers HSP70, CD63, CD81 and CD9 using specific antibodies. **(A)** Immunoblots demonstrates with the modified protocol, exosomes could be successfully and effectively isolated from ECM. MLO-Y4 cells-derived exosomes expressed all the exosome markers. Dex treatment results in reduced exosome secretion and therefore amount isolated. Densitometric quantitation of immunoblots **(B)** and Ponceau S Red staining of membranes **(C)** confirmed the reduction of exosome secretion. The reduction was not due to decreased number of cells as protein profiles from TCP were similar. **(D)** Immunoblot demonstrates that isolated exosomes were not contaminated by mitochondria membranes as no PINK1 (resident mitochondrial protein) expression was observed.

Batch	SF-media (mg/ml)	SF-media + Dex (10^{-3}M) (mg/ml)
6th	1,365	0,263
7th	1,584	1,036
8th	0,5255	0,351

Table 5.1 Exosome Concentration for subsequent batches of isolated exosomes. Concentrations of isolated exosomes were quantified by Bradford Protein Quantitation Assay. As indicated Dex treatment results in marked reduction in exosome secretion and therefore the amount that could be isolated.

membrane-targeted protein, was carried out (Figure 5.5C). As depicted in the immunoblot the exosomes isolated (batch 5) were indeed purified exosomes, and are not contaminated with mitochondrial membrane fragments. Unfortunately, there were not enough exosomes to immunoblot against PINK1 for batch 4 exosomes. These results, for the first time showed that MLO-Y4 osteocyte-like cells do release exosomes into the extracellular medium providing support that primary osteocytes are more than likely to do the same *in vivo* for intercellular communication.

Now that we have established that MLO-Y4 cells and possibly primary osteocytes produce and secrete exosomes, what then, are the physiological functions of these exosomes? Is the exosomes used as a form of waste removal to eliminate proteins that are not required by the cell or is it a form of intercellular communication to allow for the exchange of proteins or informations to external target cells. To try to address this question we examined the expression of factors known to be secreted by osteocytes that affect other bone cells. RANKL and sclerostin are two known factors secreted by osteocytes that regulate osteoclast and osteoblast formation and function respectively. Unfortunately as shown in Figure 5.5A, RANKL was not found to be expressed in exosomes and surprisingly very weakly expressed in corresponding TCP isolated from MLO-Y4 cells. This is in stark contrast to primary osteocyte which expresses abundant amounts of membrane bound and secreted RANKL *in vitro* and *in vivo*, and osteocyte-derived RANKL corresponds to almost all RANKL secreted in the bone matrix *in vivo* (Nakashima *et al*. 2011; Xiong *et al.*, 2011). On the other hand, sclerostin a potent inhibitor of osteoblast differentiation and function (Winkler *et al*., 2003; Li *et al*., 2008) was found to be expressed in both exosomes and TCP from MLO-Y4 cells. This result is the first to show that sclerostin is secreted as a cargo of exosomes and suggest that sclerostin following synthesis in the cell may be targeted to the MVB for incorporation into ILV as cargo to be secreted as part of exosomes.

Osteocytes have been proposed to be able to carry out bone resorption of the lacuna space in which it resides via a process known as osteocytic osteolysis. However, bone resorption the primary function of osteoclasts requires two important prerequisites: generation of an isolated acidic microenvironment which allows the dissolution of the

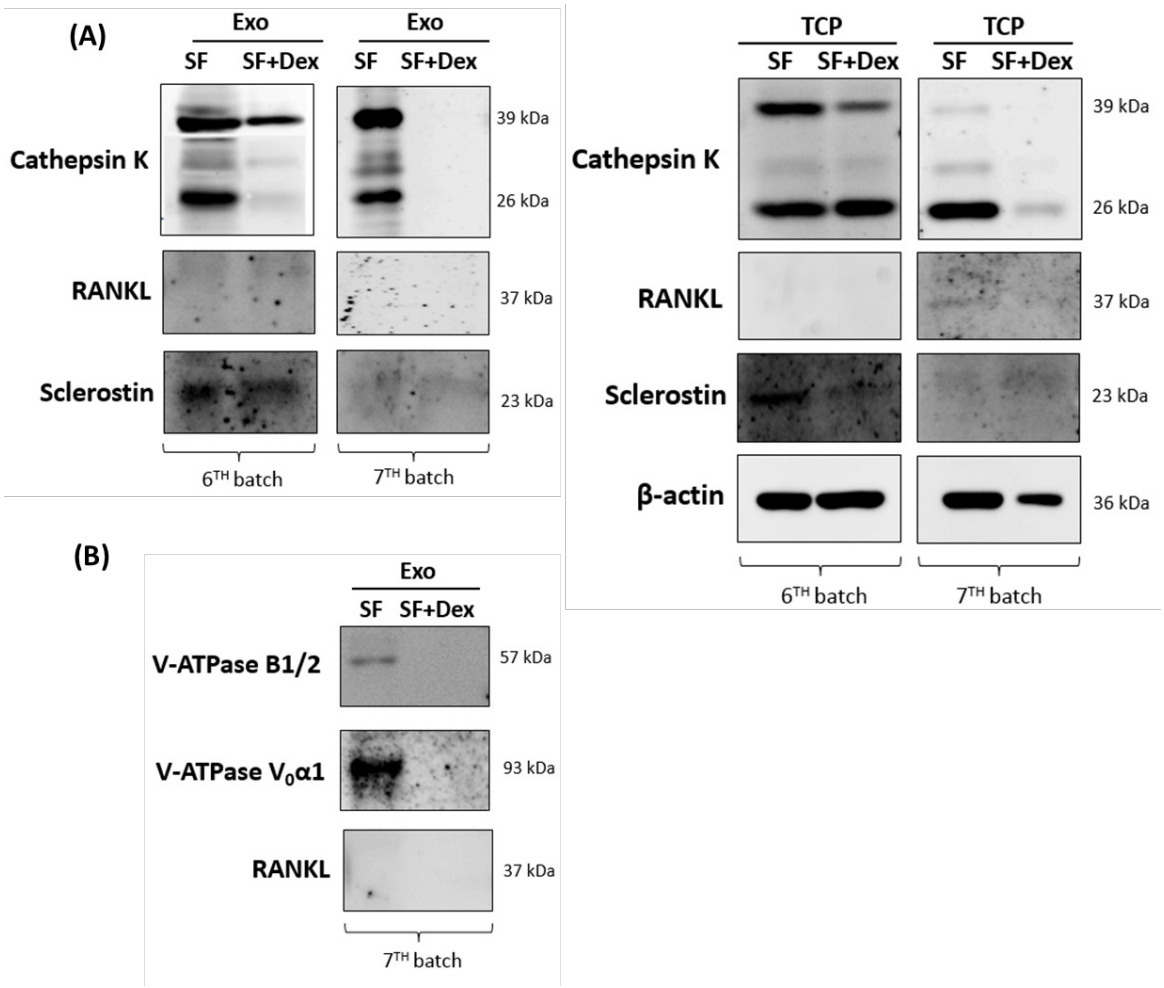

Figure 5.5. MLO-Y4 cells-derived exosomes expresses sclerostin, cathepsin K and V-ATPases. MLO-Y4 cells were maintained in 200ml of serum-free conditioned media (with or without dex) for 72hrs. ECM was harvested after incubation, was concentrated down to a smaller volume using Centricon PLUS centrifugal concentrator (10,000 NMWL) prior to differentiatial ultracentrifugation with a tabletop ultracentrifuge (Beckman Coulter Optima MAX-TL) according to a modified protocol. Isolated exosomes and TCP were resolved on a 10% SDS-Page gel and immunoblotted for RANKL, sclerostin, cathepsin K and V-ATPase V1 subunits B1/2 and V0 subunit a1 with specific antibodies. **(A)** RANKL the master regulator of osteoclast formation and function was not found to be expressed on MLO-Y4 cells-derived exosomes by immunoblot analysis but sclerostin a potent inhibitor of osteoblasts were. Interestingly, cathepsin K an proteolytic enzyme involved in osteoclastic bone resorption was also found to be abundantly expressed and processed in exosomes. (B) For cathepsin K to be processed from its inactive propeptide (~39kDa) to active mature form (26kDa) and acidic environment is required. V-ATPase proton pump (depicted by V1B1/2 and V0a1) was found to be expressed on exosomes and would provide the necessary acidic environment for cathepsin K processing and activation.

mineralized bone and the subsequent break down of the collagen matrix by cathepsin K (also activated by the acidic microenvironent). Primary osteocytes have been shown to express cathepsin K, but they do not possess the required specialized membrane compartment known as the ruffled border that is specifically utilized by the osteoclasts to isolate and acidify (via the V-ATPase proton pump) the resorption lacuna during bone resorption. Consistent with previous studies, cathepsin K was found to be abundantly expressed in TCP of MLO-Y4 cells, and very surprisingly, was also found to be highly enriched in exosomes (Figure 5.5A). More importantly, not only was the pro-immature form of cathepsin K (39kDa) was detected in the exosomes but also the cleaved activated mature form (26kDa). For cathepsin to be cleaved and activated, an acidic environment must be available. Thus we examined the exosomes for the presence of the V-ATPase proton pump complex, the machinery required for acidification process. True enough, in Figure 5.5B, exosomes expresses both the V1B1 subunit, and the V0a1 subunit, indicating that a functional V-ATPase complex is present on exosomes. The functional V-ATPase complex could provide the necessary acidic environment in the exosomes to cleave and activate cathepsin K. Collectively, these data to my knowledge is the first to provide evidence that the exosomes released by MLO-Y4 cells and possibly primary osteocytes contains factors that could affect osteoblast formation and function (sclerostin) as well enzymes (cathepsin K and V-ATPase) involved in bone resorption.

5.2.4 Effects of MLO-Y4 cells-derived Exosomes on Bone Marrow Monocytes

To test the functional outcomes of the isolated exosomes, we have started to conduct preliminary investigations into the effects of MLO-Y4-derived exosomes on other bone cells such as osteoblasts, osteoclasts and osteoclast precursor cells (bone marrow monocytes; BMMs). But due to time constraint, only some preliminary results on BMMs were obtained. Although we did not detect RANKL on the purified exosomes (Figure 5.5A), we were still interested to see whether MLO-Y4 cells-derived exosomes will be taken up by BMMs, precursors to mature osteoclasts. Isolated exosomes were labelled with Exo-Green fluorescent stain to enable the visualization of the exosomes following uptake by cells. MCSF-dependent BMMs cultured on glass coverslips were incubated with 10µl labeled exosomes for 24hrs, following by fixation in paraformaldehyde and

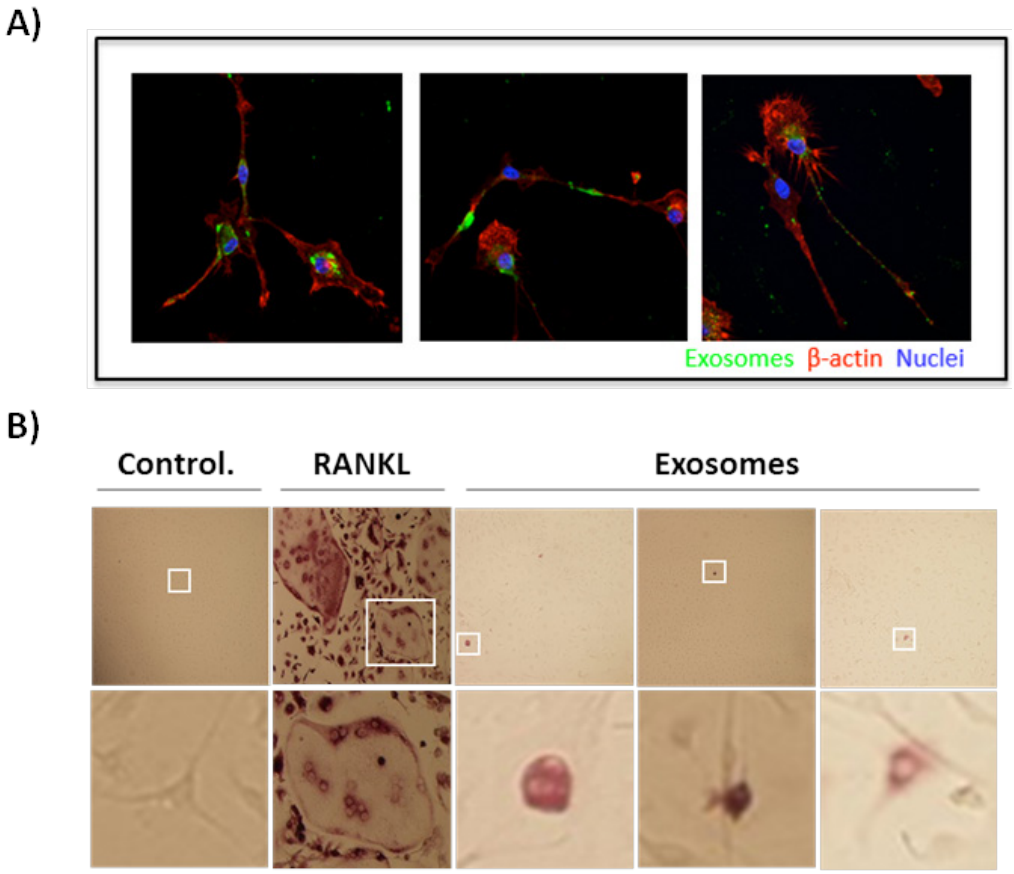

Figure 5.6. Effect of MLO-Y4 cells-derived exosomes on osteoclast precursors, bone marrow monocytes. (A) Bone marrow monocytes (BMM) cultured cultured on glass coverslips were incubated with Exo-Green labelled MLO-Y4 cells-derived exosomes for for 24 hours. Cells were fixed, immunostained with rhodamine phalloidin (actin; red) and Hoechst (nucleus; blue), and analysed for exosome uptake by immunofluorescence Accumulation of green positive exosomes were found in BMMs indicating that the exosomes were actively taken up by the cells. **(B)** Osteoclast formation induced by MLO-Y4 cells-derived exosomes. BMMs were incubated with MLO-Y4 cells-derived exosomes or RANKL for 5 days to induce osteoclast formation. Cells were then fixed and stained for TRAP, an enzymatic marker of osteoclast formation. RANKL induces large multinucleated TRAP positive osteoclast formation consistent with its role as a master regulator of osteoclast formation. BMM treated with exosome did not form osteoclasts, but did show signs of TRAP staining indicating the possibility that RANKL was expressed on exosomes but at a level that could not be detected by immunoblot analysis. Control BMMs that were untreated did not stain for TRAP at all.

immunostaining for actin and nuclei. Coverslips were then mounted onto glass slides for assessment by immunofluorescence microscopy. As illustrated in Figure 5.6, Exo-Green labelled exosomes were internalized by BMMs. Interestingly internalized exosomes were found to accumulate at specific localizations at the cell periphery in filapodia like projections as well as in the perinuclear region of the cell.

Given that BMMs uptake the exosomes, we next assessed whether the exosomes could induce osteoclast formation. MCSF-dependent BMMs were incubated with various amounts of exosomes for 5 days followed by fixation in paraformaldehyde and stained for TRAP activity, a marker of expressed when BMM differentiate down the osteoclast lineage. Soluble recombinant RANKL (200ng/ml) was used as positive control. As shown in Figure 5.5B, RANKL could induce the formation of large multinucleated "pancake" shaped osteoclasts that are positive for TRAP staining. Also note that mononuclear BMMs that are committed to differentiate down the osteoclast lineage also expressed TRAP, whereas BMMs that have not been stimulated with RANKL and therefore not committed to become an osteoclast remain TRAP negative. Interestingly, although most cells were TRAP negative in the exosomes treated groups, there are some cells that stained positive for TRAP. This indicates that there are some level of RANKL expressed on the exosomes but the amount is too low (and why it was not detectable by immunoblotting) to be able to induce all the cells to commit to the osteoclast lineage. Collectively, these preliminary results provide promising functional outlook for the effects of MLO-Y4 cells-derived exosomes on other bone cells such as the osteoblast and osteoclast.

5.3 Discussion and Conclusion

Osteocytes are bone resident cells that are entombed in the bone matrix for pretty much their entire lifespan. It has long been recognised that osteocytes communicate locally with their neighbouring osteocytes and cells on the bone surface via its dendritic process. However, how osteocytes can exert regulatory influences beyond the boundaries of the bone such as in phosphate metabolism remains largely unknown. Exosome are small extracellular microvesicles (50-100nm) that are secreted by various cells. The biological functions of exosomes are not fully understood, but may serve as a means to eliminate proteins that is useless and not required for the normal functioning of the cells. However, more recent studies suggest a more physiological important role for exosomes in intercellular communication, allowing the exchange of

proteins, membrane receptors, microRNAs, messenger RNAs, carbohydrates, organelles, and various other signaling information from the exosome-producing cells to target cells within and beyond the local microenvironment of the exosome-producing cell (Thery *et al.*, 2002; Ratajcsak *et al*., 2006; De Maio *et al*., 2011). Thus exosome secretion into the local microenvironment and circulation (Kamioka et al. 2001) could be an alternative form of communication utilized by osteocytes for intercellular communication to interact with and influence other cellular bodies beyond the bone.

Exosomes have been shown to play a role in areas such as immune response, tumour microenvironment, and stem cell biology, but yet to be described for osteocytes. Optimization of the protocol for isolating exosomes is important for exosome research, since all results subsequently obtained may not be reliable, if the purification were not accordingly performed. With several failed attempts and modifications to recommended protocol, MLO-Y4 cells-derived exosomes were for the first time successfully isolated and purified. The MLO-Y4 cells-derived exosomes were characterized by the enrichment of typical exosomal protein markers HSP70, CD63, CD9 and CD81. The quality of the isolated exosomes was further verified by the total protein profile. Exosomes should contain a large number of proteins, many of which should be distinct from the proteins detected in whole cell lysates. Furthermore, the exosomes isolated were of good purity and free from possible contamination from other membrane or organellar sources such as mitochondrial contaminations.

Interestingly, cells that were treated with Dex results in a substantial decrease in the amount of exosomes isolated. Previous studies have reported that induction of autophagy inhibits exosome secretion as these opposing mechanisms share a common convergence point, the multivesicular body (MVB) (Fader and Colombo, 2008; Fader *et al*., 2008; Simons and Raposo, 2009; Baixauli *et al*., 2014). Exosomes biogenesis and release is mediated by a complex pathway integrating with the endosomal machinery. Exosomes originate from the endosome through the inward budding of the limiting membrane of the late endosomes to form intraluminal vesicles (ILVs) which together are housed in an organelle known as the multivesicular bodies (MVBs). Once ILVs are formed, MVBs can fuse with the plasma membrane and release their cargo of ILVs to the extracellular environment as exosomes. (Buschow *et al*. 2005; Raposo and Stoorvogel, 2013). Alternatively, when cells undergo autophagy, MVBs are targeted to fuse with autophagasomes to form a prelysosomal vesicle called an amphisome which

ultimately fuse with lysosomes to form autolysosome (Gordon *et al.*, 1988; Berg *et al.*, 1998; Fader *et al.*, 2008; Fader and Colombo, 2009). In line with this, inducers of autophagy, such as rapamycin and vinblastine, increases fusion of MVBs with autophagosomes and consequently significantly decrease the release of exosomes (Fader *et al*. 2008; Wendler *et al*. 2013). However, the molecular signal and pathways that governs this switch has yet to be deciphered.

Another possible explanation for the reduced exosome secretion following Dex treatment is the alteration in morphological appearance of MLO-Y4 cells. Dex treatment induced a drastic rearrangement of the actin cytoskeleton, resulting in a loss of dendritic processes and concomitant increase in stress fibers formation ultimately switching the morphology of MLO-Y4 cells from a spindle-to-polygonal appearance. It is likely that the loss of dendritic processes would affect exosome release as dendritic processes are necessary for cell to cell communication and proposed to be the site for exosome release. Although the exact mechanism underlying this phenomenon is presently unclear, it appears to be closely coupled with the onset of autophagy. Indeed, the cytoskeleton is known to be intricately linked to both MVB, exosome and autophagosome formation and trafficking (Monastyrska *et al*., 2009; Aguilera *et al*., 2012; Zhuo *et al*., 2013; Raposo and Stoorvogel, 2013).

Despite the decrease in exosome release following dex treatment, the fact that MLO-Y4 osteocyte-like cells and more than likely primary osteocytes release exosomes was an exciting finding. So, what then, may the physiological function of these exosomes be? The tetraspanins CD9, CD81 and CD63 (Hemler *et al*. 2014) which were found to be expressed MLO-Y4 cell-derived exosomes have been shown to play important role in cell signalling, adhesion, invasion, migration, motility and fusion of immune, brain and cancer cells (Hemler 2005; Hemler 2014; Boucheix *et al*. 2001). In addition, HSP70, a heatshock protein which was consistently found to be highly expressed in MLO-Y4 cells-derived exosomes have been shown to activate immune system cells, like macrophages, dendritic cells and natural killers and to be involved in immune response to cancer (Asea A. *et al*. 2000; Gross C. *et al.* 2003; Binder *et al*. 2009; Wells *et al*. 2000). Thus taking into consideration the already studied functions of these proteins, it is plausible to suggest that exosomes released by MLO-Y4 cells and primary osteocytes, into the blood circulation, could in part modulate immune response, in conjunction with other potential biological processes.

Besides potential systemic effects, the osteocyte-derived exosomes may also have a local impact within the bone microenvironment. Sclerostin a potent inhibitor of osteoblast differentiation and bone formation is exclusively expressed by osteocytes (Winkler *et al*. 2003; Li *et al*. 2008). Interestingly, exosomes isolated from MLO-Y4 conditioned media expresses sclerostin suggesting that the sclerostin might be secreted as a cargo of osteocyte-derived exosomes to exert its inhibitory effect on bone surface lining osteoblasts and precursor cells. It is probable that sclerostin following synthesis in the cell is transported directly to endosomal membranes via chaperones such as HSP70, and then incorporated into ILV in MVBs for subsequent secretion as part of exosomal protein component. Due to time constraints, future studies will explore whether the MLO-Y4 cells-derived exosomes expressing sclerostin could inhibit osteoblastic mineralization and bone nodule formation *in vitro*.

As well as secreting sclerostin to regulate osteoblast formation and function, osteocytes are also the primary source of RANKL *in vitro* and *in vivo* (Nakashima *et al*. 2011; Xiong *et al.*, 2011). RANKL is both a membrane-bound and secreted soluble factor widely known as the most important regulator of osteoclast differentiation and, consequently, bone resorption. However immunoblotting failed to detect RANKL in MLO-Y4 cells-derived exosomes. Surprisingly RANKL was also found to be very weakly expressed TCP isolated from MLO-Y4 cells which is in stark contrast to primary osteocytes. But when we treated osteoclast precursor cells, MCSF-dependent BMMs, with the MLO-Y4 cells derived-exosomes for 5 days, a few TRAP positive cells were observed suggesting that RANKL was indeed incorporated into exosomes. TRAP is a marker for osteoclasts and precursor cells that have been committed towards the osteoclast lineage following stimulation with RANKL. However, unlike recombinant RANKL which invokes large multinucleated TRAP positive osteoclast formation, precursor cells treated with exosomes only have a few mononuclear TRAP positive BMMs with the majority of cells remaining TRAP negative BMMs. This suggest that although RANKL was expressed on MLO-Y4 cells-derived exosomes, the amount or concentration of RANKL was too low to induce efficient osteoclast formation. This is likely due to the low expression of RANKL in MLO-Y4 cells themselves. Thus we believe that exosomes derived from primary osteocyte would have higher levels of RANKL as the cells themselves expresses an abundant level of RANKL.

Finally an interesting protein enzyme was identified in MLO-Y4 cells-derived exosomes, cathepsin K. Cathepsin K is a proteolytic enzyme highly expressed in osteoclasts and required for bone resorption as it is the only known protease capable of degrade type I collagen at acidic pH (Tezuka *et al*., 1994; Inaoka *et al*., 1995; Dodds *et al*., 1998, 2001; Xia *et al.*, 1999; Pennypacker *et al.* 2009). Primary osteocytes have been shown to express cathepsin K (Qing *et al*., 2012) but what is the reason for osteocytes to express cathepsin K? Osteocytes have been proposed to be able to carry out bone resorption of the lacuna space in which it resides via a process known as osteocytic osteolysis. However, bone resorption is a specialized function carried out only by osteoclasts and requires two important prerequisites: the generation of an isolated acidic microenvironment which allows the dissolution of the mineralized bone and the subsequent break down of the collagen matrix by cathepsin K (also activated by the acidic microenvironent). Although MLO-Y4 cells and osteocytes expresses cathepsin K, they do not possess the required specialized membrane compartment known as the ruffled border that is specifically utilized by the osteoclasts to isolate and acidify (via the V-ATPase proton pump) the resorption lacuna, as well as provide the acidic condition for the cleavage of pro-cathepsin K to active mature cathepsin K during bone resorption. Thus it is not likely that osteocytes could perform bone osteolysis directly.

The identification of cathepsin K in MLO-Y4 cells-derived exosomes opens up the possibility that an alternative mechanism by which osteolysis by osteocytes could occur. More importantly, not only was the pro-immature form of cathepsin K was detected in the exosomes but also the cleaved activated mature form suggesting an acidic environment exists in the exosomes. Consistent with this was the identification of V-ATPase subunits V1B1 and the V0α1 in the same exosomes as cathepsin K. V-ATPase are the proton pump utilized by every cell in the body to acidify intracellular compartments and organelles. The identification of an intact V-ATPase complex (ie. containing both V1 and V0 domains) could provide the necessary acidic environment in the exosomes to cleave and activate cathepsin K. However, functional analysis of the potential of these cathepsin K containing exosomes to cause bone resorption needs to be further investigated in future studies.

In summary, despite the isolation of exosomes from cell culture media is a very time-consuming process, requiring large starting volumes of cell culture media and various

protocol optimization, the data in this chapter have for the first time demonstrated that MLO-Y4 osteocyte-like cells secretes exosomes. These exosomes expresses exosomal protein markers HSP70, CD63, CD81 and CD9 that have previously been shown to have various immune-modulatory effects. Furthermore, these exosomes also express variable levels of cytokines such as sclerostin and RANKL that exhibit anti-osteoblastic and pro-osteoclastogenic effects respectively. Most interestingly, MLO-Y4 cells-derived exosomes expressed an enzyme that is normally associated with bone resorption by osteoclasts providing support for the hotly debated processes of osteocytic osteolysis could likely occur. Finally, we have provided some preliminary evidence to suggest that GC (Dex)-induced autophagy could negatively impact exosome secretion. Although exosomes were isolated from a pseudo-osteocytic cell line, MLO-Y4, we are confident that primary osteocytes will also secrete exosomes probably to a higher degree than the MLO-Y4 cell line. Isolation of exosomes from primary osteocytes will be the focus of future studies.

CHAPTER SIX

OVERVIEW OF THESIS

6.1 General Discussion

Bone is a highly dynamic tissue in human body that continuously undergoes remodeling. Bone remodeling is a complex process tightly regulated by the balance of bone formation by the osteoblasts and bone resorption by the osteoclasts whose activity is modulated by bone matrix-embedded osteocytes. Perturbations in the balance of bone remodeling, leading to excessive osteoclastic bone resorption, results in debilitating osteolytic bone diseases such as osteoporosis. Osteoporosis is characterised by a systemic impairment of bone mass and microarchitecture resulting in fragility fractures (Rachner, Khosla and Hofbauer 2011).

Glucocorticoids (GCs) are extensively used for the treatment of chronic inflammatory and autoimmune diseases, but prolonged use results in reduction of bone mineral density (BMD) and increased risk of bone fragility (Weinstein 2012). GC-induced osteoporosis is the third leading form of osteoporosis and the most common cause of drug-related osteoporosis (Weinstein 2001). Patients with GC-induced osteoporosis show fewer osteoblasts and an increased prevalence of osteocyte apoptosis (Canalis et al. 2007; Weinstein et al. 1998; O`Brien et al. 2004). Furthermore, GCs also directly impact new osteoclast formation, prolong the lifespan of already formed osteoclasts, and decrease osteoblast survival. Therefore, with chronic long-term GC exposure reduces bone formation, decrease bone volume and density of trabeculae into spongy bone, leading to osteoporosis (Weinstein et al., 1998; Manolagas *et al*. 1999).

Recent studies have demonstrated that low dose GC treatment induces autophagy (self catabolism) in primary osteocytes and osteocytic cell-lines *in vitro* and *in vivo* (Xia *et al.*, 2010; Jia et al. 2011). In accordance with these studies, we also demonstrated using immunofluorescence analysis the induction of autophagy in MLO-Y4 osteocyte-like cells using the GC, dexamethasone (Dex). Dex treatment could dose and time-dependently induce the formation and accumulation of autophagic vacuoles suggesting an increased autophagic flux. Thus osteocyte autophagy, could be a firstline adaptive self-preservation mechanism utilized by osteocytes to adapt to cellular and metabolic stress from agents such as GCs. Thus, autophagy may provide a promising new target in the prevention of GC-induced bone fragility however, further investigation into the detailed molecular mechanism that regulates the development and progression of autophagy in osteocytes in response to GC treatment is required an aim that this thesis embarks to address..

GC elicit its effects by binding to its cognate receptor GR in the cytoplasm of the cell. The primary action of an activated GC-GR complex is the regulation of gene transcription (ref). Consistent with this our data in MLO-Y4 cells shows that GR is translocated from the cytoplasm to the nucleus following Dex treatment. In the nucleus, the activate GC-GR complex initiates the transcription of GC-responsive genes. Of these we identified two genes *mkp1* and *redd1* as potential targets for the actions of GC on autophagy. The proteins encoded by these gene MKP1 and REDD1 functions upstream of the mTORC1 signaling cascade, the signaling pathways considered the master regulatory pathway of autophagy (Mammucari *et al*., 2008; Esclatine *et al*. 2009; Jung et al., 2010; Ravikumar *et al*. 2010). Our gene expression analysis results revealed that both *mkp1* and *redd1* gene expression was dose and time-dependently increased following Dex treatment. However, only REDD1 protein displayed a similar increased induction profile following Dex treatment. These results suggest that the role of REDD1 in GC-induced autophagy was of more importance than MKP1. This was supported by our observations that silencing of REDD1 resulted in a marked reduction in the ability of Dex to induced autophagasome formation and thus autophagy, providing further evidence that REDD1 is functionally required to evoke GC-induced autophagic response. Interestingly, REDD1-dependent induction of autophagy have also been reported in lymphocytes (Molitoris *et al.* 2011).

We next defined the molecular mechanism by which REDD1 exert its pro-autophagic effect. REDD1 functions upstream of TSC1-TSC2 and Rheb in the mTORC1 signaling cascade (Corradetti et al. 2005). REDD1 inhibit mTORC1 activity in a TSC1-TSC2 dependent manner by activating TSC1-TSC2 GAP activity via activating phosphorylation of TSC2. Immunoblots analysis of the phosphorylation state of TSC2 following REDD1 overexpression revealed that inhibitory phosphorylation residues on TSC2, Ser939, Ser1254 and Thr1462, were not phosphorylated suggesting that TSC2 is in its active state bound to TSC1 and not to inhibitory anchoring protein 14-3-3 (Aicher et al., 2001; Huang and Manning. 2008; Ma et al., 2009; Orlova and Crino, 2010; Li et al., 2003). Consistent with an activated TSC2, we also detected activation phosphorylation at Ser1387, which is important for the activation of TSC2 GAP activity allowing active Rheb-GTP to by hydrolyzed into inactive Rheb-GDP form. However, REDD1 does not function directly in phosphorylating TSC2. REDD1 activates TSC2 by 14-3-3 protein sequestration through association of REDD1/14-3-3 complex and promoting dissociation of TSC2/14-3-3 complex (Bhasker et al., 2007;

DeYoung et al., 2008; Huang and Manning. 2008; Orlova and Crino, 2010; Regazzetti et al., 2012). Thus the overexpression of REDD1 in MLO-Y4 cells may have led to the sequestration of 14-3-3 away from TSC2 allowing it to form an active complex with TSC1. Further activating phosphorylation at Ser1387 by other kinases activates the GAP activity of TSC2 allowing it to hydrolyze Rheb-GTP to Rheb-GDP to inhibit mTORC1 activity.

In accordance with an active TSC2, mTORC1 activity was decreased by evidenced by two observations in our REDD1 overexpression studies. Firstly mTOR activation phosphorylation at Ser2448 was attenuated and second, phosphorylation status of downstream substrates S6K and ULK1 (mammalian homologue of yeast Atg1) kinases were also attenuated. The lack of inhibitory phosphorylation of ULK1 by mTORC1 allows this kinase to initiate the autophagic cascade (Stephan and Herman, 2006; Chan et al., 2007). When activated, ULK1 can bind to several autophagy-related (Atg) proteins, regulating their phosphorylation states and intracellular trafficking (Kamada et al., 2000; Young et al., 2006; Lee et al., 2007; Hara et al., 2008). Collectively, our data provides strong evidence that REDD1 plays an important role in signaling the activation of autophagy in response to GC treatment.

Autophagy induction is characterized by the mobilization of many membrane compartments throughout the cytoplasm, culminating with the formation of the autolysosome (Ravikumar *et al*. 2010). In contrast to this hypothesis, several studies have demonstrated a probable convergence between the autophagic and endosomal pathways before the formation of autolysosome (Gordon et al. 1988). It has been shown that autophagosome may fuse with a late endosome or multivesicular bodies (MVBs) leading to the formation of a prelysosomal compartment called amphisome. MVBs are large organelles that houses intraluminal vesicles which becomes what is commonly known as exosomes, when they are released into the extracellular environment. Interestingly, it has been shown that inducers of autophagy, such as rapamycin and vinblastine, increases fusion of MVBs with autophagosomes and consequently significantly decrease the release of exosomes (Fader et al. 2008; Wendler et al., 2013).

Exosome are small extracellular microvesicles secreted by various cells to functions as an alternative mechanism for intercellular communication. Osteocytes which are terminally entombed in the bone matrix has long been recognised to

communicate locally with their neighbouring osteocytes and cells on the bone surface via its dendritic process. However, how osteocytes can exert regulatory influences beyond the boundaries of the bone such as in phosphate metabolism remains largely unknown. We thus propose that exosomes secretion into the local microenvironment and circulation as an alternative form of communication utilized by osteocytes to exert influence on other cellular bodies within the local environment of the bone and beyond.

This thesis; to my knowledge is the first to show that MLO-Y4 osteocyte-like cells could secrete exosomes. Consistent with other studies, GC treatment which induces autophagy in MLO-Y4 cells significantly reduced the amount of exosomes isolated. Another possible explanation for the reduced exosome secretion following Dex treatment is changes in cytoskeletal dynamics. We observed drastic rearrangement of the actin cytoskeleton, resulting in a loss of dendritic processes and concomitant increase in stress fibers formation following Dex treatment. It is likely that this loss of dendritic processes would contribute to the decrease in exosome release. Although the exact mechanism underlying this phenomenon is presently unclear, it appears to be closely coupled with the onset of autophagy. Indeed, the cytoskeleton is known to be intricately linked to both MVB, exosome and autophagosome formation and trafficking (Monastyrska *et al*., 2009; Aguilera *et al*., 2012; Zhuo *et al*., 2013; Raposo and Stoorvogel, 2013). Taken together, the results provided further evidence that the processes of autophagy and exosome secretion are intricately linked, with cytoskeletal dynamics contributing to the regulation of both processes.

These MLO-Y4 cells-derived exosomes were characterized by the enrichment of typical exosomal protein markers HSP70, CD63, CD9 and CD81 (Hemler 2005; Hemler 2014; Boucheix *et al*. 2001; Asea A. et al., 2000; Gross C. et al., 2003; Binder *et al*. 2009; Wells *et al*. 2000). Interestingly, these protein markers have been suggest to exhibit immune-modulatory functions suggesting that exosomes released by MLO-Y4 and possibly primary osteocytes could regulate the immune response. In addition to have potential immune-modulatory role, the MLO-Y4 cells was also found to express sclerostin and RANKL, two important cytokines that have a more localized role in the bone. Sclerostin is a potent inhibitor of osteoblast differentiation and bone formation, and is exclusively expressed by osteocytes (Winkler et al. 2003; Li et al. 2008). The presence of sclerostin on exosomes suggests that following synthesis in the cell, sclerostin is transported directly to endosomal membranes via chaperones such as

HSP70, and then incorporated into ILV in MVBs for subsequent secretion as part of exosomal protein component. Once released as part of exosomes, sclerostin containing exosomes can circulate within the local bone environment and modulate osteoblast function.

Although we did not directly detect RANKL, the most important regulator of osteoclast differentiation and bone resorption (Sobacchi *et al.*, 2007), on exosomes by immunoblotting, cellular affects were observed. Some MCSF-dependent mononuclear BMMs which are the precursors to multinucleated osteoclasts were found to express TRAP, an enzymatic marker for cells that have been stimulated with RANKL to commit to the osteoclast lineage. However, unlike recombinant RANKL which invokes large multinucleated TRAP positive osteoclast formation, only a few mononuclear TRAP positive BMMs were observed in exosome treated group. This is likely due to the low expression of RANKL in MLO-Y4 cells themselves, resulting in low expression in exosomes. On the other hand, we expect exosomes from primary osteocyte which express high levels of RANKL to have more RANKL on their exosomes.

Interestingly, we identified the expression of cathepsin K and V-ATPase proton pump on MLO-Y4 cells-derived osteoclasts. So what are these proteolytic and degradative enzymes doing on the exosomes? Cathepsin K is a proteolytic enzyme highly expressed in osteoclasts required for bone resorption and is the only known protease capable of degrade type I collagen at acidic pH It is cleaved from an immature propeptide to an active mature form under acidic conditions (Tezuka *et al*., 1994; Inaoka *et al*., 1995; Dodds *et al*., 1998, 2001; Xia *et al.*, 1999; Pennypacker *et al.* 2009). Primary osteocytes have previously been shown to express cathepsin K (Qing *et al*., 2012) and thus been proposed to be able to carry out osteocytic osteolysis of the lacuna space in which it resides. However, bone resorption is a specialized function carried out exclusively by osteoclasts and requires two important prerequisites. One being the expression of cathepsin K, the other is the generation of an isolated acidic microenvironment which allows the dissolution of the mineralized bone and the subsequent break down of the collagen matrix by cathepsin K (activated by the acidic microenvironent). Although MLO-Y4 cells and osteocytes expresses cathepsin K, they do not possess the required specialized membrane compartment known as the ruffled border that is specifically utilized by the osteoclasts to isolate and acidify (via the V-ATPase proton pump) the resorption lacuna. Thus it is not likely that osteocytes could

perform bone osteolysis directly. The identification of cathepsin K and V-ATPase proton pump in MLO-Y4 cells-derived exosomes opens up the possibility that osteolysis may occur via the actions of the exosomes. More importantly, not only was the pro-immature form of cathepsin K was detected in the exosomes but also the cleaved activated mature form suggesting an acidic environment exists in the exosomes. However, how this is achieved requires further functional analysis in future studies.

Overall, the results from the studies carried out in this thesis have provided an molecular mechanism via which glucocorticoids, in this case, dexamethasone induces autophagy in an osteocytic-like cell line MLO-Y4. The upregulation of REDD1 by Dex treatment inhibited the activity of a major negative regulator of autophagy, mTORC1, in a TSC2-dependent manner. Furthermore, this thesis for the first time provided evidence to support exosome secretion by MLO-Y4 cells, and these exosomes appears to express proteins that could exert both local bone and system effects. Furthermore, we have further shown an intricate interplay between autophagy and exosome secretion with induction of one lead to the inhibition of the other. Finally, an alternative mechanism to osteocytic osteolysis via exosomes may have been uncovered.

6.2 Future Directions

Due to time constraints, there were a lot of potential mechanisms for both autophagy and exosome secretion that was not explored. Firstly for autophagy, optimization of the silencing protocol and confirmation of REDD1 silencing via gene and protein expression needs to be carried out. Once done, further examination of the effects of REDD1 silencing on the mTORC1 signaling pathway would have provided a good comparative measure for REDD1 overexpression. Similarly, the direct effects of GC on the mTORC1 signaling should be explored and compared to REDD1 overexpression to show that REDD1 overexpression could mimic the GC effects. This will provide further support that REDD1 indeed carry out the effects of GC. It would also been ideal to further decipher the autophagy signaling cascade downstream of ULK1 activation under the various experimental conditions, that is, GC induction with and without REDD1 silencing and REDD1 overexpression.

Another avenue of future studies is to explore the role of MKP1 in GC-induced autophagy. MKP1 although MKP1 also inhibits mTORC1 activity in a TSC2-dependent manner, the molecular mechanism is different to REDD1 (Ma *et al.,* 2005). MKP1

functions further upstream of REDD1 in the mTORC1 signaling cascade. Thus, similar experiments such as MKP1 overexpression and silencing with or with GC-treatment shed information on the role of MKP1 in the signaling events. It would be ideal for both MKP1 and REDD1 overexpression experiments to be able to visualize the induction of autophagy induction in the absence of GC treatment via immunofluorescence microscopy. However, this would require using a fluorescent probe that utilizes a different wavelength to GFP, such as Cyto-ID Red. Alternatively, REDD1 and MKP1 could be fused to another fluorescent tag like mCHERRY or RFP, which would allow the use of Cyto-ID Green.

For the exosomes, we have only started to pick at the very beginning of a very much largely unexplored field Immunoblotting of known secreted proteins that could be express on exosomes is a very slow process and limited by the availability of good antibodies. Thus it would be ideal to examine the protein profile of osteocyte-derived exosomes and compare it with TCP by proteomic analyses. This will potentially provide up to hundreds or thousands of protein candidates that could be differentially expressed on the surface of the exosome as well as those that a trapped within the exosomal lumen as compared to TCP. Furthemore, we could also compare protein profiles of osteocyte-derived exosomes with exosomes derived from other bone cells such as osteoblasts and osteoclasts. Furthermore, how induction of autophagy by stressors such as glucocorticoids affect exosome protein profile would be of great interest. This may actually provide further insight into the molecular interplay between autophagy and exosome secretion.

Another way to explore the interplay between autophagy and exosome secretion is to monitor changes in the trafficking events of the MVB under an autophagic state or an exosome secretory state. This could be achieved by the use of live-cell immunofluorescence confocal imaging and staining the MVB with a marker such as CD63 and see what happens in the presence of an autophagy (which could be counterstained with Cyto-ID) inducer like glucocorticoids. Live-cell imaging would allow for the tracking and monitoring of the change from secretory to degradative states in real time. Furthermore, investigation of the trafficking events (involvement of Rab GTPases) will also like shed light on the regulation of autophagosome, MVB, and exosome biogenesis and subcellular distribution in the presence or absence of autophagy inducer like glucocorticoids.

Functional studies using exosomes would be experiment high on the "to-do" list. Our very preliminary results for the effects of MLO-Y4-derived exosomes on osteoclast formation shows promise although no "true" osteoclast was formed but TRAP positivity was a start. Thus trying to isolate and larger quantity of exosomes using alternative isolation methods such as immunoisolation, to repeat the experiment will likely provide even more exciting results. Furthermore other than examining osteoclast formation, we could also explore the effects on osteoclast bone resorption to see whether osteocyte-derived exosomes could regulate the bone resorption process. In addition, given sclerostin was found to be expressed on the exosomes, osteoblast differentiation and function (mineralization and bonr formation) should be explored. Functional analyses would not only be limited to bone cells as the isolated exosomes also expresses proteins that's been implicated to have immune-modulatory effects. Thus examination of osteocyte-derived exosomes on immune cells and macrophages would provide further evidence to support osteocyte regulation of cellular and metabolic processes beyond the bobe.

Although the data presented for both autophagy and exosomes are promising, they are early preliminary data and requires much further investigations. The biggest drawback is the use of MLO-Y4 cells as the cell source for the exosomes. It would be ideal to utilize primary osteocytes from bones to isolate exosomes. However, it is very difficult to isolate primary osteocytes from skeletally mature bones, and usually require the use of neonate mice. Furthermore, once extracted, primary osteocytes rapidly dedifferentiate to an osteoblastic/fibroblastic phenotype within a few days making functional assessments very difficult. This is because *in vitro* monolayer cutlures does not provide the necessary environment and mechanical stimulation to maintain their osteocytic phenotype. Until a robust isolation and *in vitro* culture condition for primary osteocytes are established, osteocyte-like cell lines such as MLO-Y4 are the best representative for the functional analysis of this bone cell.

In all, if possible in Brazil, I hope to be able to continue further studies and contribute to this field both scientifically and medically. Hopefully the further studies could be in collaboration with colleagues and friends at the Centre for Orthopaedic Research at the University of Western Australia.

CHAPTER SEVEN

REFERENCES

7.1 References

Aarden, EM., et al. (1994). "Function of osteocytes in bone." J Cell Biochem **55**(3): 287-299.

Abraham, S. M., et al. (2006). "Antiinflammatory effects of dexamethasone are partly dependent on induction of dual specificity phosphatase 1." J Exp Med **203**(8): 1883-1889.

Adachi, T., et al. (2009). "Calcium response in single osteocytes to locally applied mechanical stimulus: differences in cell process and cell body." J Biomech **42**(12): 1989-1995.

Aguilera, M. O., et al. (2012). "The actin cytoskeleton participates in the early events of autophagosome formation upon starvation induced autophagy." Autophagy **8**(11): 1590-1603.

Aicher, L. D., et al. (2001). "Tuberin phosphorylation regulates its interaction with hamartin. Two proteins involved in tuberous sclerosis." J Biol Chem **276**(24): 21017-21021.

Alers, S., et al. (2012). "Role of AMPK-mTOR-Ulk1/2 in the regulation of autophagy: cross talk, shortcuts, and feedbacks." Mol Cell Biol **32**(1): 2-11.

Alessi, DR., et al. (2009). "New insights into mTOR signaling: mTORC2 and beyond." Sci Signal **2**(67): pe27.

Anisimov, VN., et al. (2010). "Rapamycin extends maximal lifespan in cancer-prone mice." Am J Pathol **176**(5): 2092-2097.

Asea, A., et al. (2000). "HSP70 stimulates cytokine production through a CD14-dependant pathway, demonstrating its dual role as a chaperone and cytokine." Nat Med **6**(4): 435-442.

Ashcroft, B. A., et al. (2012). "Determination of the size distribution of blood microparticles directly in plasma using atomic force microscopy and microfluidics." Biomed Microdevices **14**(4): 641-649.

Axe, EL., et al. (2008). "Autophagosome formation from membrane compartments enriched in phosphatidylinositol 3-phosphate and dynamically connected to the endoplasmic reticulum." J Cell Biol **182**(4): 685-701.

Babij, P., et al. (2003). "High bone mass in mice expressing a mutant LRP5 gene." J Bone Miner Res **18**(6): 960-974.

Baixauli, F., et al. (2014). "Exosomes and autophagy: coordinated mechanisms for the maintenance of cellular fitness." Front Immunol **5**: 403.

Beauchamp, E. M. and L. C. Platanias (2013). "The evolution of the TOR pathway and its role in cancer." Oncogene **32**(34): 3923-3932.

Berg, TO., et al. (1998). "Isolation and characterization of rat liver amphisomes. Evidence for fusion of autophagosomes with both early and late endosomes." J Biol Chem **273**(34): 21883-21892.

Bhaskar, P. T. and N. Hay (2007). "The two TORCs and Akt." Dev Cell **12**(4): 487-502.

Binder, R. J. (2009). "CD40-independent engagement of mammalian hsp70 by antigen-presenting cells." J Immunol **182**(11): 6844-6850.

Bonewald, LF. (2011). "The amazing osteocyte." J Bone Miner Res **26**(2): 229-238.

Bonewald, LF. (2006). "Mechanosensation and Transduction in Osteocytes." Bonekey Osteovision **3**(10): 7-15.

Boucheix, C., et al. (2001). "Tetraspanins and malignancy." Expert Rev Mol Med **2001**: 1-17.

Bouillon, R. and T. Suda (2014). "Vitamin D: calcium and bone homeostasis during evolution." Bonekey Rep **3**: 480.

Buschow, SI., et al. (2005). "Exosomes contain ubiquitinated proteins." Blood Cells Mol Dis **35**(3): 398-403.

Canalis, E., et al. (2007). "Glucocorticoid-induced osteoporosis: pathophysiology and therapy." Osteoporos Int **18**(10): 1319-1328.

Chan, E. Y., et al. (2007). "siRNA screening of the kinome identifies ULK1 as a multidomain modulator of autophagy." J Biol Chem **282**(35): 25464-25474.

Chen, K., et al. (2014). "Decreased activity of osteocyte autophagy with aging may contribute to the bone loss in senile population." Histochem Cell Biol.

Corradetti, MN. and KL. Guan (2006). "Upstream of the mammalian target of rapamycin: do all roads pass through mTOR?" Oncogene **25**(48): 6347-6360.

Corradetti, MN., et al. (2005). "The stress-induced proteins RTP801 and RTP801L are negative regulators of the mammalian target of rapamycin pathway." J Biol Chem **280**(11): 9769-9772.

Cowin, SC., et al. (1991). "Candidates for the mechanosensory system in bone." J Biomech Eng **113**(2): 191-197.

De Maio, A. (2011). "Extracellular heat shock proteins, cellular export vesicles, and the Stress Observation System: a form of communication during injury, infection, and cell damage. It is never known how far a controversial finding will go! Dedicated to Ferruccio Ritossa." Cell Stress Chaperones **16**(3): 235-249.

DeYoung, M. P., et al. (2008). "Hypoxia regulates TSC1/2-mTOR signaling and tumor suppression through REDD1-mediated 14-3-3 shuttling." Genes Dev **22**(2): 239-251.

Dodds, R. A., et al. (1998). "Cathepsin K mRNA detection is restricted to osteoclasts during fetal mouse development." J Bone Miner Res **13**(4): 673-682.

Dodds, R. A., et al. (2001). "Human osteoclast cathepsin K is processed intracellularly prior to attachment and bone resorption." J Bone Miner Res **16**(3): 478-486.

Esclatine, A., et al. (2009). "Macroautophagy signaling and regulation." Curr Top Microbiol Immunol **335**: 33-70.

Fader, CM. and MI. Colombo (2009). "Autophagy and multivesicular bodies: two closely related partners." Cell Death Differ **16**(1): 70-78.

Fader, CM., et al. (2008). "Induction of autophagy promotes fusion of multivesicular bodies with autophagic vacuoles in k562 cells." Traffic **9**(2): 230-250.

Gattineni, J., et al. (2009). "FGF23 decreases renal NaPi-2a and NaPi-2c expression and induces hypophosphatemia in vivo predominantly via FGF receptor 1." Am J Physiol Renal Physiol **297**(2): F282-291

Gordon, PB. and PO. Seglen (1988). "Prelysosomal convergence of autophagic and endocytic pathways." Biochem Biophys Res Commun **151**(1): 40-47.

Gross, C., et al. (2003). "Heat shock protein 70-reactivity is associated with increased cell surface density of CD94/CD56 on primary natural killer cells." Cell Stress Chaperones **8**(4): 348-360.

Hadjidakis, DJ. and Androulakis, II (2006). "Bone remodeling." Ann N Y Acad Sci **1092**: 385-396

Hamasaki, M., et al. (2013). "Autophagosomes form at ER-mitochondria contact sites." Nature **495**(7441): 389-393.

Hara, K., et al. (2002). "Raptor, a binding partner of target of rapamycin (TOR), mediates TOR action." Cell **110**(2): 177-189.

Hara, T., et al. (2008). "FIP200, a ULK-interacting protein, is required for autophagosome formation in mammalian cells." J Cell Biol **181**(3): 497-510.

Harrison, DE., et al. (2009). "Rapamycin fed late in life extends lifespan in genetically heterogeneous mice." Nature **460**(7253): 392-395.

Heino, TJ., et al. (2002). "Osteocytes inhibit osteoclastic bone resorption through transforming growth factor-beta: enhancement by estrogen." J Cell Biochem **85**(1): 185-197.

Heitman, J., et al. (1991). "Targets for cell cycle arrest by the immunosuppressant rapamycin in yeast." Science **253**(5022): 905-909.

Hemler, M. E. (2005). "Tetraspanin functions and associated microdomains." Nat Rev Mol Cell Biol **6**(10): 801-811.

Hemler, M. E. (2014). "Tetraspanin proteins promote multiple cancer stages." Nat Rev Cancer **14**(1): 49-60.

Huang, J. and B. D. Manning (2008). "The TSC1-TSC2 complex: a molecular switchboard controlling cell growth." Biochem J **412**(2): 179-190.

Huiskes, R., et al. (2000). "Effects of mechanical forces on maintenance and adaptation of form in trabecular bone." Nature **405**(6787): 704-706.

Inaoka, T., et al. (1995). "Molecular cloning of human cDNA for cathepsin K: novel cysteine proteinase predominantly expressed in bone." Biochem Biophys Res Commun **206**(1): 89-96.

Inoki, K., et al. (2003). "Rheb GTPase is a direct target of TSC2 GAP activity and regulates mTOR signaling." Genes Dev **17**(15): 1829-1834

Jager, S., et al. (2004). "Role for Rab7 in maturation of late autophagic vacuoles." J Cell Sci **117**(Pt 20): 4837-4848.

Jia, J., et al. (2011). "Glucocorticoid dose determines osteocyte cell fate." Faseb j **25**(10): 3366-3376

Jing, D., et al. (2014). "In situ intracellular calcium oscillations in osteocytes in intact mouse long bones under dynamic mechanical loading." Faseb j **28**(4): 1582-1592.

Juhasz, G. and TP. Neufeld (2006). "Autophagy: a forty-year search for a missing membrane source." PLoS Biol **4**(2): e36.

Julien, LA., et al. (2010). "mTORC1-activated S6K1 phosphorylates Rictor on threonine 1135 and regulates mTORC2 signaling." Mol Cell Biol **30**(4): 908-921.

Jung, CH., et al. (2010). "mTOR regulation of autophagy." FEBS Lett **584**(7): 1287-1295.

Kamada, Y., et al. (2000). "Tor-mediated induction of autophagy via an Apg1 protein kinase complex." J Cell Biol **150**(6): 1507-1513.

Kamioka, H., et al. (2001). "A three-dimensional distribution of osteocyte processes revealed by the combination of confocal laser scanning microscopy and differential interference contrast microscopy." Bone **28**(2): 145-149.

Kassel, O., et al. (2001). "Glucocorticoids inhibit MAP kinase via increased expression and decreased degradation of MKP-1." Embo j **20**(24): 7108-7116.

Keller, S., et al. (2007). "CD24 is a marker of exosomes secreted into urine and amniotic fluid." Kidney Int **72**(9): 1095-1102.

Kim, DH., et al. (2002). "mTOR interacts with raptor to form a nutrient-sensitive complex that signals to the cell growth machinery." Cell **110**(2): 163-175.

King, MA., et al. (2008). "Rapamycin inhibits polyglutamine aggregation independently of autophagy by reducing protein synthesis." Mol Pharmacol **73**(4): 1052-1063.

Kochl, R., et al. (2006). "Microtubules facilitate autophagosome formation and fusion of autophagosomes with endosomes." Traffic **7**(2): 129-145.

Larsson, T., et al. (2004). "Transgenic mice expressing fibroblast growth factor 23 under the control of the alpha1(I) collagen promoter exhibit growth retardation, osteomalacia, and disturbed phosphate homeostasis." Endocrinology **145**(7): 3087-3094

Leboime, A., et al. (2010). "Osteoporosis and mortality." Joint Bone Spine **77 Suppl 2**: S107-112.

Lee, S. B., et al. (2007). "ATG1, an autophagy regulator, inhibits cell growth by negatively regulating S6 kinase." EMBO Rep **8**(4): 360-365.

Li, X., et al. (2005). "Sclerostin binds to LRP5/6 and antagonizes canonical Wnt signaling." J Biol Chem **280**(20): 19883-19887.

Li, X., et al. (2008). "Targeted deletion of the sclerostin gene in mice results in increased bone formation and bone strength." J Bone Miner Res **23**(6): 860-869.

Loewith, R., et al. (2002). "Two TOR complexes, only one of which is rapamycin sensitive, have distinct roles in cell growth control." Mol Cell **10**(3): 457-468.

Lu, N. Z., et al. (2006). "International Union of Pharmacology. LXV. The pharmacology and classification of the nuclear receptor superfamily: glucocorticoid, mineralocorticoid, progesterone, and androgen receptors." Pharmacol Rev **58**(4): 782-797.

Ma, L., et al. (2005). "Phosphorylation and functional inactivation of TSC2 by Erk implications for tuberous sclerosis and cancer pathogenesis." Cell **121**(2): 179-193.

Ma, X. M. and J. Blenis (2009). "Molecular mechanisms of mTOR-mediated translational control." Nat Rev Mol Cell Biol **10**(5): 307-318.

Mammucari, C., et al. (2008). "Downstream of Akt: FoxO3 and mTOR in the regulation of autophagy in skeletal muscle." Autophagy **4**(4): 524-526.

Manolagas, S. C. and R. S. Weinstein (1999). "New developments in the pathogenesis and treatment of steroid-induced osteoporosis." J Bone Miner Res **14**(7): 1061-1066.

Mathivanan, S., et al. (2010). "Exosomes: extracellular organelles important in intercellular communication." J Proteomics **73**(10): 1907-1920.

Mayer, C. and I. Grummt (2006). "Ribosome biogenesis and cell growth: mTOR coordinates transcription by all three classes of nuclear RNA polymerases." Oncogene **25**(48): 6384-6391

Mendoza, M. C., et al. (2011). "The Ras-ERK and PI3K-mTOR pathways: cross-talk and compensation." Trends Biochem Sci **36**(6): 320-328.

Mirams, M., et al. (2004). "Bone as a source of FGF23: regulation by phosphate?" Bone **35**(5): 1192-1199.

Molitoris, J. K., et al. (2011). "Glucocorticoid elevation of dexamethasone-induced gene 2 (Dig2/RTP801/REDD1) protein mediates autophagy in lymphocytes." J Biol Chem **286**(34): 30181-30189.

Monastyrska, I., et al. (2009). "Multiple roles of the cytoskeleton in autophagy." Biol Rev Camb Philos Soc **84**(3): 431-448.

Mullen, CA., et al. (2013). "Osteocyte differentiation is regulated by extracellular matrix stiffness and intercellular separation." J Mech Behav Biomed Mater **28**: 183-194.

Nakashima, T., et al. (2011). "Evidence for osteocyte regulation of bone homeostasis through RANKL expression." Nat Med **17**(10): 1231-1234.

Noda, T. and Y. Ohsumi (1998). "Tor, a phosphatidylinositol kinase homologue, controls autophagy in yeast." J Biol Chem **273**(7): 3963-3966.

O'Brien, C. A., et al. (2004). "Glucocorticoids act directly on osteoblasts and osteocytes to induce their apoptosis and reduce bone formation and strength." Endocrinology **145**(4): 1835-1841

Onal, M., et al. (2013). "Suppression of autophagy in osteocytes mimics skeletal aging." J Biol Chem **288**(24): 17432-17440

Orlova, K. A. and P. B. Crino (2010). "The tuberous sclerosis complex." Ann N Y Acad Sci **1184**: 87-105.

Pajevic, P. D. (2009). "Regulation of bone resorption and mineral homeostasis by osteocytes." IBMS BoneKEy 6**:** 63-70.

Pennypacker, B., et al. (2009). "Bone density, strength, and formation in adult cathepsin K (-/-) mice." Bone **44**(2): 199-207.

Piekarski, K. and M. Munro (1977). "Transport mechanism operating between blood supply and osteocytes in long bones." Nature **269**(5623): 80-82.

Poole, KE., et al. (2005). "Sclerostin is a delayed secreted product of osteocytes that inhibits bone formation." Faseb j **19**(13): 1842-1844

Proud, CG. (2007). "Amino acids and mTOR signalling in anabolic function." Biochem Soc Trans **35**(Pt 5): 1187-1190.

Pyo, JO., et al. (2012). "Molecules and their functions in autophagy." Exp Mol Med **44**(2): 73-80.

Qin, A., et al. (2012). "V-ATPases in osteoclasts: structure, function and potential inhibitors of bone resorption." Int J Biochem Cell Biol **44**(9): 1422-1435.

Rachner, TD., et al. (2011). "Osteoporosis: now and the future." Lancet **377**(9773): 1276-1287

Raposo, G. and W. Stoorvogel (2013). "Extracellular vesicles: exosomes, microvesicles, and friends." J Cell Biol **200**(4): 373-383.

Ratajczak, J., et al. (2006). "Embryonic stem cell-derived microvesicles reprogram hematopoietic progenitors: evidence for horizontal transfer of mRNA and protein delivery." Leukemia **20**(5): 847-856.

Ravikumar, B., et al. (2010). "Regulation of mammalian autophagy in physiology and pathophysiology." Physiol Rev **90**(4): 1383-1435.

Regazzetti, C., et al. (2012). "Regulated in development and DNA damage responses - 1 (REDD1) protein contributes to insulin signaling pathway in adipocytes." PLoS One **7**(12): e52154.

Riminucci, M., et al. (2003). "FGF-23 in fibrous dysplasia of bone and its relationship to renal phosphate wasting." J Clin Invest **112**(5): 683-692.

Rochefort, GY., et al. (2010). "Osteocyte: the unrecognized side of bone tissue." Osteoporos Int **21**(9): 1457-1469.

Rubinsztein, DC., et al. (2011). "Autophagy and aging." Cell **146**(5): 682-695.

Sarbassov, DD., et al. (2004). "Rictor, a novel binding partner of mTOR, defines a rapamycin-insensitive and raptor-independent pathway that regulates the cytoskeleton." Curr Biol **14**(14): 1296-1302.

Scott, RC., et al. (2004). "Role and regulation of starvation-induced autophagy in the Drosophila fat body." Dev Cell **7**(2): 167-178.

Sheng, MH., et al. (2014). "Role of Osteocyte-derived Insulin-Like Growth Factor I in Developmental Growth, Modeling, Remodeling, and Regeneration of the Bone." J Bone Metab **21**(1): 41-54.

Simons, M. and G. Raposo (2009). "Exosomes--vesicular carriers for intercellular communication." Curr Opin Cell Biol **21**(4): 575-581.

Sobacchi, C., et al. (2007). "Osteoclast-poor human osteopetrosis due to mutations in the gene encoding RANKL." Nat Genet **39**(8): 960-962.

Stephan, J. S. and P. K. Herman (2006). "The regulation of autophagy in eukaryotic cells: do all roads pass through Atg1?" Autophagy **2**(2): 146-148.

Sugawara, Y., et al. (2005). "Three-dimensional reconstruction of chick calvarial osteocytes and their cell processes using confocal microscopy." Bone **36**(5): 877-883.

Tatsumi, S., et al. (2007). "Targeted ablation of osteocytes induces osteoporosis with defective mechanotransduction." Cell Metab **5**(6): 464-475.

Tezuka, K., et al. (1994). "Molecular cloning of a possible cysteine proteinase predominantly expressed in osteoclasts." J Biol Chem **269**(2): 1106-1109.

Thery, C., et al. (2002). "Exosomes: composition, biogenesis and function." Nat Rev Immunol **2**(8): 569-579.

Tooze, S. A. and T. Yoshimori (2010). "The origin of the autophagosomal membrane." Nat Cell Biol **12**(9): 831-835.

Villarroya-Beltri, C., et al. (2014). "Sorting it out: Regulation of exosome loading." Seminars in Cancer Biology (In press)

Wang, X., et al. (2008). "The role of MAP kinase phosphatase-1 in the protective mechanism of dexamethasone against endotoxemia." Life Sci **83**(19-20): 671-680.

Wang, Z., et al. (2003). "Dexamethasone-induced gene 2 (dig2) is a novel pro-survival stress gene induced rapidly by diverse apoptotic signals." J Biol Chem **278**(29): 27053-27058.

Weinbaum, S., et al. (1994). "A model for the excitation of osteocytes by mechanical loading-induced bone fluid shear stresses." J Biomech **27**(3): 339-360.

Weinstein, RS., et al. (1998). "Inhibition of osteoblastogenesis and promotion of apoptosis of osteoblasts and osteocytes by glucocorticoids. Potential mechanisms of their deleterious effects on bone." J Clin Invest **102**(2): 274-282.

Weinstein, RS. (2001). "Glucocorticoid-induced osteoporosis." Rev Endocr Metab Disord **2**(1): 65-73.

Weinstein, RS. (2012). "Glucocorticoid-induced osteoporosis and osteonecrosis." Endocrinol Metab Clin North Am **41**(3): 595-611

Wells, A. D. and M. Malkovsky (2000). "Heat shock proteins, tumor immunogenicity and antigen presentation: an integrated view." Immunol Today **21**(3): 129-132.

Wendler, F., et al. (2013). "Cancer becomes wasteful: emerging roles of exosomes (dagger) in cell-fate determination." J Extracell Vesicles **2**.

Winkler, DG., et al. (2003). "Osteocyte control of bone formation via sclerostin, a novel BMP antagonist." Embo j **22**(23): 6267-6276.

Wullschleger, S., et al. (2006). "TOR signaling in growth and metabolism." Cell **124**(3): 471-484.

Wyttenbach, A., et al. (2008). "Amelioration of protein misfolding disease by rapamycin: translation or autophagy?" Autophagy **4**(4): 542-545.

Xiao, Y. Q., et al. (2006). "Oxidants selectively reverse TGF-beta suppression of proinflammatory mediator production." J Immunol **176**(2): 1209-1217.

Xia, L., et al. (1999). "Localization of rat cathepsin K in osteoclasts and resorption pits: inhibition of bone resorption and cathepsin K-activity by peptidyl vinyl sulfones." Biol Chem **380**(6): 679-687.

Xia, X., et al. (2010). "Glucocorticoid-induced autophagy in osteocytes." J Bone Miner Res **25**(11): 2479-2488.

Xiong, J., et al. (2011). "Matrix-embedded cells control osteoclast formation." Nat Med **17**(10): 1235-1241.

Yamamoto, A., et al. (1998). "Bafilomycin A1 prevents maturation of autophagic vacuoles by inhibiting fusion between autophagosomes and lysosomes in rat hepatoma cell line, H-4-II-E cells." Cell Struct Funct **23**(1): 33-42.

Yamazaki, Y., et al. (2002). "Increased circulatory level of biologically active full-length FGF-23 in patients with hypophosphatemic rickets/osteomalacia." J Clin Endocrinol Metab **87**(11): 4957-4960.

Young, A. R., et al. (2006). "Starvation and ULK1-dependent cycling of mammalian Atg9 between the TGN and endosomes." J Cell Sci **119**(Pt 18): 3888-3900.

Zhang, K., et al. (2006). "E11/gp38 selective expression in osteocytes: regulation by mechanical strain and role in dendrite elongation." Mol Cell Biol **26**(12): 4539-4552.

Zhao, S., et al. (2002). "MLO-Y4 osteocyte-like cells support osteoclast formation and activation." J Bone Miner Res **17**(11): 2068-2079.

Zhao, W., et al. (2000). "Osteocyte and osteoblast apoptosis and excessive bone deposition accompany failure of collagenase cleavage of collagen." J Clin Invest **106**(8): 941-949.

Zhuo, C., et al. (2013). "Proteomics analysis of autophagy-deficient Atg7-/- MEFs reveals a close relationship between F-actin and autophagy." Biochem Biophys Res Commun **437**(3): 482-488.